AJ

Vortex-Induced Vibration of Flexible Cylinders in Sheared Flows

by

Tae-Young Chung

B.S., Seoul National University, Korea

(1975)

M.S., Seoul National University, Korea

(1977)

Submitted in Partial Fulfillment of the

Requirements for the Degree of

Doctor of Philosophy

in Ocean Engineering

at the

Massachusetts Institute of Technology

May 1987

Signature of Author Tae young Chung

Department of Ocean Engineering

May 21, 1987

Certified by J Kim Vandiver

Professor J. Kim Vandiver

Thesis Supervisor

Accepted by _____

Professor A. Douglas Carmichael

Chairman, Departmental Graduate Committee

Vortex-Induced Vibration of Flexible Cylinders in Sheared Flows

by

Tae-Young Chung

Submitted to the Department of Ocean Engineering
on May 21, 1987 in partial fulfillment of the requirements
for the Degree of Doctor of Philosophy

Abstract

A series of field experiments was performed to investigate the response characteristics of flexible cylinders in sheared flows. The test matrix varied from uniform to highly sheared flow, and from very low to high tension. The observed dynamic characteristics varied from single mode lockin to the response characteristics of cables of infinite length. The role of hydrodynamic damping is investigated in some detail and is shown to be very important under sheared conditions. An important finding is that the hydrodynamic damping ratio decreases with increasing frequency.

Dimensional analysis reveals additional parameters required to characterize the response under sheared flow conditions. A response prediction method is proposed for the vortex-induced vibration of cables in sheared flows based on a Green's function approach. The predicted response shows good agreement with the measured response.

Thesis Supervisor:Dr. J. Kim Vandiver

Professor of Ocean Engineering

Acknowledgements

I would like to express my appreciation to my thesis advisor, Professor J. Kim Vandiver. The successful completion of this thesis is in great part due to his guidance and suggestions. I would like to extend my appreciation to my thesis committee, consisting of Professors Ira Dyer, Nicholas M. Patrikalakis and Dr. George Triantafyllou for their willingness to hear and critique.

I wish to thank R. J. Shyu for his help during experiments and especially Junghan Lee who prepared and carried out experiments with me from the very beginning. Thanks is also extended to Mrs. Sheila McNary for her patience in typing this manuscript.

This work was sponsored by Exxon Production Research, Shell Development Company, Conoco Inc.,Unocal, the Technology Assessment and Research Program of the Minerals Management Service, and the Naval Research Laboratory. Special thanks is given to the Lawrence Hydroelectric Associates for allowing us to use the canal and necessary facilities for conducting the experiments.

I am indebted to the Korea Science and Engineering Foundation for its financial support during my first two years in M.I.T.

I would like to thank my parents for their prayerful support and finantial support with love.

Lastly, and most importantly, I thank my wife , Insook , for her constant encouragement and patience in completion of this work. A special thanks goes to my children, Woosuk and Yousun , who made my stay at MIT enjoyable.

Contents

List of Figures

List of Tables

Chapter 1

Introduction

Many cylindrical offshore structures are in areas of strong currents and are subjected to vortex-induced vibration. Fatigue life estimates are required in the design of these structures, and good response predictions to vortex-induced vibration are essential for making this determination.

The vortex-induced vibration of long-tensioned cylinders in a uniform flow can be predicted reasonably well on the basis of existing experimental data. However, real ocean currents are not spatially and directionally uniform. In contrast to the uniform flow case, a sheared flow can excite flexible cylinders at spatially varying frequencies, thus making prediction more difficult.

Most previous attempts to predict vortex-induced vibration of flexible cylinders have been devoted to the uniform flow case. Some attempts have been made to predict response in sheared flows. However, due to the lack of publicly available response data for long flexible cylinders in sheared flows, these models remain unrefined and untested. Therefore, this study began with field experiments which were carried out to investigate the dynamic response characteristics of long, tensioned, flexible cylinders in sheared flows. Experiments were performed on a horizontal cable, 57 ft. 3 in. long, which was exposed to sheared flows ranging from 0 to about 4 ft/sec. These experiments measured sheared flow profiles, tensions, and biaxial accelerations at six locations along the cable. The experiments are described in Chapter 5.

Chapter 2 presents the necessary background information common to the field of flow induced vibration. Particular attention is given to the knowledge base relating to response in sheared flows. Chapter 3 presents a dimensional analysis discussion in which the well-known important parameters are reviewed and some new ones are introduced which are important in response prediction in sheared flows.

Chapter 4 presents a response prediction model which is capable of predicting multi-modal response in sheared conditions and is capable of modeling the spatial response variation discovered in the experimental results. A hydrodynamic damping model is included.

Chapters 6 and 7 present experimental results, for a test matrix in which the flow was varied from uniform to highly sheared. The tension was varied from very high, resulting in a few well-spaced modes, to very low, which resulted in a very high modal density which characterizes the response of cables of infinite length. An important experimental result was the observation of substantial variation in response amplitude and frequency from high to low velocity regions of the cylinder. Hydrodynamic damping is shown to be responsible.

The experimental results and the predicted results are compared in chapter 8. Sensitivity analysis for the several important input parameters in the prediction model are also carried out in chapter 8.

Finally, chapter 9 summarizes the key results of this research.

Chapter 2

Background

2.1 Flow Around a Stationary Circular Cylinder (in a Uniform Flow)

When a fluid flows about a stationary circular cylinder, vortices are shed and periodic wakes are formed as a result of flow separation.

The ultimate configuration of vortices downstream in the wake is asymmetrical (predicted from a stability analysis by Von Karman, as shown in Figure 2.1). The vortices are shed into the wake at the frequency, f_s , which is a function of flow velocity, U , cylinder diameter, D , and Reynolds number, $R_e = UD/\nu$:

$$f_s = S_t \frac{U}{D} \tag{2.1}$$

where S_t is the Strouhal number which depends on the Reynolds number, as shown in Figure 2.2.

A periodic lift force acts on the body at the vortex shedding frequency , f_s , as a result of the asymmetrical arrangement of vortices. A dimensional analysis shows that the lift force is a function of Reynolds number and of the group $\rho_w U^2 D$. The Reynolds number dependency is accounted for in a suitably determined lift coefficient, C_L , and

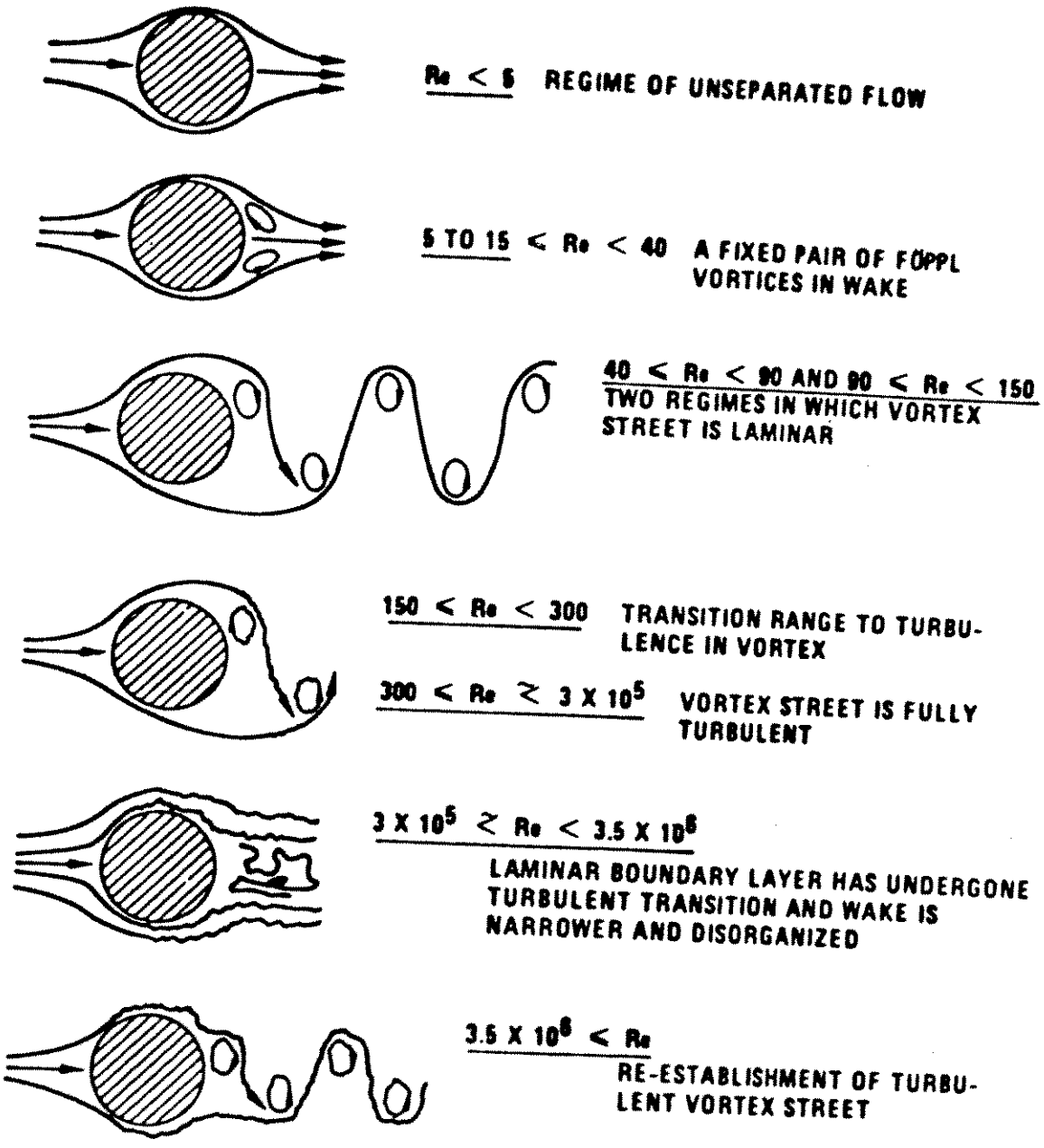

Figure 2.1: Regimes of fluid flow across circular cylinder (from Blevins 1977)

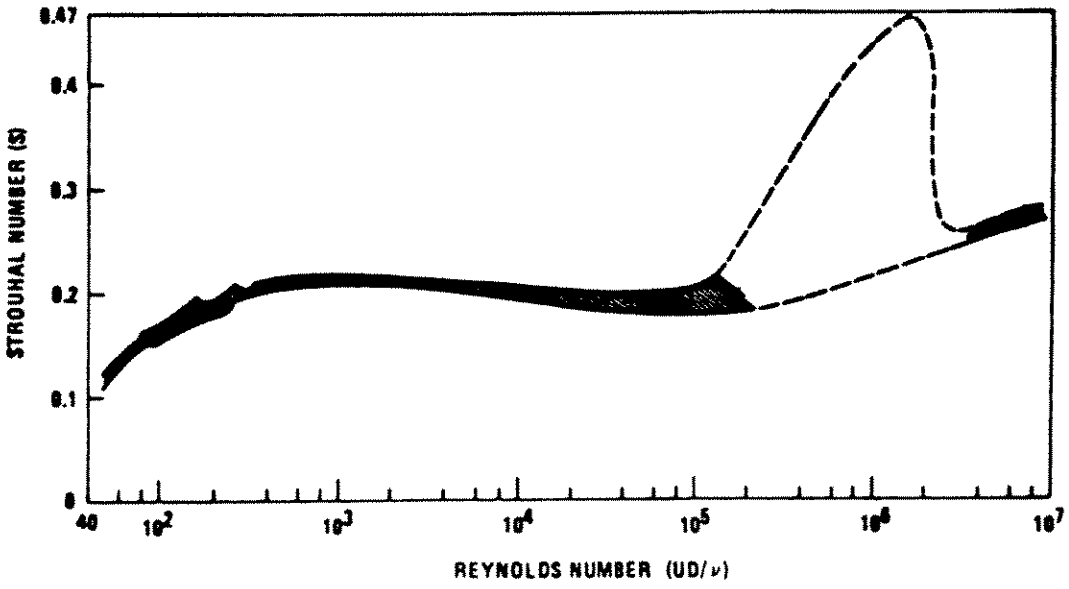

Figure 2.2: Reynolds number dependency of the Strouhal number for circular cylinders(from Blevins 1977)

the lift force per unit length along the cylinder can then be written approximately as:

$$f_L(x,t) = \frac{1}{2}\rho_w U^2 D C_L(Re) e^{i\omega_s t} \tag{2.2}$$

where

ω_s = vortex shedding frequency in rad/sec ($= 2\pi f_s$)
ρ_w = fluid density
U = flow velocity
D = cylinder diameter

The typical values of Strouhal number, S_t , and lift coefficient, C_L , for non-moving circular cylinders are 0.2 and 0.5, respectively for a Reynolds number between 3×10^2 and 2×10^5 . The above model is approximate because the lift force is periodic but not exactly sinusoidal as implied by this model. Higher harmonics of lower amplitude are present in the lift force.

2.2 Effect of Cylinder Oscillation on the Wake (in a Uniform Flow)

If the cylinder is flexible or flexibly mounted, interaction may arise between the vortex-shedding mechanism and the cylinder oscillation. This implies that the cylinder oscillations may influence the vortex shedding process, as shown schematically in Figure 2.3. As a result of this interaction the analytical or numerical prediction of vortex-induced vibration has proven to be extremely difficult. That is why most of the research of the past has emphasized experiments.

The most studied phenomenon caused by this interaction is lockin (or synchronization) of the vortex shedding frequency to the structure's vibrating frequency (usually a structural natural frequency). Many authors have given comprehensive reviews related to this lockin phenomena (Sarpkaya 1979 [16], Griffin and Ramberg 1982 [6],

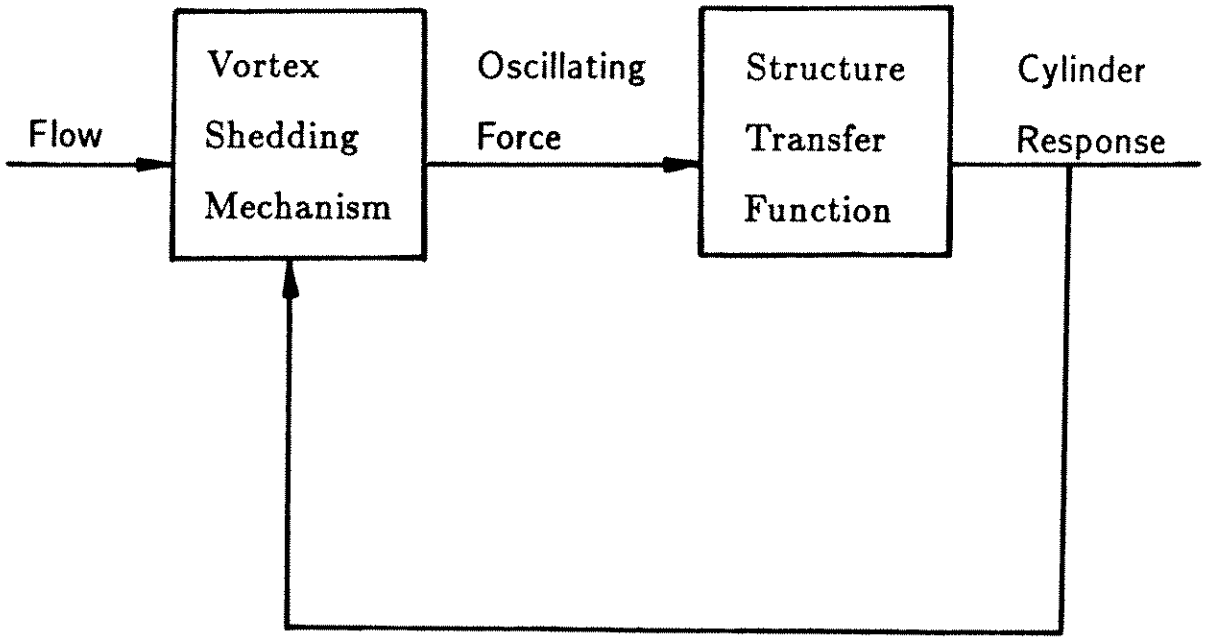

Figure 2.3: Interaction between the vortex-shedding mechanism and cylinder oscillation

King 1977[12], and Blevins 1977 [1]). At lockin, the cylinder motion takes influences the frequency of the shedding of vortices in apparent violation of the Strouhal relationship described by Equation (2.1). At lockin, the structural oscillation is synchronized to the vortex shedding frequency often resulting in increased structural response. The increase in cylinder oscillation is restricted by self-limiting decreases in vortex strength and increases in fluid damping due to large oscillation of the cylinder.

Figure 2.4 shows one example of lockin phenomena. Tsahalis measured the response of the center of a pipe span, which had a specific gravity of 2.25 (Tsahalis 1984[18]). Figure 2.4 shows his results in the case of steady current, where the reduced velocity is based on the natural frequency in still water. It might seem to the casual observer that the vibrating frequency of the cylinder in the lockin region is almost constant. However, it is significant that the vibrating frequency does not remain constant but varies in the lockin range. This is evidence that the added mass coefficient is changing with flow speed and therefore with reduced velocity.

The response of cylindrical structures in uniform flows is sometimes characterized by a broad lockin region or bandwidth. Lockin bandwidth is thought to be dependent on structural damping, hydrodynamic damping, the ratio of cylinder mass per unit length to displaced fluid mass, and on a parameter known as the reduced velocity. The reduced velocity is defined by $U/(f_n D)$, where U is the flow velocity, D is the diameter of the cylinder, and f_n is the natural frequency of the structure. Generally, the natural frequency of the structure, f_n , is calculated using an assumed constant added mass coefficient of value 1. For consistency one should define the natural frequency in one particular way and adhere to that definition. For the purpose of calculating natural frequencies and reduced velocities, an added mass coefficient to 1.0 is used in this thesis. A more detail discussion will be presented in Section 3.2.3.

The added mass coefficient is, in fact, widely varying during large amplitude oscillation with separated flow (Sarpkaya 1977[15] and reproduced in Botelho 1982[2]). In his experiment, Sarpkaya measured the forces acting on a rigid cylinder forced to vibrate transverse to a uniform flow and decomposed it into two orthogonal components

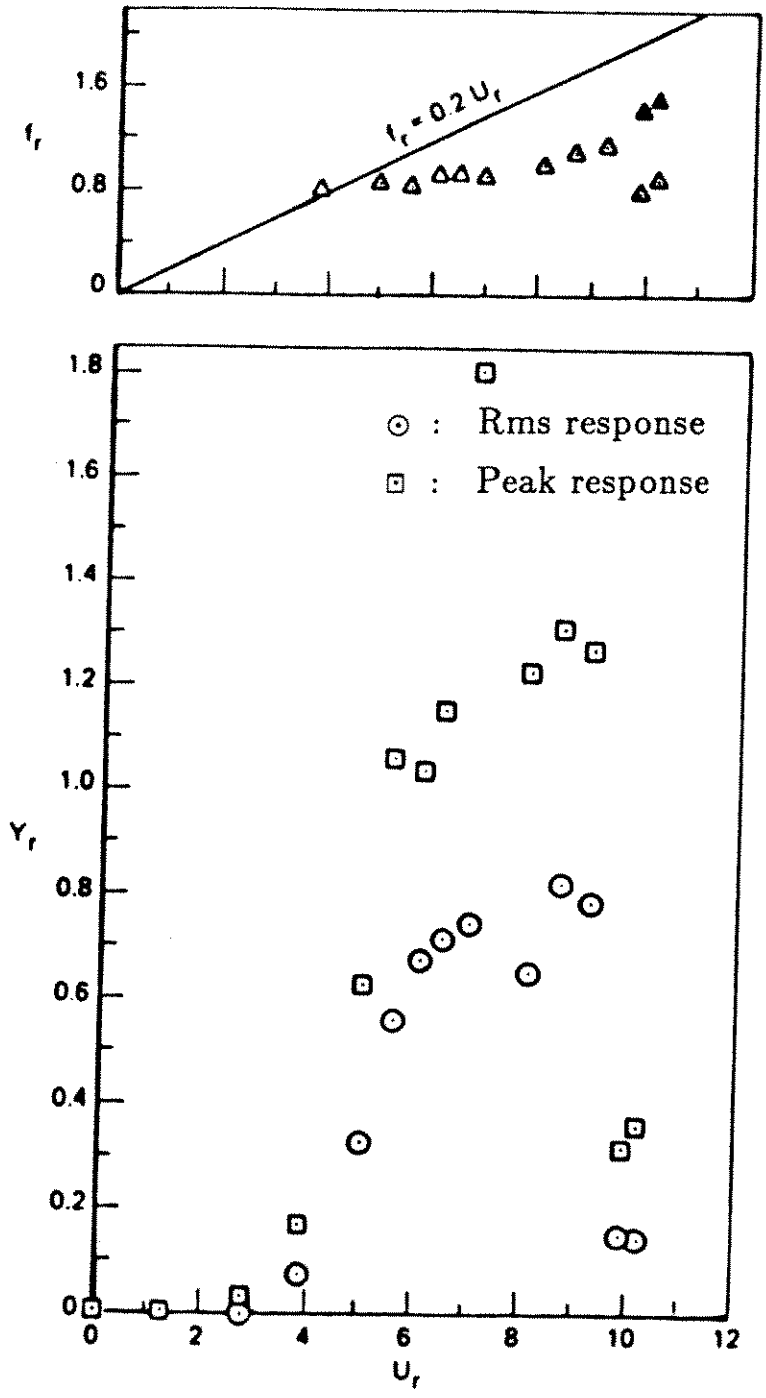

Figure 2.4: Cross-flow response at the center of a flexible pipe in uniform flows (from Tsahalis 1984)

(inertia coefficient, C_{mh} , and drag coefficient, C_{dh}) defined by:

$$f(t) = \frac{1}{2}\rho_w U^2 D(C_{mh}\sin\omega t - C_{dh}\cos\omega t) \tag{2.3}$$

Figure 2.5 shows the result of that experiment where reduced velocity was defined by $V_r = UT/D$, where T represents the period of transverse oscillation.

2.3 Shear Flow Effect on the Dynamic Response Characteristics of Flexible Cylinders

The vortex-induced vibration of long flexible cylinders in uniform flows often exhibits the lockin of one mode (Jong and Vandiver 1983[8]). However, real ocean currents are not spatially and directionally uniform. Vortex shedding from stationary cylinders in non-uniform (sheared) flow occurs in cells of different frequencies and of finite spanwise length. Figure 2.6 shows a typical example of the power spectra of vortex wakes for various spanwise positions of a stationary cylinder in a linear sheared flow (Stansby 1976[17]). Stansby carried out experiments in an open-return wind tunnel to investigate the frequencies of vortex shedding from 25.4 mm diameter circular cylinders with $L/D = 16$ in a linear sheared flow. The frequency of vortex shedding in a cell approximately follows the local Strouhal relationship:

$$f_s(x) = S_t V(x)/D \tag{2.4}$$

where S_t is the Strouhal number, $V(x)$ is the local flow velocity, and D is the diameter of the cylinder. This three-dimensional vortex shedding mechanism in a sheared flow makes the vortex-induced vibration problem more complicated and unpredictable.

A few non-dimensional parameters characterizing the sheared flow have been proposed (Griffin 1985[5,4], Kim 1984[10]). The most popular one is the steepness parameter defined by:

$$\beta = \frac{D}{V_{ref}}\frac{dV(x)}{dx} \tag{2.5}$$

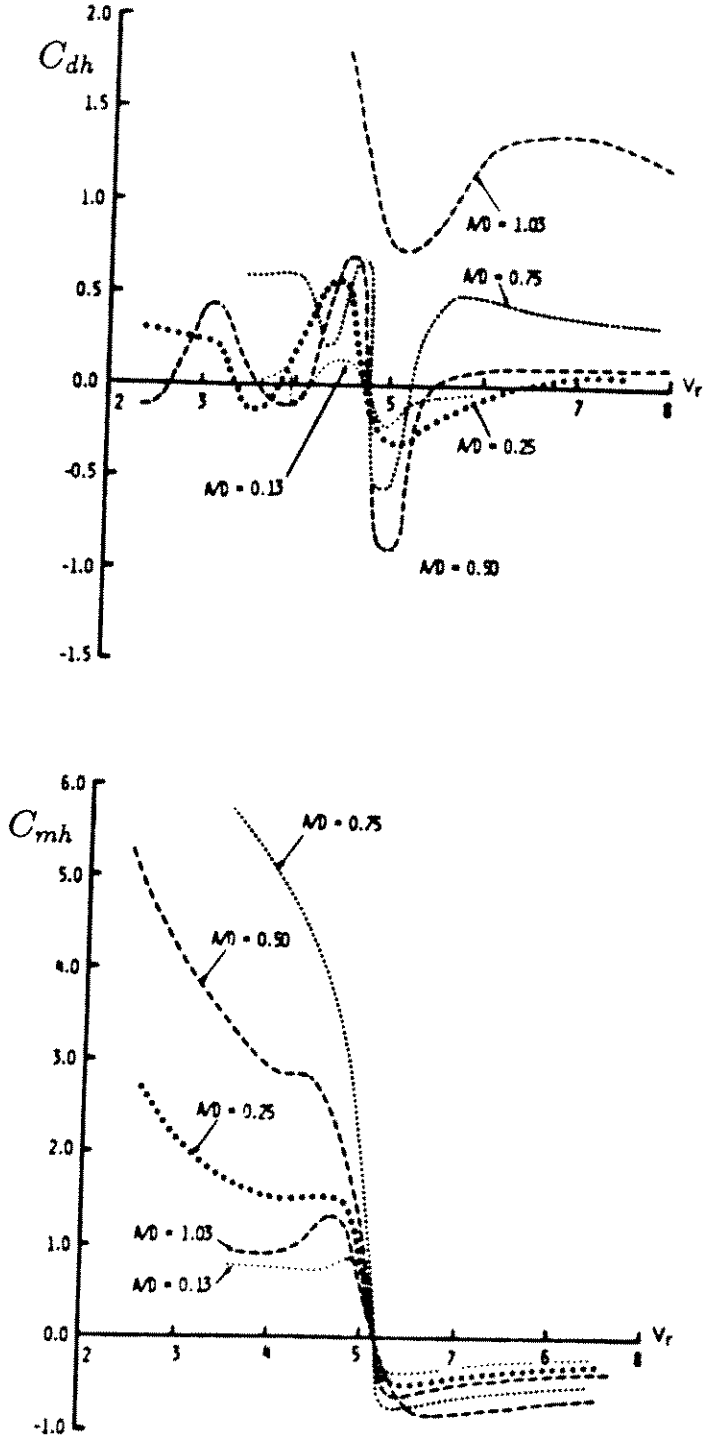

Figure 2.5: Inertia coefficient C_{mh} and drag coefficient C_{dh} versus reduced velocity for various values of normalized amplitude (from Sarpkaya 1977 and Botelho 1982)

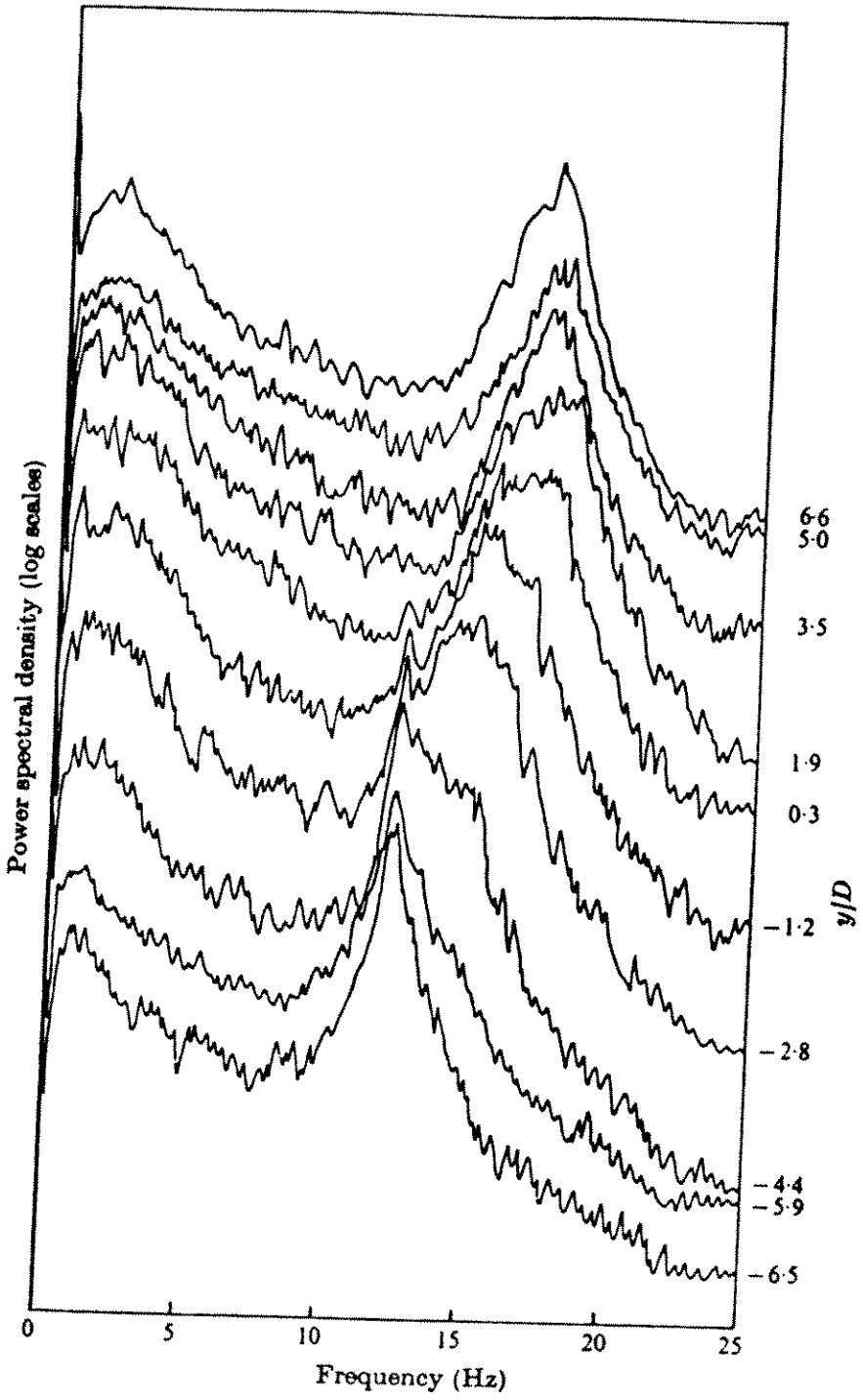

Figure 2.6: Spectra of the wake at various spanwise positions for the stationary cylinder with $L/D = 16$(from Stansby 1976)

where $\frac{dV(x)}{dx}$ is the rate of change of sheared flow velocity along the cylinder, D is the cylinder diameter, and V_{ref} is a reference velocity located at a selected point on the cylinder. In a linear sheared flow case, the steepness parameter is:

$$\beta = \frac{D}{V_{ref}} \frac{dV(x)}{dx} = \frac{D}{V_{ref}} \frac{\Delta V}{L} \tag{2.6}$$

where V_{ref} is the flow velocity at the center location of the cylinder, ΔV is the difference between the maximum and minimum flow velocities, and L is the length of the cylinder.

Another important shear-related parameter was proposed by Kim for use in estimation of the likelihood of lockin in sheared flow (Kim 1984[10]). It is simply the number of natural modes, N_s , excited by the locally varying vortex shedding frequencies occurring over the entire length of the cylinder:

$$N_s = n(f)\Delta f_s \tag{2.7}$$

where $n(f)$ is the modal density of the cylinder and Δf_s is the excitation bandwidth due to sheared flow.

The excitation bandwidth, Δf_s , is defined by:

$$\Delta f_s = S_t \frac{\Delta V}{D} \tag{2.8}$$

where ΔV is the difference between the maximum and minimum velocities encountered on the cylinder.

These additional parameters are not adequate to estimate the behavior of flexible cylinders in sheared flows. As will be shown, mode shape and hydrodynamic damping also play important roles.

Chapter 3

Discussion of Important Dimensionless Groups in a Sheared Flow

3.1 General Description

Dimensional analysis is generally useful in understanding complicated physical mechanisms. It has been commonly used to find the appropriate scaling laws for model tests, which are used to predict full-scale performance. In this chapter, non-dimensional parameters which govern the dynamic response characteristics of a tensioned cable in a sheared flow are discussed.

A great deal is already known about vortex-induced vibration and therefore a completely blind dimensional analysis is not appropriate here. Experimental information already available will be used to direct this discussion to the most significant points. This analysis builds on the understanding of response in uniform flows.

3.2 Dimensional Analysis of a Tensioned Cable in a Uniform Flow

The parameters known to be important in determining the dynamic behavior of a constant tension uniform cable in a uniform flow are:

- Response Parameters

  (1) amplitude of vibration(y)

  (2) frequency of vibration (f_v)

- Structural Parameters

  (1) length of the cylinder (L)

  (2) diameter of the cylinder (D)

  (3) structural mass per unit length (m_s)

  (4) tension (T)

  (5) structural damping ratio (ζ_s)

- Flow Parameters

  (1) density of water (ρ_w)

  (2) viscosity (μ)

  (3) flow velocity (U)

Ten independent parameters have been identified. According to the Pi theorem these may be arranged into 7 independent dimensionless groups. One convenient set is identified below.

y/D = dimensionless amplitude

L/D = aspect ratio

$UD\rho_w/\mu$ =Reynolds number=UD/ν, where $\nu = \mu/\rho_w$ = kinematic viscosity

$\rho_w D^2/m_s$ = mass ratio

$U/f_v D$ = reduced velocity

ς =damping ratio=$\varsigma_s + \varsigma_h$

where ς_h represents hydrodynamic damping ratio

$f_v/\frac{1}{2L}\sqrt{\frac{T}{m}}$ = ratio of vibration frequency to the first natural frequency

$=f_v/f_1$

Damping ratio, ς , requires brief further discussion. For flow induced vibration the damping has two components, internal material or structural damping and external hydrodynamic damping. Hydrodynamic damping depends upon the correlation between lift forces and cylinder motion. It is very small under uniform flow lockin conditions, but is very important for sheared flows.

The dimensional analysis discussion will proceed for the present, in terms of response in a uniform flow exhibiting principally individual modal response. One of the 7 dimensionless groups can be made to depend upon the other six.

$$F(\frac{y}{D}, \frac{L}{D}, \frac{UD}{\nu}, \frac{\rho_w D^2}{m_s}, \frac{U}{f_v D}, \varsigma, \frac{f_v}{f_1}) = 0 \tag{3.1}$$

The significance of each of the groups as they are presently understood is presented next. Most of these parameters can be extended directly to the sheared flow case and when appropriate such extensions are pointed out. Many of them become functions of local position on the cable.

3.2.1 The Length to Diameter Ratio (L/D)

The length to diameter ratio, L/D , is closely related to the hydrodynamic effects of end boundaries. Small values of L/D imply more influence from the ends. However, typical values of the length-to-diameter ratio of marine cables and risers in deep water are in excess of 250. For such values of length-to-diameter ratio the effect of boundary conditions are negligible, and the parameter L/D is of no special significance in characterizing the response of long cables in the ocean.

3.2.2 Reynolds Number ($R_e = \frac{UD}{\nu}$)

The vortex formation process near a cylindrical structure is influenced by the Reynolds number. However, the Strouhal number remains almost constant, for large ranges in Reynolds number (refer Figure 2.2). Therefore, variation in Reynolds numbers may only be important in certain transition regions. The Reynolds number will vary with position in a sheared flow.

3.2.3 Mass Ratio ($\eta = \frac{\rho_w D^2}{m_s}$)

The relationship between mass ratio, η , and specific gravity, $s.g.$, is

$$s.g. = \frac{m_s}{\frac{\pi}{4}\rho_w D^2} = \frac{4}{\pi\eta} \tag{3.2}$$

The bandwidth of the large amplitude response lockin range depends upon the mass ratio as is illustrated in Figure 3.1. Rms displacement of cross-flow vibration for four different mass ratios are plotted. As the ratio of fluid density to structural density increases, so does the bandwidth measured in reduced velocity terms. Figure 3.2 is a plot of the lockin region of a vibrating cylinder in water as a function of reduced velocity and specific gravity. In this example the threshold of lockin has been defined as 0.2 diameters rms response. The response amplitude at lockin depends on damping. A commonly used parameter, the reduced damping or response parameter as it is known, combines mass ratio and damping. Past practice has been to use only these combined parameters to predict response. The mass ratio must be used separately to correctly predict the lockin bandwidth.

3.2.4 Reduced Velocity ($V_r = \frac{U}{f_v D}$)

Reduced velocity is a key parameter in evaluating the likelihood of lockin. As can be seen in Figure 3.1, the maximum cross-flow amplitudes occur in the range of $5 \leq V_r \leq 9$ depending on mass ratio. Within this range the vortex shedding frequency may be the same as one of the natural frequencies of the structure. Strictly speaking,

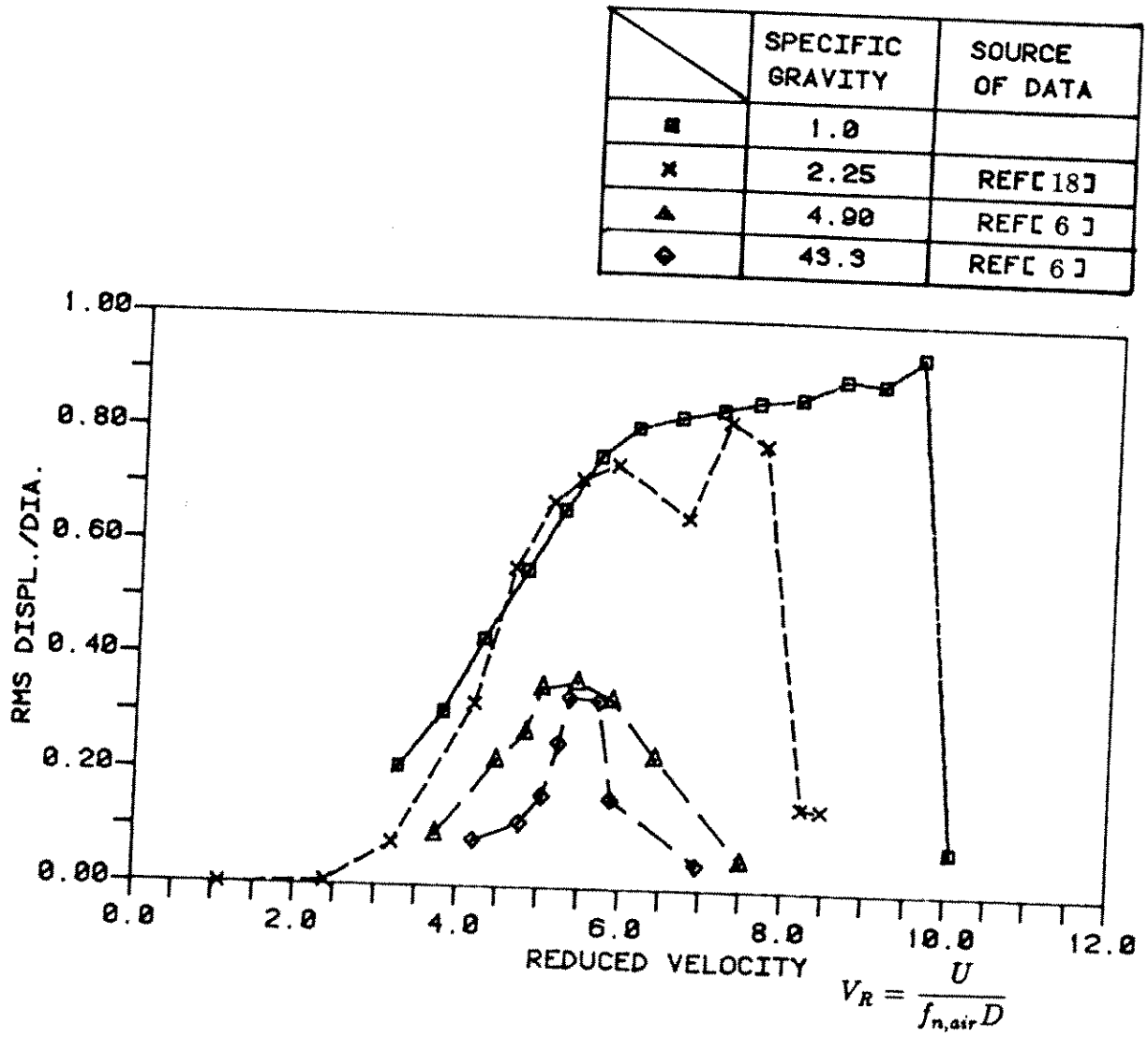

Figure 3.1: Cross-flow vibration responses for several cylinders having different specific gravities

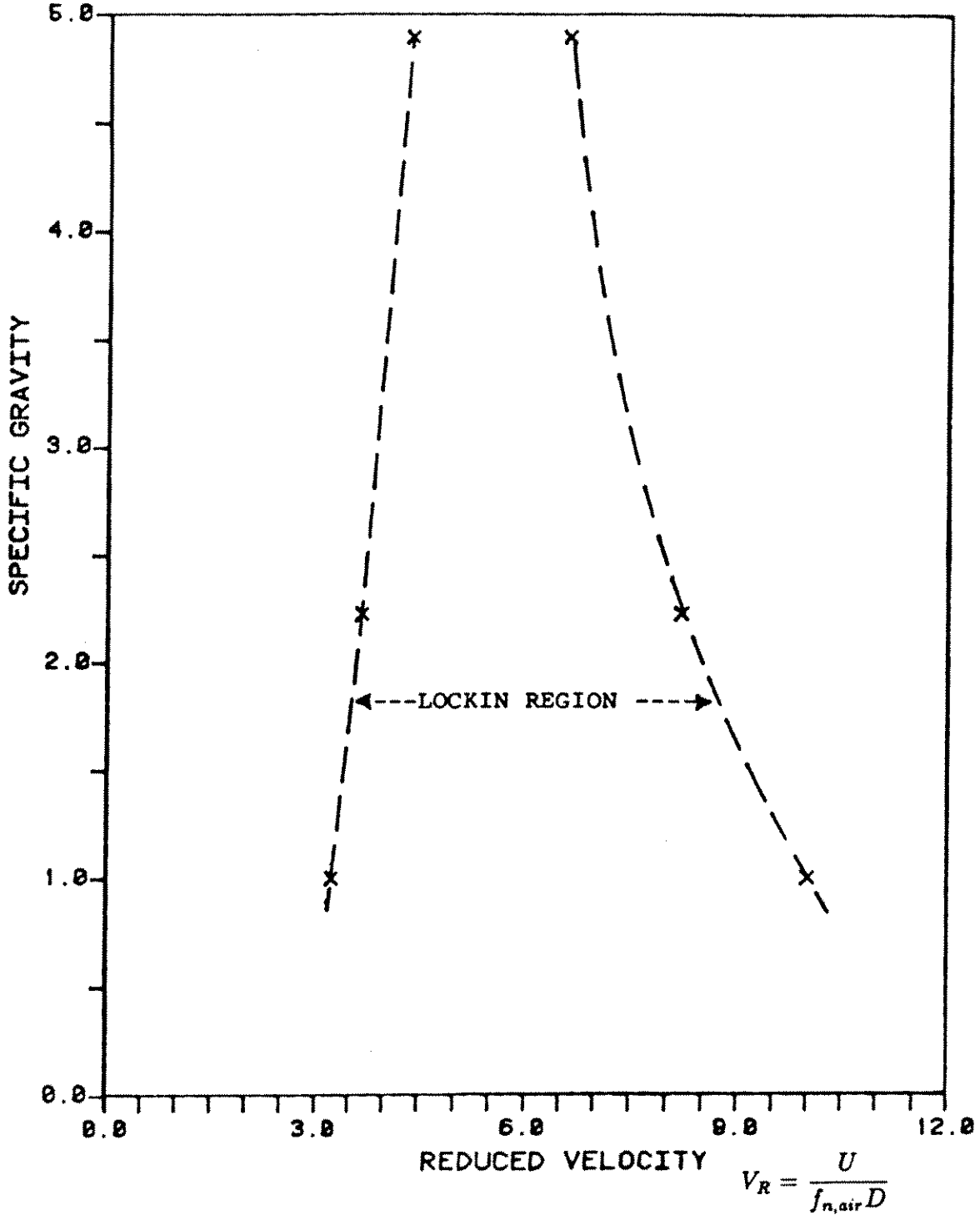

Figure 3.2: Lockin region depedence on specific gravities

the Strouhal number is defined only for rigid non-moving cylinders.

$$S_t = f_s \frac{D}{U} \tag{3.3}$$

However, it is useful to have a simple device for estimating the vortex shedding frequency for a long flexible cable. Perhaps the most likely response frequency corresponds to a reduced velocity of about 5.5. In equivalent Strouhal number terms this is $S_t \simeq 0.17$. Henceforth the concept of a Strouhal number will be applied to estimate a vortex shedding frequency.

3.2.5 Damping Ratio (ς)

An infinite cable of total mass per unit length m , including added mass, and a damping constant, r , per unit length per unit transverse velocity will have a damping ratio given by

$$\varsigma = \frac{r}{4\pi f_v m} \tag{3.4}$$

such that waves traveling down the cable at a frequency f_v will be attenuated exponentially according to

$$e^{-\frac{2\pi}{\lambda}\Delta x \varsigma} \tag{3.5}$$

when Δx is the distance traveled and λ is the wave length at f_v. If the frequency is different from the local vortex shedding frequency then, r , the damping constant, must include substantial local hydrodynamic losses, as well as internal material losses.

If the cable is short, so that it is appropriate to define a modal damping ratio, then

$$\varsigma_n = \frac{r}{4\pi f_n m} \tag{3.6}$$

Where, it has been assumed that r and m are constant over the length of the cable. When they are not, then the individual modal damping and modal mass must be computed first, leading to

$$\varsigma_n = \frac{R_n}{4\pi f_n M_n} \tag{3.7}$$

where

R_n =modal damping constant

M_n =modal mass

Once the damping ratio has been established it is necessary to consider the subject of half power bandwidth and modal overlap, as they will affect vortex-induced vibration response.

3.2.6 Ratio of Vibration Frequency to the First Natural Frequency (f_v/f_1)

Ratio of vibration frequency to the first natural frequency, f_v/f_1 , reveals the approximate mode number of the excited mode. For constant tension uniform cables the higher natural frequencies are simply integer multiples of the lowest, f_1. Since the vortex shedding frequency, f_s, and the cross-flow vibration response frequency, f_v, are essentially the same in a uniform flow, this ratio tells one which mode is most likely to be excited.

Vibration to vortex shedding frequency ratio, f_v/f_s, is 1.0 under uniform flow lockin conditions, but may depart substantially from 1.0 under sheared flow conditions. For example if one mode is being principally excited on a portion of the cable where the $f_v/f_s = 1.0$ then the whole cable will respond at that frequency. Outside of the excitation region the dominant vibration will not coincide with the local vortex shedding frequency and the major hydrodynamic effect will be to damp the motion. Thus this ratio is a good indicator of power flow in versus power flow out regions of the cable.

3.2.7 Reduced Damping, also known as the Response Parameter

A very common additional parameter used to determine lockin response behavior is the response parameter (or reduced damping) which is found by combining the mass

ratio and the damping ratio. The maximum response amplitude has been determined to be a function of this combination (see Figure 3.3, also refer to Griffin 1982[6]). The reduced damping is defined by

$$k_s = \frac{2m_s\delta_s}{\rho_w D^2} = \frac{4\pi m_s \zeta_s}{\rho_w D^2} \tag{3.8}$$

where

k_s = reduced damping

δ_s = logarithmic decay ratio

$\frac{\rho_w D^2}{m_s}$ = mass ratio of a cable

ζ_s = structural damping ratio

However, the author believes that the mass ratio and the damping ratio should not be combined together. These two non-dimensional parameters are valuable independently (as discussed in 3.2.3 and 3.2.5, respectively) and in reference Vandiver 1985[19].

3.3 Important Additional Dimensionless Groups for Cable Response in a Sheared Flow

All of the parameters discussed to this point are important in the sheared flow case. Some must be interpreted locally on the cable as a function of local values of flow velocity or vortex shedding frequency. One additional set of parameters is needed to characterize the shear flow itself. For a complicated shear, a number of parameters are necessary. For a linearly varying shear the flow profile can be specified by two parameters, usually by a reference velocity and a rate of change of velocity, or the maximum and minimum values of velocity in the shear.

A popular combination is known as the steepness parameter defined in equation (2.5).

$$\beta = \frac{D}{V_{ref}}\frac{dV(x)}{dx} = \frac{D}{V_{ref}}\frac{\Delta V}{L} \tag{3.9}$$

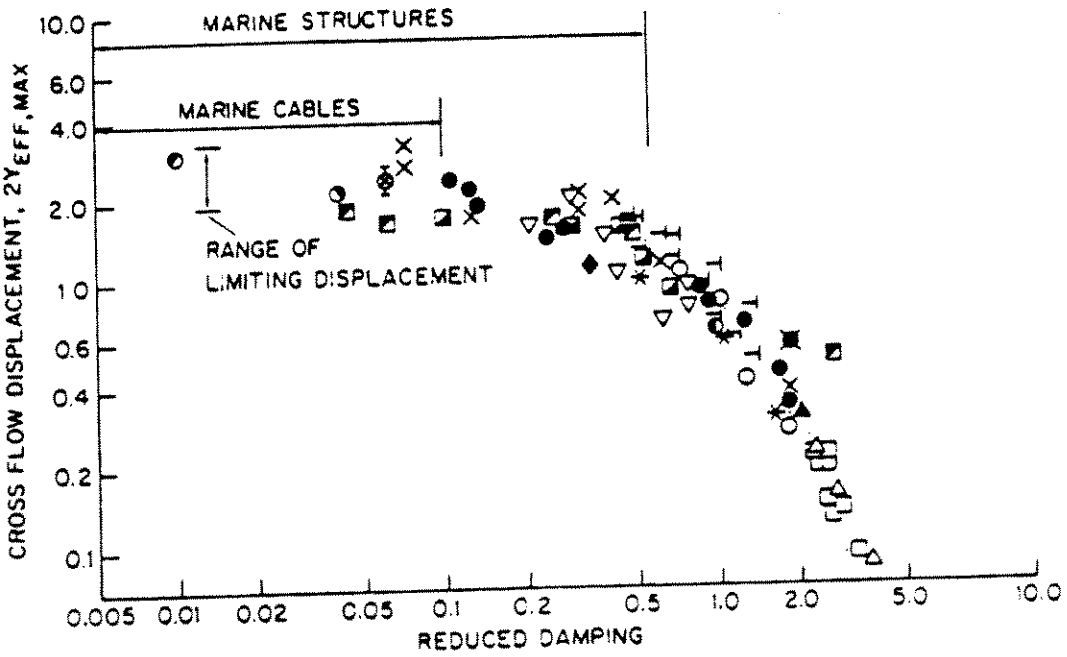

Figure 3.3: Cross-flow displacement dependence on reduced damping

where ΔV is the total change in velocity over the length and V_{ref} is the velocity at some reference point. V_{ref} in this paper is taken to be V_{max}. For the purposes of this paper, the two parameters used to describe a linear shear are V_{max} and ΔV. These can be expressed in dimensionless groups by

$$\frac{f_{s,max}}{f_1} \qquad \text{and} \qquad \frac{\Delta f_s}{f_1} = N_s \tag{3.10}$$

where

$$f_{s,max} = S_t \frac{V_{max}}{D} \tag{3.11}$$

and

$$\Delta f_s = S_t \frac{\Delta V}{D} \tag{3.12}$$

In equation (3.10), $f_{s,max}/f_1$ represents the highest excited mode in the shear, and $\Delta f_s/f_1$ represents the total number of modes excited by the sheared flow.

The non-dimensional amplitude of a tensioned cable in a linearly varying sheared flow can be a function of several non-dimensional parameters. Among the most important are:

$$F(\frac{y}{D}, \frac{\rho_w D^2}{m_s}, \varsigma, \frac{f_{s,max}}{f_1}, \frac{\Delta f_s}{f_1}) = 0 \tag{3.13}$$

3.4 The Ratio of Half Power Bandwidth to Modal Spacing

It is interesting to compare the modal spacing and the half-power bandwidth of a cable. In the case of a constant tension uniform cable, the natural frequency of the nth mode is given by:

$$\omega_n = \frac{n\pi}{L}\sqrt{\frac{T}{m_s + \frac{\pi}{4}C_a\rho_w D^2}} = n\omega_1 \tag{3.14}$$

where

n = the mode number

L = length of a cable

T = tension of a cable

m_s = structural mass per unit length

C_a = added mass coefficient

ρ_w = density of water

D = diameter of a cable

ω_1 = first natural frequency

Therefore, the modal frequency spacing between two adjacent modes of a simple cable is equal to the first natural frequency, ω_1.

$$\omega_1 = \frac{\pi}{L}\sqrt{\frac{T}{m_s + \frac{\pi}{4}C_a\rho_w D^2}} \tag{3.15}$$

The last dimensionless group identified in Section 3.2 was the ratio f_v/f_1 , where f_v is assumed equal to the vortex shedding frequency, f_s. For a uniform constant tension cable this ratio is approximately the number, n, of the mode excited by the flow.

$$n = \frac{f_v}{f_1} \qquad \text{because} \qquad f_v = f_n = nf_1 \tag{3.16}$$

The half-power bandwidth of the nth mode of a structure is given by:

$$\Delta_{\frac{1}{2}} = 2\zeta_n\omega_n \tag{3.17}$$

which for a simple cable is simply

$$\Delta_{\frac{1}{2}} = 2n\zeta_n\omega_1 \tag{3.18}$$

For a simple constant tension uniform cable, the modal spacing is ω_1 and the ratio of the half power bandwidth to the modal spacing, here defined as N , is given by

$$N = 2n\zeta_n \tag{3.19}$$

N is a measure of the overlap between modes and will prove to be very important in understanding sheared flow response. A simple interpretation is that it is the number of modes contained within the half power bandwidth of any particular mode

of interest. When N is small, single mode lockin may occur. When N is large, infinite cable behavior is seen. This topic will be discussed at length later.

It is useful to have an expression for the mode number n for a simple cable in a uniform flow with velocity U , and a vortex shedding frequency, f_s , approximated by the Strouhal frequency.

$$\frac{f_s}{f_1} = n = \frac{2L}{C_p} S_t \frac{U}{D} \tag{3.20}$$

where

n = mode number excited by the flow

L = length of a cable

C_p = phase velocity of a cable

S_t = Strouhal number

U = flow velocity

D = diameter of a cable

This expression may be used to estimate a local value of N for very long cables with slowly varying properties.

$$N(x) = 2\varsigma \frac{2L}{C_p} S_t \frac{V(x)}{D} \tag{3.21}$$

where x is a position coordinate in the cable and $V(x)$ is the local flow velocity.

Noting the relationship between frequency and wave number, $k = 2\pi f_s / C_p$, yields

$$\frac{\pi}{2} N(x) = \varsigma k(x) L \tag{3.22}$$

Therefore, another interpretation of $N(x)$ is that over a propagation distance, L , a wave of frequency, f_s , will be attenuated by the factor $e^{-\frac{\pi}{2}N(x)} = e^{-\varsigma k(x) L}$. Therefore for values of $N(x)$ greater than about 2, waves will largely die out while propagating over the length of the cable and infinite cable behavior will be observed.

Chapter 4

The Response Prediction Model in a Sheared Flow

4.1 General Description

The vortex-induced vibrations of long-tensioned cylinders in uniform flow can be predicted reasonably well on the basis of experimental data (Sarpkaya 1979[16], Blevins 1977[1], Griffin 1982[6]). A few attempts have been made to predict the response in a sheared flow (Wang 1986[21], Patrikalakis and Chryssostomidis 1986[13]). These response prediction methods for sheared flows were based on the superposition of normal modes. The amplitude of each mode was determined using information gotten from experimental results in uniform flows. Under the assumption of small damping, the total response amplitude was obtained by a sum-of-squares superposition of resonant modes only[21]:

$$\frac{A(x)}{D} = \{\sum (\frac{A_n}{D} \frac{\Psi(x)}{\Psi_{n,max}})^2\}^{1/2} \tag{4.1}$$

However, this approach cannot model the spatial attenuation observed in the response for the highly sheared flow case shown later in this thesis (refer to Figure 7.10). When there is significant damping, non-resonant modal response becomes an important portion of the total response and must be included in response prediction calculations.

In reference[13] the nonlinear coupling with non-resonant modes was accounted for.

In mode superposition models, the non-resonant modes are required to correctly obtain the spatial attenuation. Many modes may be required to obtain the correct solution. If the Green's function is available, it gives more accurate results with less computational effort because it is equivalent to a superposition of an infinity of modes.

The prediction of the response of a flexible cylinder to vortex shedding may be thought of as consisting of four major components: an excitation model, a structural model, a damping model, and a solution technique. In this chapter, a response prediction method is proposed for the vortex-induced vibration of a long-tensioned cylinder in sheared flow, based on the Green's function approach. Detailed descriptions of the response prediction model including hydrodynamic damping and lift force models are given in the following sections.

4.2 A Proposed Linear Random Vibration Model of Exciting Force and Structural Response

In a sheared flow, the vortex shedding process excites the cable through a complex interaction, in which the motion affects the exciting forces in a poorly understood feedback mechanism. However, for steady state solutions a simple non-feedback model of the exciting forces can be successfully used to approximate the correct response.

In uniform flow especially at lockin, the response is periodic in nature with sharp spectral peaks. However, the typical measured response spectrum in a highly sheared flow is characterized by a broad band random process.

Cylinder motions in the flow are a non-linearly correlated combination of cross-flow and in-line components. The correlation is due to a common source of excitation (the vortices) and not due to mechanical coupling in the structure. The cross-flow response is typically much greater than the in- line response (Jong 1984[7], Vandiver and Jong[20]). The approach taken in this research is to compute the cross-flow response first, ignoring any influence of the in-line motion. If in-line motion is desired,

then relationships discovered by Jong and Vandiver[20] may be used to predict it, after the cross-flow results are obtained.

Based on the preceding assumptions and arguments, a linear random vibration model is used to predict the cross-flow vibration response of a tensioned long cylinder to vortex shedding in a sheared flow.

In a linear one-dimensional continuous system, the displacement response spectrum at a location may be specified by the following integral equation:

$$S_{yy}(x,\omega) = \int_0^L d\xi \int_0^L d\xi' S_{f_\xi f_{\xi'}}(\xi,\xi',\omega) G(x/\xi) G^*(x/\xi') \tag{4.2}$$

where

$S_{yy}(x,\omega)$ = the displacement response spectrum at location x

$S_{f_\xi f_{\xi'}}(\xi,\xi',\omega)$ = the lift force spectrum

$G(x/\xi)$ = the Green's function due to excitation at the location $x = \xi$

$G^*(x/\xi')$ = conjugate of the Green's function due to excitation at the location $x = \xi'$

The mean square value of the response displacement at a location is obtained by integrating the displacement spectrum in the frequency domain.

$$E[y^2(x,t)]_{at\ x} = \int_0^\infty S_{yy}(x,\omega) d\omega \tag{4.3}$$

The Green's function of the system includes the structural modelling information as well as the hydrodynamic damping description. The lift force spectrum model, to be discussed in Section 4.4, includes all aspects of the hydrodynamic exciting forces. The solution technique used in this thesis is a straightforward discrete numerical integration of equations (4.2) and (4.3).

4.3 Green's Function of a Finite Cable

The forced vibration of a finite cable with constant tension and uniformly distributed mass in a sheared flow can be described by an equation of motion.

$$m\frac{\partial^2 y(x,t)}{\partial t^2} + R\frac{\partial y(x,t)}{\partial t} - T\frac{\partial y^2(x,t)}{\partial x^2} = f(x,t) \tag{4.4}$$

where

$y(x,t)$ = cross-flow response displacement
m = structural mass per unit length including added mass
$R\frac{\partial y(x,t)}{\partial t}$ = damping force including hydrodynamic damping force
T = tension
$f(x,t)$ = lift force per unit length due to vortex-shedding

The fixed end boundary conditions are given by:

$$\begin{cases} y(0,t) = 0 \\ y(L,t) = 0 \end{cases} \tag{4.5}$$

where L is the length of cable.

In equation (4.4), $f(x,t)$ is varying in space and time. In order to get a solution for such conditions, the solutions to particular loadings in space and in time must be derived first. The response of the system to a unit harmonic force acting at a single point is called the Green's function. The extension to general loading in space is possible using the superposition principle.

The Green's function, $G(x/\xi)$, for the cable without damping is given by[3]:

$$G(x/\xi) = \begin{cases} \frac{1}{T}\frac{\sin kx \sin k(L-\xi)}{k \sin kL} & (0 \le x < \xi) \\ \\ \frac{1}{T}\frac{\sin k\xi \sin k(L-x)}{k \sin kL} & (\xi < x \le L) \end{cases} \tag{4.6}$$

where

x = response measurement point

ξ = excitation point

T = tension along the cable

k = wave number$(= \omega/C_p)$

ω = excitation frequency

C_p = phase velocity of the cable$(= \sqrt{\frac{T}{m}})$

The response of the cable $y(x,t)$ to a unit harmonic force acting at ξ is thus:

$$y(x,t) = G(x/\xi)e^{-i\omega t} \tag{4.7}$$

The Green's function, $G(x/\xi)$, for the cable with damping is obtained by replacing the wave number, k , in equation (4.6) by the complex wave number, $k + ik\varsigma$, where ς represents the damping ratio of the cable. The relationship between ς and R in equation (4.4) is given by:

$$\varsigma = \frac{R}{2\omega m} \tag{4.8}$$

The Green's function, $G(x/\xi)$, for the cable with damping is given by:

$$G(x/\xi) = \begin{cases} \frac{1}{T}\frac{\sin(k+ik\varsigma)x\,\sin(k+ik\varsigma)(L-\xi)}{(k+ik\varsigma)\sin(k+ik\varsigma)L} & (0 \le x < \xi) \\ \\ \frac{1}{T}\frac{\sin(k+ik\varsigma)\xi\,\sin(k+ik\varsigma)(L-x)}{(k+ik\varsigma)\sin(k+ik\varsigma)L} & (\xi < x \le L) \end{cases} \tag{4.9}$$

The general forms $\sin(x+iy)$ in equation (4.9) can be expressed in terms of their real and imaginary parts:

$$\sin(x+iy) = \sin x \cosh y + i \cos x \sinh y \tag{4.10}$$

Applying equation (4.10) to equation (4.9), we can get the Green's function:

$$G(x/\xi) = \begin{cases} \frac{1}{T}(\sin kx \cosh k\varsigma x + i \cos kx \sinh k\varsigma x) \\ \times\{\sin k(L-\xi)\cosh k\varsigma(L-\xi) + i\cos k(L-\xi)\sinh k\varsigma(L-\xi)\} \\ \div\{(k+ik\varsigma)(\sin kL\cosh k\varsigma L + i\cos kL\sinh k\varsigma L)\} \\ \qquad\qquad \text{for} \qquad (0 \le x < \xi) \\ \\ \frac{1}{T}(\sin k\xi \cosh k\varsigma \xi + i \cos k\xi \sinh k\varsigma \xi) \\ \times\{\sin k(L-x)\cosh k\varsigma(L-x) + i\cos k(L-x)\sinh k\varsigma(L-x)\} \\ \div\{(k+ik\varsigma)(\sin kL\cosh k\varsigma L + i\cos kL\sinh k\varsigma L)\} \\ \qquad\qquad \text{for} \qquad (\xi < x \le L) \end{cases} \tag{4.11}$$

At resonance of the nth mode, kL in equation (4.11) is given by:

$$kL = n\pi \tag{4.12}$$

and Green's function in equation (4.11) becomes

$$G(x/\xi) = \begin{cases} \frac{1}{T}(\sin \frac{n\pi x}{L} \cosh \frac{n\pi\varsigma x}{L} + i \cos \frac{n\pi x}{L} \sinh \frac{n\pi\varsigma x}{L}) \\ \times\{\sin \frac{n\pi(L-\xi)}{L}\cosh \frac{n\pi\varsigma(L-\xi)}{L} + i\cos \frac{n\pi(L-\xi)}{L}\sinh \frac{n\pi\varsigma(L-\xi)}{L}\} \\ \div\{\pm i\frac{n\pi}{L}(1+i\varsigma)\sinh n\pi\varsigma\} \\ \qquad\qquad \text{for} \qquad (0 \le x < \xi) \\ \\ \frac{1}{T}(\sin \frac{n\pi\xi}{L} \cosh \frac{n\pi\varsigma\xi}{L} + i \cos \frac{n\pi\xi}{L} \sinh \frac{n\pi\varsigma\xi}{L}) \\ \times\{\sin \frac{n\pi(L-x)}{L}\cosh \frac{n\pi\varsigma(L-x)}{L}) + i\cos \frac{n\pi(L-x)}{L}\sinh \frac{n\pi\varsigma(L-x)}{L}\} \\ \div\{\pm i\frac{n\pi}{L}(1+i\varsigma)\sinh n\pi\varsigma\} \\ \qquad\qquad \text{for} \qquad (\xi < x \le L) \end{cases} \tag{4.13}$$

It is interesting to investigate the behavior of the Green's function given in equation (4.13) for two extreme cases. One of the extreme cases is the case when the resonant mode, n , and the damping ratio,ς , have small values so that the value of $n\varsigma$ satisfies the condition:

$$n\varsigma < 0.2 \qquad \text{or} \qquad n\pi\varsigma = \varsigma kL < 0.6 \tag{4.14}$$

Then, the first order approximation of the Green's function in equation (4.13) is given by:

$$G(x/\xi) = \frac{1}{T} \frac{\sin\frac{n\pi x}{L} \sin\frac{n\pi(L-\xi)}{L}}{\frac{n^2\pi^2}{L}\varsigma} \tag{4.15}$$

where

T = tension

n = mode number of the nth mode

ς = damping ratio $(R/2\omega m)$

Using the relationship

$$\omega_n^2 = \frac{n^2\pi^2}{L^2}\frac{T}{m} \tag{4.16}$$

we can get another form of the Green's function given in equation (4.15):

$$\begin{aligned} G(x/\xi) &= \frac{\sin\frac{n\pi x}{L} \sin\frac{n\pi(L-\xi)}{L}}{\omega_n^2 M\varsigma} \\ &= \frac{\sin\frac{n\pi x}{L} \sin\frac{n\pi(L-\xi)}{L}}{2\varsigma K_n} \end{aligned} \tag{4.17}$$

where

M = total mass of a cable including added mass $(= mL)$

K_n = modal stiffness of the nth mode

The Green's function in equation (4.17) shows exactly the same result with the frequency response function of the nth mode resonance obtained from the normal mode method, using the response of one mode only. This case can be interpreted in terms

of wave attenuation also. For values of $\varsigma kL < 0.6$, a wave travelling a distance L is not severely attenuated.

Another extreme is the case when the resonant mode number, n , has a larger value, the excitation point, ξ , and the response measurement point, x , are far from the end boundaries of the cable, and the damping ratio, ς, is less than 1. When these conditions are satisfied and the following condition is true

$$n\varsigma \gg 1 \qquad \text{or} \qquad n\pi\varsigma = \varsigma kL \gg \pi \tag{4.18}$$

then the Green's function in equation (4.13) is given by:

$$G(x/\xi) = \begin{cases} \dfrac{ie^{ik(\xi-x)}e^{-k\varsigma(\xi-x)}}{2Tk} & (0 \le x < \xi) \\ \\ \dfrac{ie^{ik(x-\xi)}e^{-k\varsigma(x-\xi)}}{2Tk} & (\xi < x \le L) \end{cases} \tag{4.19}$$

The Green's function in equation (4.19) shows exactly the same result with the Green's function of an infinite cable, in which waves are damped out travelling from one end to the other.

Figure 4.1(A) shows an harmonic exciting force at the midpoint of a string at the natural frequency of the fifth mode. Figure 4.1(B) is a plot of the magnitude squared of the Green's function to that input when the modal damping ratio of the fifth mode is 1%. The Green's function is an exact solution, equivalent to summing an infinite number of normal modes. However, in this case, a calculation of the response of the fifth mode contribution only would have appeared essentially the same. This response is typical of a "short" lightly damped cable. For this case $n\varsigma = 0.05(\varsigma kL = 0.05\pi)$.

Figure 4.1(C) is the response of the same string, excited by a unit force at the natural frequency of the 99th mode, with a modal damping of 10% ($n\varsigma = 9.9$ and $\varsigma kL = 9.9\pi$). This response is characteristic of an infinite cable response. Excitation at the mid-point is never felt at the ends. To get the right answer by mode superposition would have required well in excess of 100 modal contributions.

Figure 4.1(D) is for excitation at the ninth mode natural frequency with a damping of 10% ($n\varsigma = 0.9$ and $\varsigma kL = 0.9\pi$). Some vibration energy reaches the ends, but it is

substantially damped. This string exhibits intermediate behavior.

The critical parameter to determine whether the cable acts like infinite cable or not is the product $n\varsigma$ where n is the mode number of the highest resonantly excited mode in the system. Three cases have been described here. In terms of this parameter they are

n	ς	$n\varsigma$	$n\pi\varsigma = \varsigma kL$
5	0.01	0.05	0.05π
9	0.10	0.9	0.9π
99	0.10	9.9	9.9π

When $n\varsigma$ is less than 0.2 then it is "short" in the dynamic sense used here and single mode resonant response will dominate the total response. Between 0.2 and 3 significant attenuation occurs over the length of the cable, but an infinite cable response model is not adequate. However, normal mode superposition may be used except that one may need from $2n$ to $3n$ terms because non-resonant modal contributions are essential in the correct solution. When $n\varsigma$ exceeds 3, then, except when excited near an end, the cable can be considered to behave dynamically as if it were infinite in length. When excited near an end, a semi-infinite model may be used. For $n\varsigma > 3$, mode superposition models are not very useful, because a large number of modes are required.

In Chapter 3, modal overlap was discussed and the parameter $N = 2n\varsigma_n$ was introduced. In the preceding discussion $n\varsigma = N/2$. So another way of thinking of the quantity $n\varsigma$ is that $2n\varsigma$ is the number of modes contained within the half power bandwidth of mode n, for a constant tension uniform cylinder.

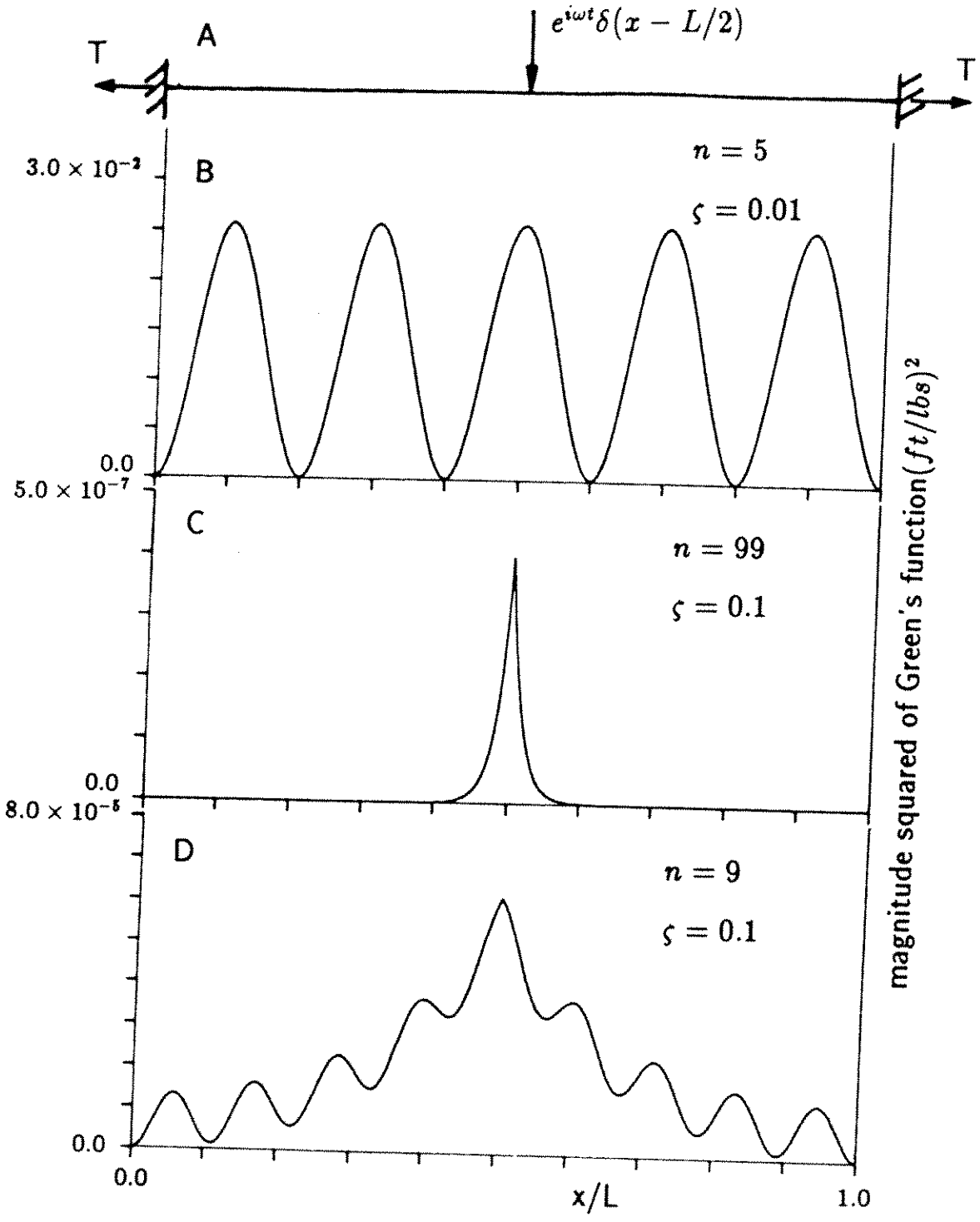

Figure 4.1: Three different cases of Green's function squared for unit harmonic force acting at the center of a cable

4.4 Hydrodynamic Lift Force and Damping Models

The most difficult components of the response prediction model of a flexible cylinder in a sheared flow are the hydrodynamic lift force and damping.

In Reference(Wang et al. 1986[21]) the cylinder is divided into an hydrodynamically excited region and an hydrodynamically damped region for each mode. A conceptually similar example is shown in Figure 4.2 where the sheared flow shown is depicted as injecting power into the cylinder in a region at frequencies which excite principally the second mode. Outside of the region, the fluid extracts energy from the cylinder in the same frequency band. At other frequencies the region of power flow in and out will be located differently. Partitioning the cylinder into such regions may be reasonable, but substantial improvement is needed in the method used by Wang et al.

There is not too much known about hydrodynamic damping of vortex-induced vibration in a sheared flow. However, experiments show that hydrodynamic damping is small under lockin conditions and large when the vibration frequency and vortex shedding frequency are different. Two hydrodynamic damping models will be introduced and discussed. One is deduced from a non-linear Morison equation model and the other is from a direct linear damping model based on dimensional analysis.

As a lift force model, a linear lift force cross spectrum model having a Gaussian distribution form in frequency and space domain is taken.

The proposed hydrodynamic damping and lift force models are described in the following subsections in detail.

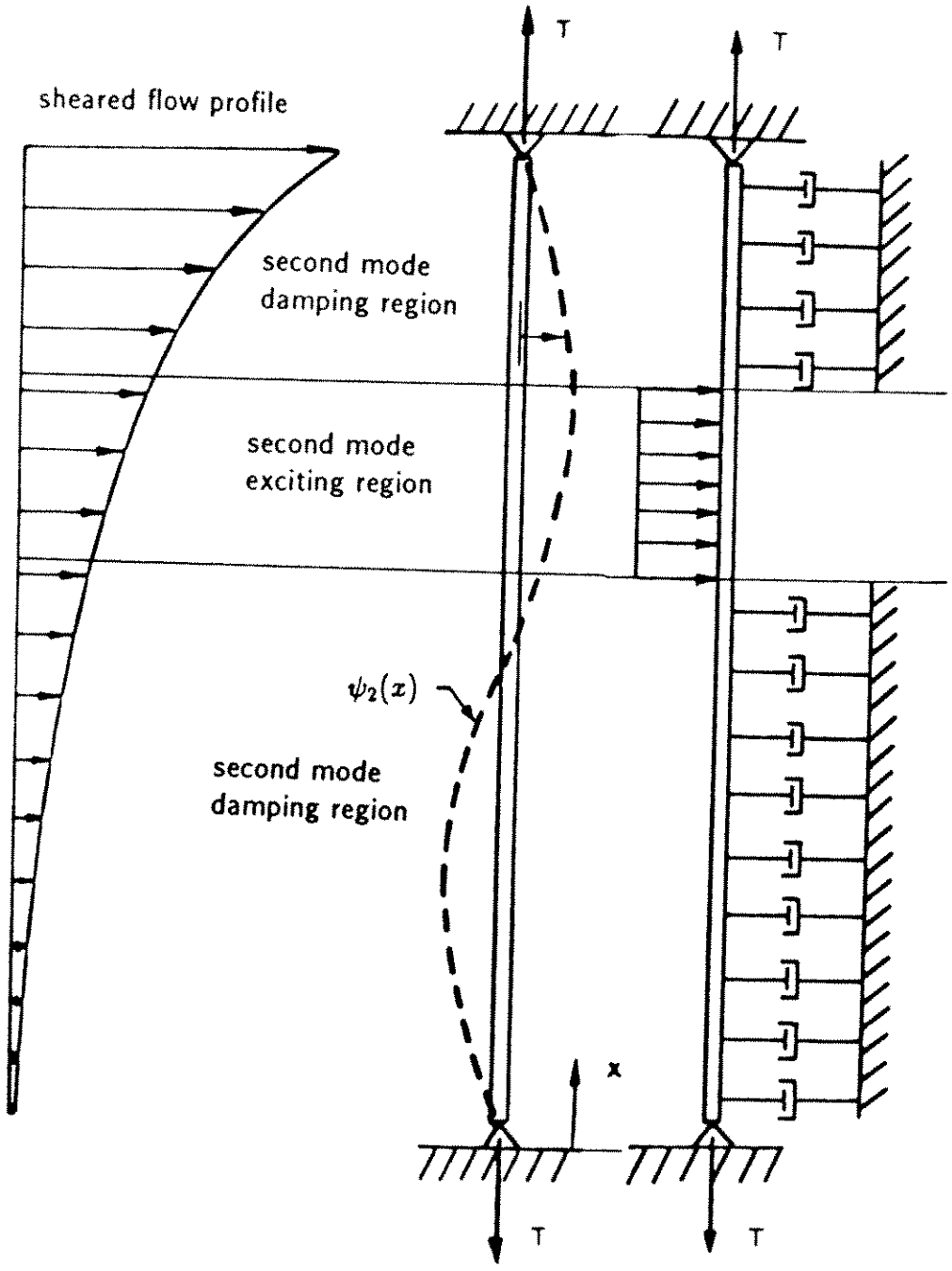

Figure 4.2: A conceptual drawing of the regions of fluid damping and fluid excitation for the 2nd mode vibration

4.4.1 Hydrodynamic Damping Model

Hydrodynamic Damping Model from the Morison Equation

At any specific location an instantaneous drag force per unit length may be defined as the force in the direction of the instantaneous relative fluid flow. The fluid velocity relative to the cable is the vector sum of the free stream velocity $V(x)$ and the negative of the local cross-flow cable velocity $\dot{y}(x,t)$, as shown in Figure 4.3. The in-line cable velocity $\dot{z}(x,t)$ is assumed small and is neglected (it could be included if a more precise estimate was required). If one assumes the drag force to be proportional to the relative velocity squared, then the drag force takes the form given below.

$$\mid F_D(x,t) \mid = \frac{1}{2}\rho_w C_D D(V^2 + \dot{y}^2) \tag{4.20}$$

let

$$B = \frac{1}{2}\rho_w C_D D$$

The component of this force in the y direction is by simple trigonometry given by

$$F_y(x,t) = -B\dot{y}\sqrt{V^2 + \dot{y}^2} \tag{4.21}$$

Such a model of damping or dissipative forces ignores the effect of the vortex shedding process itself. When wake synchronization occurs for some region, there is a high correlation between cylinder motion and vortex shedding phenomena. Under such conditions the sectional force may be in phase with the velocity and hence may input power to the system. Vibration at frequencies which are uncorrelated with the local lift forces will lead to damping and vibration at frequencies which are correlated to lift forces is responsible for the power flow into the cable. The model of damping must be able to distinguish between regions of power in and power out, as a function of frequency and location. For example, if a wave length which is excited on a cylinder at 5 Hz travels into a region of the cylinder which is shedding vortices at 2 Hz, the 5 Hz waves will be damped out in the same region that 2 Hz waves are being excited. In

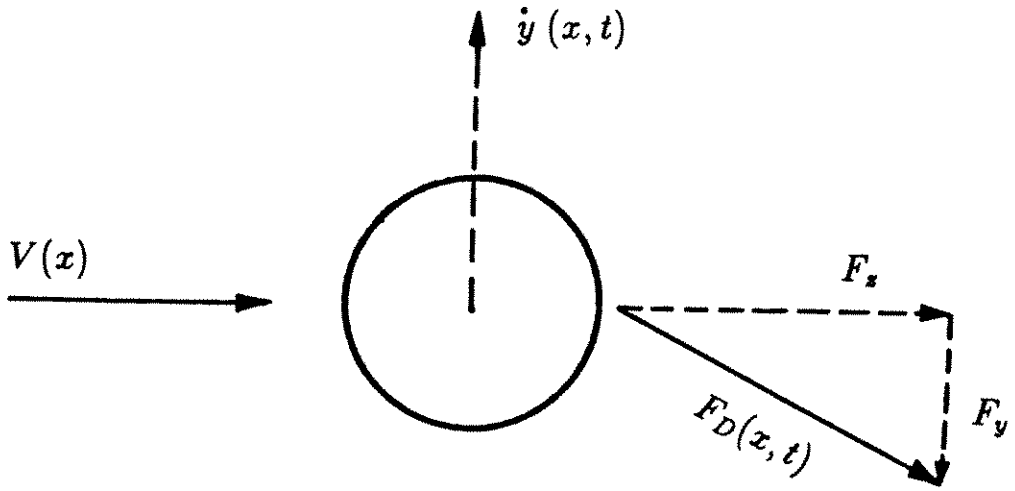

Figure 4.3: Drag force vector decomposition

very long cables in sheared flows correlation lengths will be relatively short compared to the total cable length and for the purpose of computing damping, a damping which is in effect everywhere may be adequate when calculating attenuation between points.

The damping force in equation (4.21) is a non-linear function of $\dot{y}$. It is helpful to find a linear equivalent damping constant $R(x)$ per unit length such that:

$$Damping\ \ force = -R(x)\dot{y} \tag{4.22}$$

An estimate can be obtained for a linear equivalent damping constant $R(x)$ for sinusoidal oscillations, if the requirement is imposed that the equivalent linear system dissipates the same energy per cycle as the non- linear one. In other words, it is required that

$$\frac{1}{T}\int_0^T R(x)\dot{y}^2 dt = \frac{1}{T}\int_0^T B\dot{y}^2\sqrt{V^2+\dot{y}^2}dt \tag{4.23}$$

where T is one period of oscillation.

For values of $\dot{y}^2(x,t) \leq \frac{V^2(x)}{2}$ the linear equivalent damping takes the following approximate form.

$$R(x) = BV[1+\frac{3}{8}\frac{\dot{y}^2}{V^2}] = \gamma BV(x) \tag{4.24}$$

where

$$\gamma \equiv [1+\frac{3}{8}\frac{\dot{y}^2}{V^2}] \qquad 1.0 \leq \gamma \leq 1.2$$

A Direct Linear Hydrodynamic Damping Model

Alternatively, one might assume that a linear damping model which is proportional to $\dot{y}(x,t)$ is as reasonable and justifiable as the Morison equation. This suggests

$$F_y(x,t) = -R(x)\dot{y}(x,t) \tag{4.25}$$

where $R(x)$ represents a linear hydrodynamic damping constant per unit length. $R(x)$ may depend on several physical parameters:

$$R(x) = F\{\rho_w, V(x), y(x), D, \omega(x), \mu\} \tag{4.26}$$

where

ρ_w : water density

$V(x)$: local flow velocity at location x

y : amplitude of response at location x

D : cylinder diameter

$\omega(x)$: vibrating frequency of response at location x

μ : viscosity of water

From dimensional analysis, drag coefficient C_{DV} for vortex-induced cross-flow vibration can be defined by:

$$C_{DV} = \frac{R}{\frac{1}{2}\rho_w DV(x)} = F\{\frac{y}{D}, \frac{V(x)}{\omega(x)D}, \frac{V(x)D}{\mu}\} \tag{4.27}$$

And the hydrodynamic damping constant for vortex-induced cross-flow vibration takes the form given by:

$$R(x) = \frac{1}{2}\rho_w C_{DV} DV(x) \tag{4.28}$$

To yield the same amount of damping, the two damping models have the following relationship.

$$C_{DV} = C_D(1 + \frac{3}{8}\frac{\dot{y}^2}{V^2}) \tag{4.29}$$

The Morison form is used in the remainder of this thesis. Two cases shall be evaluated:

i. infinite effective length cables

ii. finite cables

Damping for Infinite Effective Length Cables

In reference (Kim et al. 1986[11]), it is shown that when the vortex shedding frequencies correspond to very high cable natural frequencies, then energy put into the cable at one point decays exponentially with distance travelled, ultimately dying out before reflecting from the boundaries. The cables behave dynamically as if they

were infinite in length. As a result the response spectrum at any specific location is dominated by the local hydrodynamic forces as is the case in Figure 4.2(C). The local rms cylinder velocity in such cases can be evaluated. Locally the rms velocity is given approximately by the product of the local rms amplitude, y_{rms} , and the local dominant vibration frequency, ω_v , which is assumed to be the same as the local vortex shedding frequency, ω_s . The local vibration frequency can be expressed in terms of the reduced velocity at that location, which can be assumed to be approximately 5 for a wide range of Reynolds numbers.

$$V_R = \frac{2\pi V(x)}{\omega_v D} \simeq 5 \tag{4.30}$$

Substituting yields an estimate for the local rms cross-flow cylinder velocity.

$$\dot{y}_{rms} = \omega_v y_{rms} = \frac{2\pi V(x) y_{rms}}{5D} \tag{4.31}$$

For infinite length cables y_{rms} has been observed to vary from 0.1 to 0.5 diameters (refer Kim et al. 1986[11]). Substituting into equation (4.24) the equivalent damping constant becomes

$$R(x) = BV(x)[1 + \frac{3}{8}(\frac{2\pi y_{rms}}{5D})^2] \tag{4.32}$$

For values of y_{rms}/D between 0.1 and 0.5 this expression reduces to

$$R(x) = \gamma BV(x) \tag{4.33}$$

where γ is a parameter which accounts for the y_{rms} term in equation (4.32). The range of γ is from 1.0 to 1.15 and depends on the rms response. The local linear equivalent hydrodynamic damping ratio is given by

$$\varsigma_h = R(x)/2\omega m \tag{4.34}$$

where the subscript h means damping due to hydrodynamic sources and m is the local mass per unit length, including added mass and ω is any vibration frequency component of interest. The local mass per unit length, m, can be expressed as:

$$m = \rho_w \frac{\pi D^2}{4}(s.g. + C_a) \tag{4.35}$$

where $s.g.$ is the specific gravity of the cable and C_a is the added mass coefficient. Substitution for m and B, and combining the results of equations (4.30), (4.33), and (4.34) leads to:

$$\varsigma_h = \frac{5C_D\gamma\omega_s}{2\pi^2(s.g. + C_a)\omega} \tag{4.36}$$

In Chapter 7 experimental results are presented in detail. For the purpose of illustration some of the results from the Lawrence tests are used briefly here. A cable, vibrating under uniform flow lockin conditions, was struck impulsively. In the experiment, $s.g. = 1.34$, $C_a = 1.0$, and equation (4.36) reduces to:

$$\varsigma_h = 0.11C_D\gamma\omega_s/\omega \tag{4.37}$$

This is a remarkable result because it shows that the damping ratio is inversely proportional to frequency.

In the impulse propagation test the energy in the impulse was centered on about 18 Hz, and the principal shedding frequency was 3 Hz. Therefore the hydrodynamic damping ratio is estimated to be:

$$\begin{aligned} \varsigma_h &= 0.018C_D\gamma \\ &= 4.2\% \quad \text{for} \quad C_D = 2.0 \quad \text{and} \quad \gamma = 1.15 \end{aligned} \tag{4.38}$$

The measured total damping was 4 to 6%, as will be described in Section 7.4, depending on which specific test one observed. The spatial attenuation of the impulse is shown in Figure 7.13. For these tests $\dot{y}^2$ was sometimes greater than $V^2/2$ and the factor γ might need to be even larger than used here. Even though this test was on a finite cable, the comparison is a valid one, because the impulse response data considered only travelling wave attenuation between spatially separated locations, and with a frequency content quite different from the local shedding frequency. The same would be the case for an infinite cable. For the cable the structural damping (measured in air) was less than 0.3%.(refer Appendix A)

If one neglected the contribution of $\dot{y}$ in equations (4.24) and (4.32) then γ would equal one and a lower bound on the hydrodynamic damping of a wave passing along

a cylinder would be obtained. In the above example, with a C_d of 2.0, this minimum damping ratio is 3.6% at 18 Hz. A drag coefficient of 2.0 has been used because the flow was uniform and the steady state response was essentially lockin at 3 Hz.

If one wishes to predict the attenuation between two points on an infinite cable, separated by a distance l , the correct expression would be

$$\frac{y(x+l)}{y(x)} = e^{-\varsigma kl} \tag{4.39}$$

where

$$k = 2\pi/\lambda = \omega/C_p$$

Here, λ is the vibration wave length, C_p is the wave propagation speed, and ω is the vibration frequency of interest. For a fixed distance l, over which the shedding frequency varies a small amount so that the average shedding frequency can be used in equation (4.36), then by substitution for ς in equation (4.39), an expression for attenuation between the two points is arrived at which is independent of the vibration frequency, ω .

$$e^{-\varsigma kl} = e^{\frac{-5C_D\gamma\omega_s l}{2\pi^2(s.g.+C_a)C_p}} \tag{4.40}$$

This frequency independence was also seen in the Lawrence impulse response tests. Figure 7.13 shows the response spectra computed from a short time series which included an impulse. The two spectra are from positions $L/6$ and $L/2$. The low frequency peaks are due to the flow induced vibration, but the plateau between 15 and 24 Hz is the impulse vibration energy. This plateau gets lower the farther the pulse propagates, but the plateau stays flat indicating that the attenuation between the two locations, within the measurement accuracy of this experiment, was independent of frequency between 15 and 24 Hz.

Hydrodynamic Damping for Finite Cables

In the case of an infinite cable it was appropriate to compute local values of the damping. However, for short cylinders which are excited in their low modes, the

individual modal damping ratios are of interest. Equations (4.20) to (4.23) are still valid. However, the hydrodynamic modal damping constant, $R_{h,n}$, for mode n must be computed as follows

$$R_{h,n} = \int_0^L R(x)\Psi_n^2(x)dx \tag{4.41}$$

For constant tension cables and uniform cables with pinned ends the mode shapes are given by

$$\Psi_n(x) = \sin(\frac{n\pi x}{L}) \tag{4.42}$$

Using similar reasoning as in the infinite cable case one may estimate the $\dot{y}$ contribution in $R(x)$ as in equations (4.30) to (4.33). If the $\dot{y}$ contribution is included in a parameter γ then $R(x) = \gamma BV(x)$. γ rises to 1.3 for an rms anti node displacement of 0.7 diameters. Assuming a shear velocity which increases from zero linearly to a maximum value

$$V(x) = V_p x/L \tag{4.43}$$

then

$$R(x) = \gamma BV_p x/L \tag{4.44}$$

where γ may be varied from 1.0 to 1.3 to account for the effect of $\dot{y}$ on $R(x)$, and V_p is the maximum or peak velocity in the flow.

One might argue that γ should also be a function of x because y_{rms} is a function of x. However, the user may simply elect to choose an average or an upper or lower bound for γ and reduce the complexity of his damping estimate. An average value will be used here. Far more serious potential errors exist in the partitioning of the cylinder into damped and forced regions for each mode of interest. This discussion will proceed by first assuming that the damping acts over the entire cylinder. This will yield an upper bound on the modal damping constant. Substituting the expression for $R(x)$ in equation (4.44) into equation (4.41) and conducting the integral over the entire length yields for $R_{h,n}$ the following,

$$R_{h,n} = \gamma BV_p L/4 \tag{4.45}$$

The damping ratio may now be computed:

$$\varsigma_{h,n} = R_{h,n}/2\omega_n M_n \tag{4.46}$$

where M_n is the modal mass, $mL/2$, and ω_n is the natural frequency. This reduces to

$$\varsigma_{h,n} = \frac{\gamma \rho_w C_D D V_p}{8\omega_n m} = \frac{\gamma C_D V_R(\omega_p/\omega_n)}{4\pi^2(s.g. + C_a)} \tag{4.47}$$

Let

$$V_R = 5, \qquad C_a = 1.0 \qquad \text{and} \qquad s.g. = 1.34$$

then

$$\varsigma_{h,n} = 0.06\gamma C_D(\omega_p/\omega_n) \tag{4.48}$$

The damping is independent of mode number for the peak excited mode ($\omega_p = \omega_n$), and therefore $\varsigma_{h,p} = 0.06\gamma C_D$. Recall the parameter γ accounts for the increase in the damping constant due to the cylinders own motion and varies from 1 to about 1.3. Therefore, for a $C_D = 1.5$, the maximum hydrodynamic damping ratio of the highest excited mode is from 9 to 12%. All lower modes are larger by the ratio ω_p/ω_n.

The expression in equation (4.41) for $R_{h,n}$ assumes that for any given mode, energy is lost to the fluid at all points on the cable. This contradicts the idea that there are regions of the cable where due to the sheared flow, the wake is locally capable of locking in with the motion of a particular mode, and that no hydrodynamic damping should be included from such regions (Vandiver 1985[19], Wang et al. 1986[21]). Reducing the range of the integral in equation (4.41) will reduce the modal damping estimate. Evaluation of the experimental data from Lawrence indicates that the upper bound damping predicted by equation (4.48) is indeed too large.

For a general sheared flow case, a more precise model of the hydrodynamic modal damping constant for mode n is suggested by defining the range of the integral in equation (4.41). Let

$$R_{h,n,max} = \int_0^L R(x)\Psi_n^2(x)dx \tag{4.49}$$

then $R_{h,n}$ can be expressed as

$$R_{h,n} = H R_{h,n,max}$$

where

$$H = \frac{\int_0^{X_n - L_c} V(x)\Psi_n^2(x)dx + \int_{X_n+L_c}^{L} V(x)\Psi_n^2(x)dx}{\int_0^L V(x)\Psi_n^2(x)dx} \tag{4.50}$$

where $H \leq 1$ for all circumstances and X_n is the location most favorable for a resonant condition to exist between the vortex shedding process and mode n. L_c is the correlation length, or separation distance that causes the correlation between the lift forces at two locations to drop below a specified value. The correlation length will be defined more precisely in a few paragraphs. For now it is sufficient to say that a portion of cylinder $2L_c$ in length is the region into which most of the power will flow for mode n. Outside of this region will account for the dominant source of hydrodynamic damping for mode n.

In the excitation model which will be described in the next section, the spatial cross-correlation of the lift force spectrum is probabilistically defined as a Gaussian random process with the correlation length being defined as the standard deviation. Figure 4.4 showes a conceptual drawing of the hydrodynamic damping and lift force spatial correlation model.

Ramberg and Griffin measured wake velocity signals behind vibrating flexible cables using hot wire anemometers in an open jet wind tunnel and they calculated the spatial cross-correlation coefficient of the wake velocity signals(Ramberg and Griffin 1976[14]). It was found that for the portion of a vibrating cable over which the vortex shedding and vibration frequencies are locked together, the spatial cross-correlation coefficient between any two locations in the wake behind that portion approached unity, being only limited by turbulence. In that case, the correlation length in the excitation model will be infinite. However, in a sheared flow several modes can be excited simultaneously by the flow and the correlation length should be finite. For example, at two adjacent resonant locations, X_n and X_{n+1} , for the nth and $(n+1)$th mode respectively in a sheared flow the wakes should not be correlated.

As the correlation length in the proposed excitation model, the span corresponding to the half modal spacing in vortex shedding frequency is taken. For the linear sheared

flow case the correlation length coefficient, l_c , defined by:

$$l_c = \frac{L_c}{L} \simeq \frac{1}{2N_s} \tag{4.51}$$

where

L_c = the correlation length

L = the cylinder length

N_s = the number of modes excited by a linear sheared flow

For very long cables in a sheared flow for which N_s will be very large, then the ratio of the power-in region for each mode to total cylinder length, $2L_c/L$, will be very small and $H \simeq 1$.

The hydrodynamic modal damping ratio is obtained by estimating the value of H numerically:

$$\varsigma_{h,n} = H\varsigma_{h,n,max} = H\frac{R_{h,n,max}}{2\omega_n M_n} \tag{4.52}$$

The total damping ratio for the nth mode is the sum of hydrodynamic modal damping and structural damping for the nth mode:

$$\varsigma_n = \varsigma_{s,n} + \varsigma_{h,n} \tag{4.53}$$

where

ς_n = total damping ratio for the nth mode

$\varsigma_{s,n}$ = structural damping ratio for the nth mode

$\varsigma_{h,n}$ = hydrodynamic damping ratio for the nth mode

4.4.2 Lift Force Spectrum Model

The excitation force per unit length in a sheared flow can be modelled as a spatially distributed excitation (Kennedy 1979[9]):

$$f(x,t) = \frac{1}{2}\rho_w D V^2(x) C_L(x,t) \tag{4.54}$$

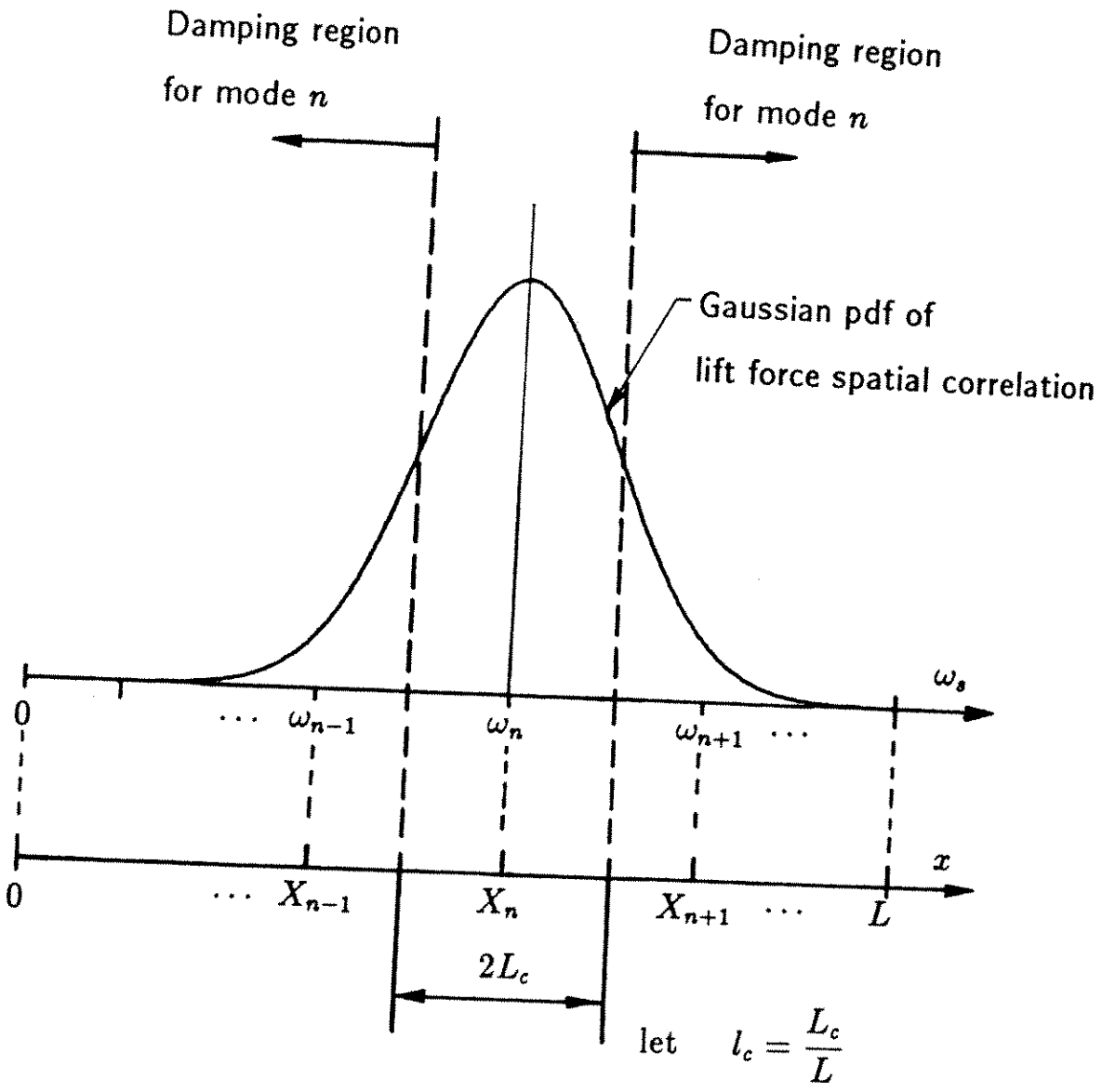

Figure 4.4: A conceptual drawing of the hydrodynamic damping and lift force spatial correlation model

where

ρ_w = water density

D = cylinder diameter

$V(x)$ = flow velocity at x

$C_L(x,t)$= local, time varying lift coefficient

If we assume that the local lift coefficient $C_L(x,t)$ is a random variable having the characteristics of being zero mean, Gaussian and time stationary-ergodic, then we can completely characterize the local lift coefficient by the space-time correlation function or its power spectrum.

A lift force coefficient spectral model in a sheared flow should have the following characteristics. At any particular location the lift force should have a bandlimited spectrum centered on the dominant local vortex shedding frequency. This local spectrum is correlated to that at neighboring locations by a spatial correlation function.

At any particular location, the peak frequency of the lift force coefficient spectrum corresponds to the local shedding frequency, $\omega_s(x)$:

$$\omega_s(x) = 2\pi S_t V(x)/D \tag{4.55}$$

If we adopt a Gaussian description for the frequency dependent portion of the local lift force coefficient spectrum, then the functional form will appear as:

$$e^{-(\omega-\omega_s)^2/2b^2} \tag{4.56}$$

where

ω = excitation frequency (rad)

ω_s = local mean vortex shedding frequency (rad)

b = one standard deviation of the local mean vortex shedding frequency

However, experience has shown that higher harmonics appear in the response in both deterministic (lockin) and random response conditions. To account for this the model used here includes higher harmonic terms. Therefore the final form of local lift force coefficient spectrum will be proportional to:

$$e^{-(\omega-\omega_s)^2/2b^2} + C_{L,2}e^{-(\omega-2\omega_s)^2/2(2b)^2} + C_{L,3}e^{-(\omega-3\omega_s)^2/2(3b)^2} + \cdots \qquad (4.57)$$

where

$C_{L,2}$ = coefficient of the 2nd harmonic

$C_{L,3}$ = coefficient of the 3rd harmonic

The bandwidths of higher harmonics were assumed to increase in proportion to the center frequency.

Combining these bandwidth and correlation length models leads to the following form of the lift coefficient spectrum.

$$\begin{aligned} S_{C_L}(\xi,\xi',\omega) = & \frac{C_L^2}{b\sqrt{\pi}}\{e^{-(\omega-\omega_s)^2/2b^2} + C_{L,2}e^{-(\omega-2\omega_s)^2/2(2b)^2} + C_{L,3}e^{-(\omega-3\omega_s)^2/2(3b)^2} + \ldots\} \\ & \times\{e^{-(\omega-\omega_s')^2/2b^2} + C_{L,2}e^{-(\omega-2\omega_s')^2/2(2b)^2} + C_{L,3}e^{-(\omega-3\omega_s')^2/2(3b)^2} + \ldots\} \\ & \times e^{-(\xi-\xi')^2/2(l_cL)^2} \times sgn[G(x/\xi)G^*(x/\xi')] \end{aligned} \qquad (4.58)$$

where

C_L^2 = mean square lift force coefficient

ω_s = local mean vortex shedding frequency at $x = \xi$

ω_s' = local mean vortex shedding frequency at $x = \xi'$

b = one standard deviation of the local mean vortex shedding frequency

$C_{L,2}$ = coefficient of the 2nd harmonic

$C_{L,3}$ = coefficient of the 3rd harmonic

l_c = L_c/L = coefficient determining the spatial correlation between ξ and ξ'

The bandwidth of the excitation spectrum may depend on the turbulence of incident flow or it may depend on the motion of the cylinder and unsteady fluctuations in the vortex formation process. In a very low turbulence flow the lift force bandwidth on a stationary cylinder is very narrow. If the turbulence level is high (as it was at Lawrence) then we may expect the excitation bandwidth to depend on it, as estimated below. If one standard deviation of the local mean flow velocity due to turbulence is ΔV_{rms}, then the standard deviation of the local mean vortex shedding frequency in the lift force spectrum, b is given by:

$$b = 2\sqrt{2}\pi S_t \Delta V_{rms}/D \tag{4.59}$$

For the Lawrence experiments the turbulence was 20 to 30% of the mean flow speed. In this case the turbulence dominates the bandwidth estimate.

Given the lift coefficient spectrum as defined in equation (4.58) the lift force spectrum can be written as:

$$S_{f_\xi f_{\xi'}}(\xi, \xi', \omega) = [\frac{1}{2}\rho_w V^2(\xi) D][\frac{1}{2}\rho_w V^2(\xi') D] S_{C_L}(\xi, \xi', \omega) \tag{4.60}$$

where

$S_{f_\xi f_{\xi'}}(\xi, \xi', \omega)$ = lift force spectrum
$V(\xi)$ = flow velocity at $x = \xi$
$V(\xi')$ = flow velocity at $x = \xi'$
ρ_w = water density
D = cylinder diameter
$S_{C_L}(\xi, \xi', \omega)$ = lift force coefficient spectrum

This model is used to predict the response observed in the Lawrence experiments.

Chapter 5

The Field Experiments

5.1 General Description

Field experiments were carried out to study the response characteristics of a cable in sheared flow. The experiments included:

1. A survey of the sheared flow profiles used in response tests.
2. Measurement of the accelerations of the test cable at six locations during response tests.
3. Measurement of the tension of the test cable during response testing.
4. Continuous measurement of the flow velocity at a single reference point during response testing for comparison to the value obtained from the survey of the sheared flow profile.

Figure 5.1 shows the block diagram of the experiment.

In the field, all analog signals were digitized and stored on floppy disks using a DEC MINC-23 computer.

In the following sections, more detailed descriptions of the experimental set-up are given.

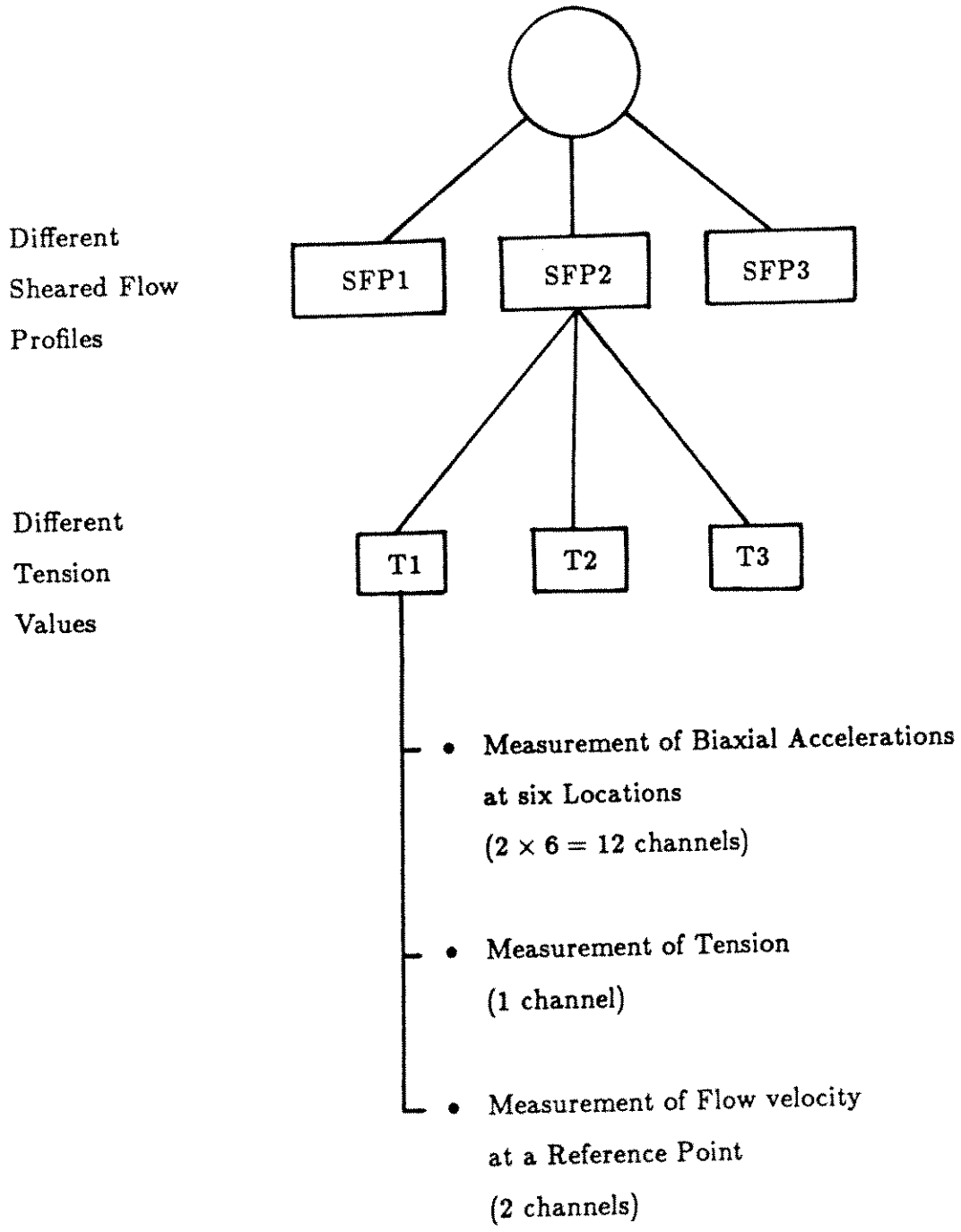

Figure 5.1: Block diagram of the Lawrence experiment

5.2 Test Site

Field experiments were carried out at Lawrence, Massachusetts during the summer of 1986. The site chosen for the experiment shown in Figure 5.2 was a 58 ft. wide canal located beside the Merrimack River. About 250 ft. upstream of the test site was a gate house where the flow rate and the flow profile were controlled by adjusting the heights of 3 sets of submerged, vertically moving gates, which opened from the bottom first. Originally, the gate house had 4 sets of gates, but one of them was out of order and closed. A continuous variation of sheared flow profiles can be made by adjusting the heights of the gates. Figure 5.3 shows the arrangement of the test site.

5.3 Test Cable

A 57 ft. 3 in. long instrumented test cable was made. The test cable consisted of one outer rubber hose and seven kevlar cables inside of the outer rubber hose. The braided kevlar cables each carried seven insulated conductors. Figure 5.4(B) shows the cross-section of the test cable. The specifications of the outer rubber hose, inner kevlar cables, and assembled test cable are given in Table 5.1. Of the 7 kevlar cables, 3 were used in holding the tension given by the winch, 3 were used as signal conducting cables, and one was used as a spare. Each kevlar cable had a breaking strength of 800 pounds.

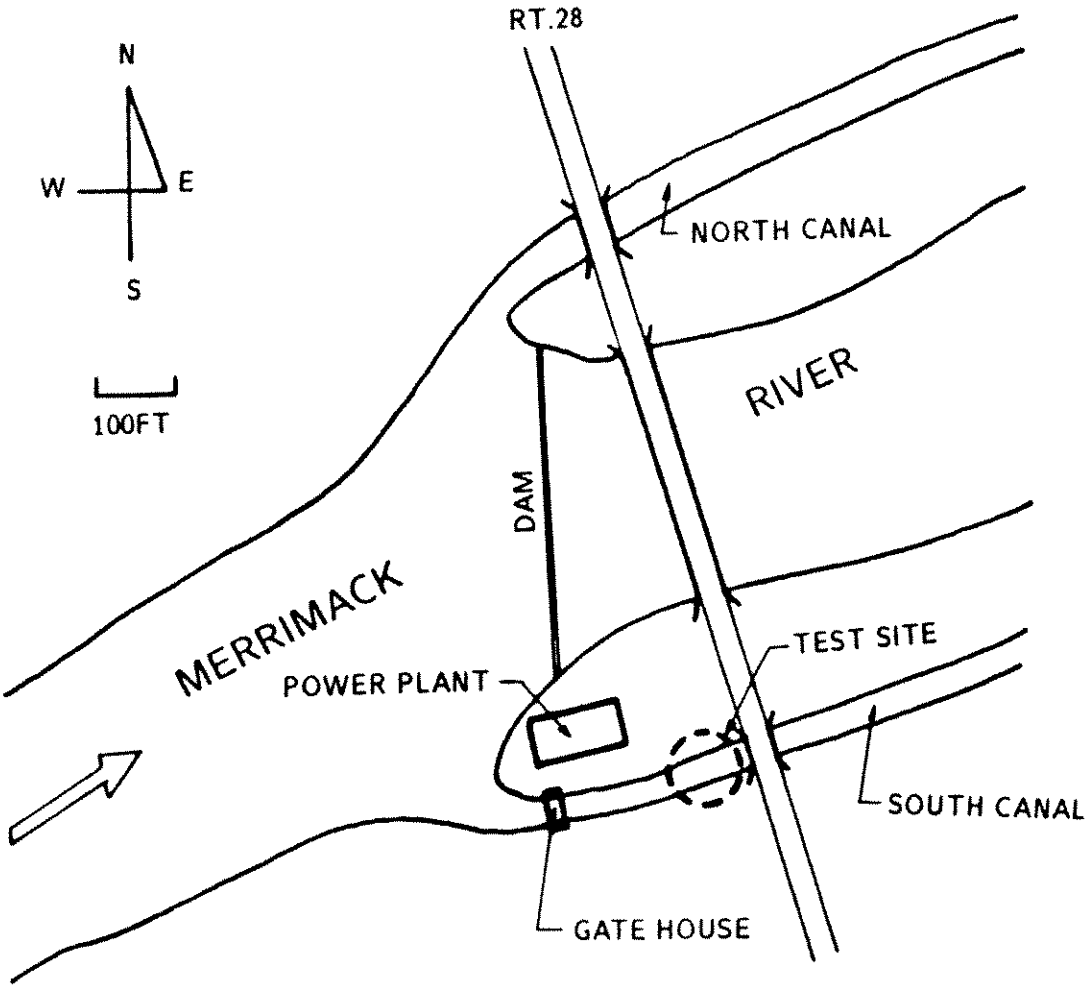

Figure 5.2: Lawrence canal test site(Lawrence, Massachusetts)

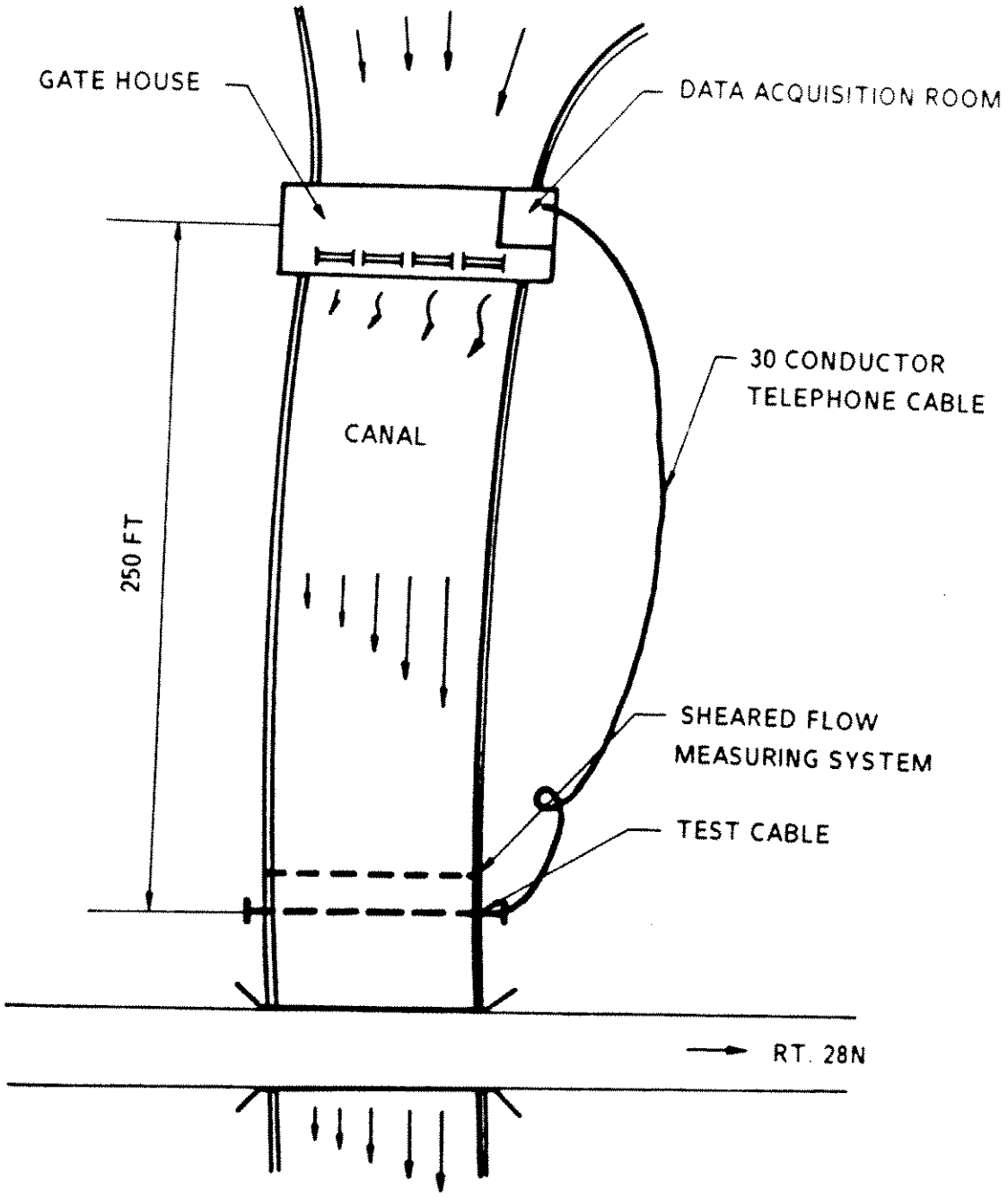

Figure 5.3: Test site arrangement

Table 5.1: Specification of the test cable

	Test cable	Rubber hose	Kevlar cable
Outer diameter (inches)	1.125	1.125	0.162
Mass per unit length in air $(slug/ft)$	0.0179	0.0145	0.00032
Length (ft) (at Tension=500 lbs)	57.25		
Specific gravity	1.34		

Six pairs of accelerometers were placed at L/8, L/6, L/4, L/2, 11L/16, and 13L/16, starting from the north end as shown in Figure 5.4(A). The accelerometers were SUNDSTRAND MINI-PAL MODEL 2180 SERVO ACCELEROMETERS which were sensitive to the direction of gravity. Each was 1/2 inch in diameter by 1.5 inches in length. The bi-axial pairing of these accelerometers made it possible to determine their orientation and hence made possible extraction of real vertical and horizontal accelerations of the test cable at the six locations.

The seven conductors in each of the three kevlar cables carried DC power and signals for two pairs of accelereometers.

5.4 Test Cable Supporting System

Two supporting frames were constructed of steel pipe to hold the ends of the test cable. These were designed to be attached to an existing 1.5 inch diameter steel post on the south side of the canal and to a steel fence on the north side. Figure 5.5 depicts these supporting frames.

5.5 Tension Adjusting and Measuring Systems

The tension adjustment was accomplished by using a hand-operated "come along" winch (capacity 1 ton). Tension was measured by a SENSOTEC Model RM/2099 LOAD CELL (Range 0-2000 lbs.). The output signal from the tension load cell passed with the current meter and acceleration signals through a 270 ft. long, 30 conductor telephone cable to the data acquisition room, where the signals were conditioned and digitized. Figure 5.6 shows the tension adjusting and measuring system.

5.6 Sheared Flow Measuring System

The flow velocity was measured by a Neil Brown Instrument Systems DRCM-2 Acoustic Current Meter located 5 ft. upstream of the test cable. Sheared flow velocity profiles were determined by taking flow velocity data at several locations along the canal width. A simple traversing mechanism was constructed to carry the acoustic current meter to any position between the canal walls as shown in Figure 5.7. The current meter was suspended from a pulley wheel which rolled freely on a taut, horizontal steel cable. An endless loop of nylon cord, like a clothesline, was used to manually position the current meter. The location of the current meter could be read from an odometer attached to the pulley system.

(A) LOCATION OF ACCELEROMETERS

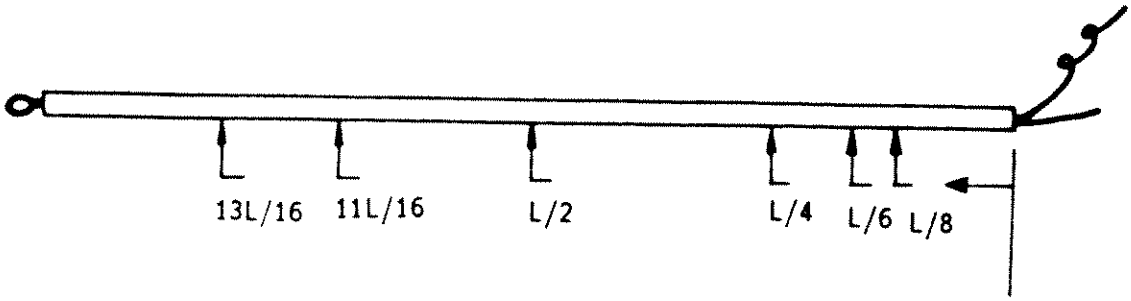

(B) CROSS SECTION OF TEST CABLE

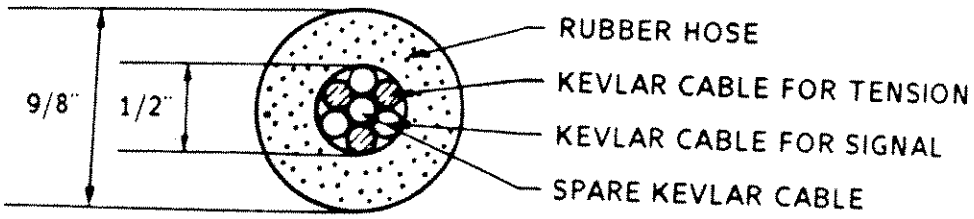

Figure 5.4: Test cable construction

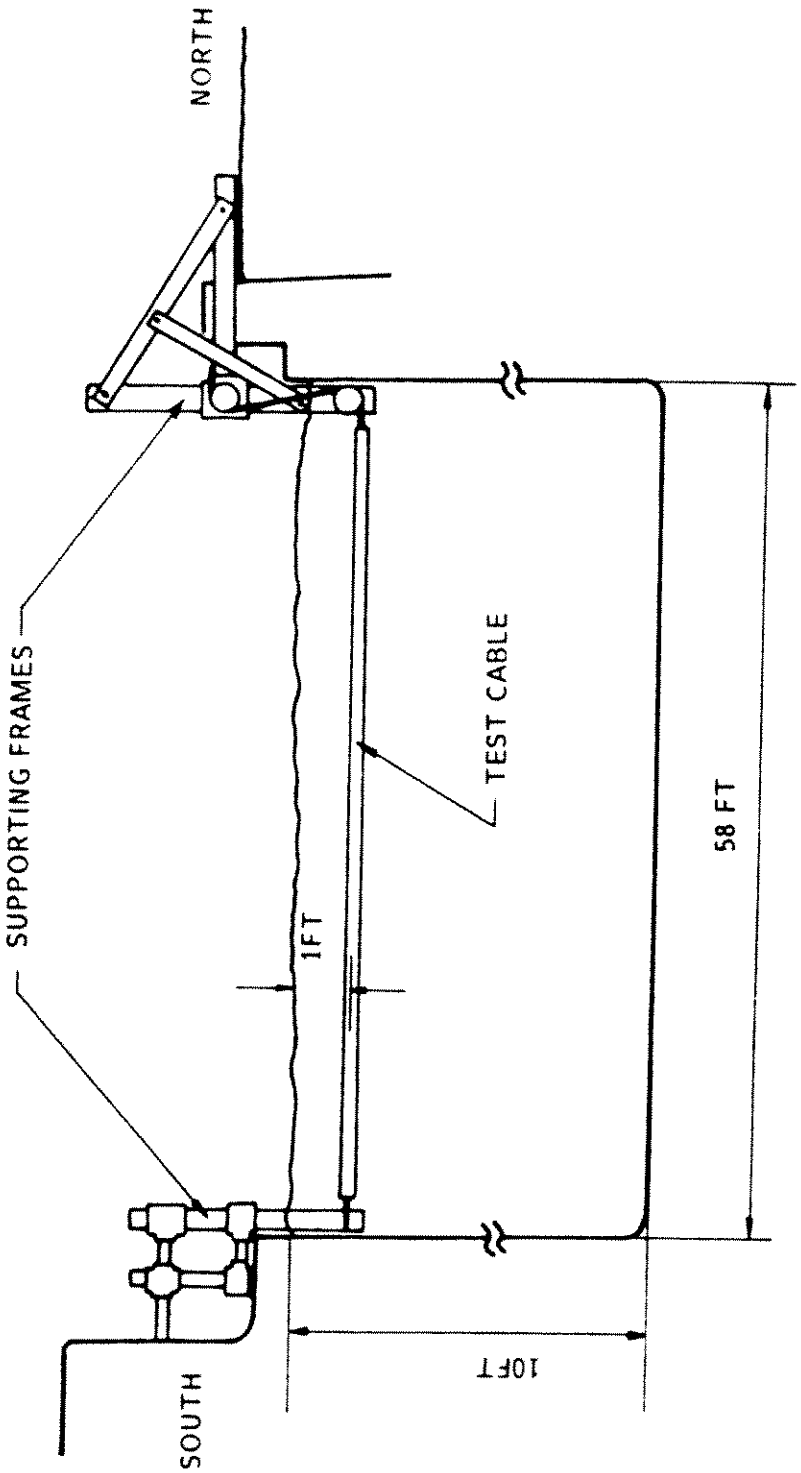

Figure 5.5: Cable support system

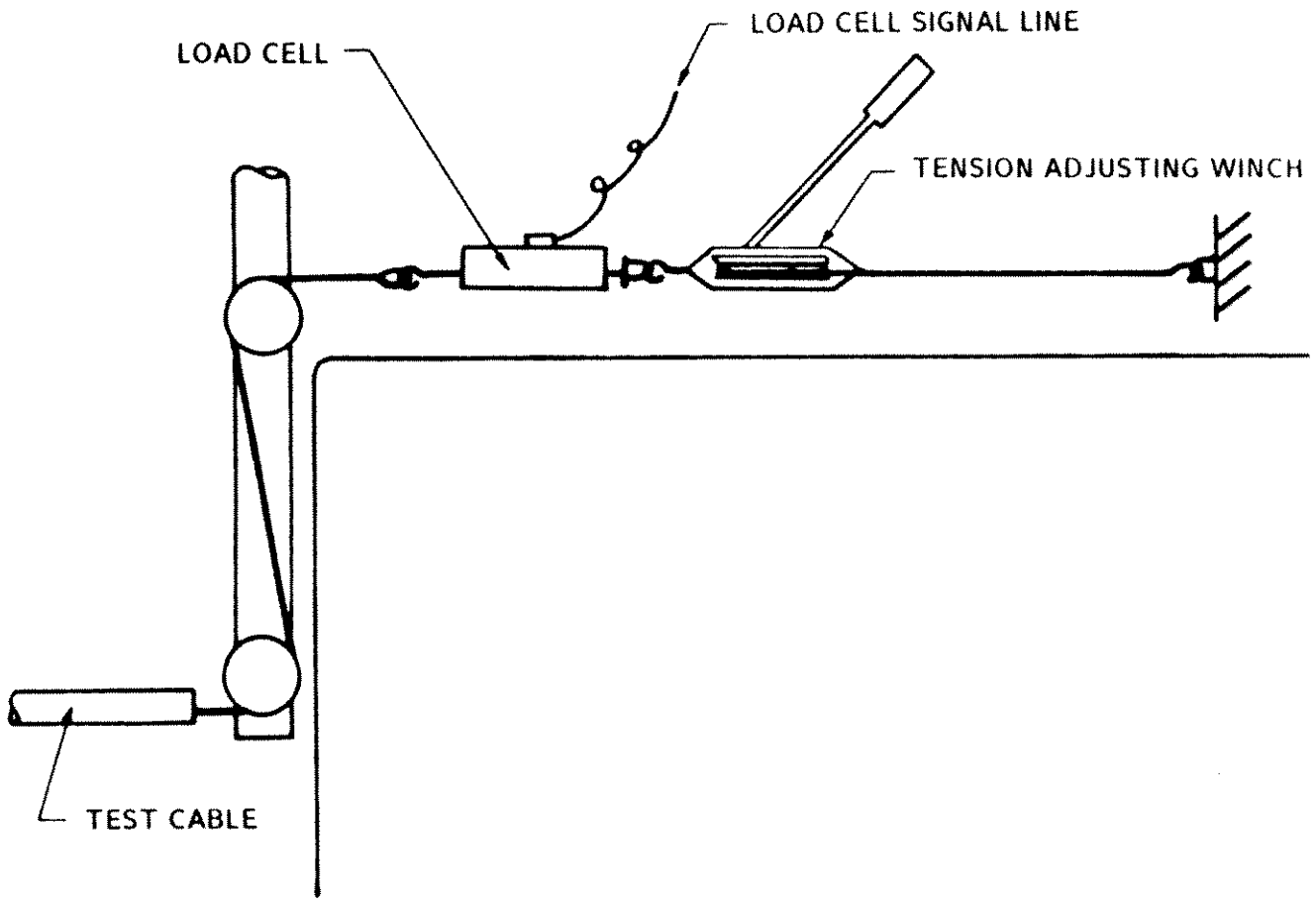

Figure 5.6: Tension adjusting and measuring system

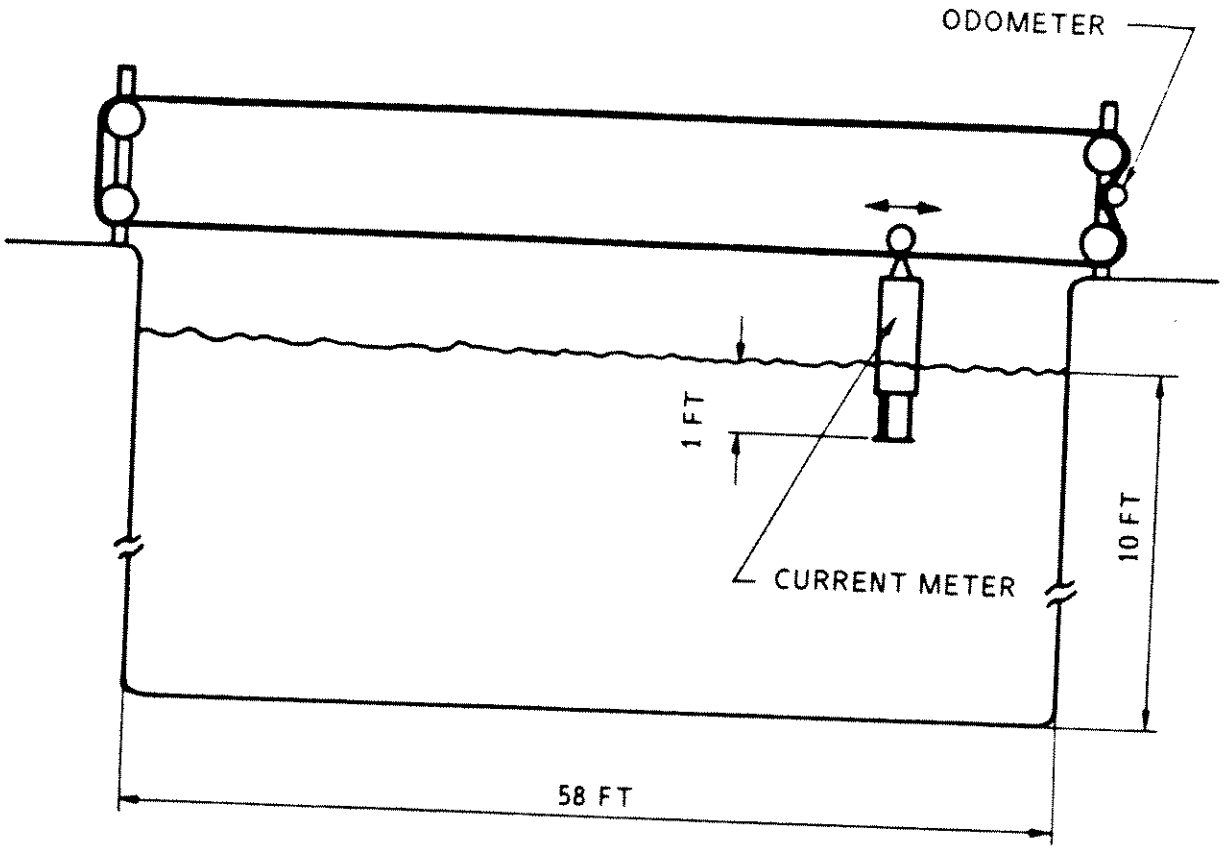

Figure 5.7: Sheard flow measuring system

Chapter 6

Data Reduction Methods

6.1 General Description

This chapter describes the general data processing procedures used for analyzing the measured signals obtained during the field experiments. The data processing consisted of two main parts:

1. Evaluation of the sheared flow velocity profiles
2. Investigation of acceleration data for a specified sheared profile and tension

Detailed descriptions of the data processing for each measurement are given in the following sections.

6.2 Survey of Sheared Flow Velocity Profile

The sheared flow velocity profile for each flow condition was determined by taking flow velocity data at several locations along the canal width. At each location, 1050

data points were taken over a period of 4 min. 22.5 sec. The sampling frequency was 4 Hz.

The current meter outputs consisted of the magnetic heading and the magnitude of the flow velocity. The flow velocity parallel to the canal was determined by vector decomposition.

$$V_p = V\cos(\phi - \theta) \tag{6.1}$$

where

V_p = the flow velocity parallel to the canal

V = flow velocity magnitude

θ = compass heading of the canal

ϕ = instantaneous magnetic heading of the velocity

The measured magnetic heading of the canal was 65 degrees. Figure 6.1 shows a typical example of the raw current speed and direction signal and Figure 6.2 shows the spectrum of that raw current velocity signal. The lowest turbulence frequencies in the range of $0 \sim 0.02Hz$ dominate the flow spectrum as shown in Figure 6.2. These lowest turbulence frequencies were associated with large eddies, up to 10feet in diameter which were convected downstream from the gatehouse.

The mean and standard deviation of the flow velocity was calculated. The standard deviation of velocity increases as the steepness of the sheared flow velocity profile increases. Table 6.1 shows one example of the statistical results of flow velocity for a particular sheared flow condition and Figure 6.3 shows the corresponding sheared flow profile along the canal width. The velocity error bands in Figure 6.3 represents $\pm$one standard deviation from the mean flow velocity at each location. The flow was at all times and at all spaces highly turbulent as indicated in Figure 6.1 and table 6.1. The rms turbulence level was about 20% of the mean of the profile.

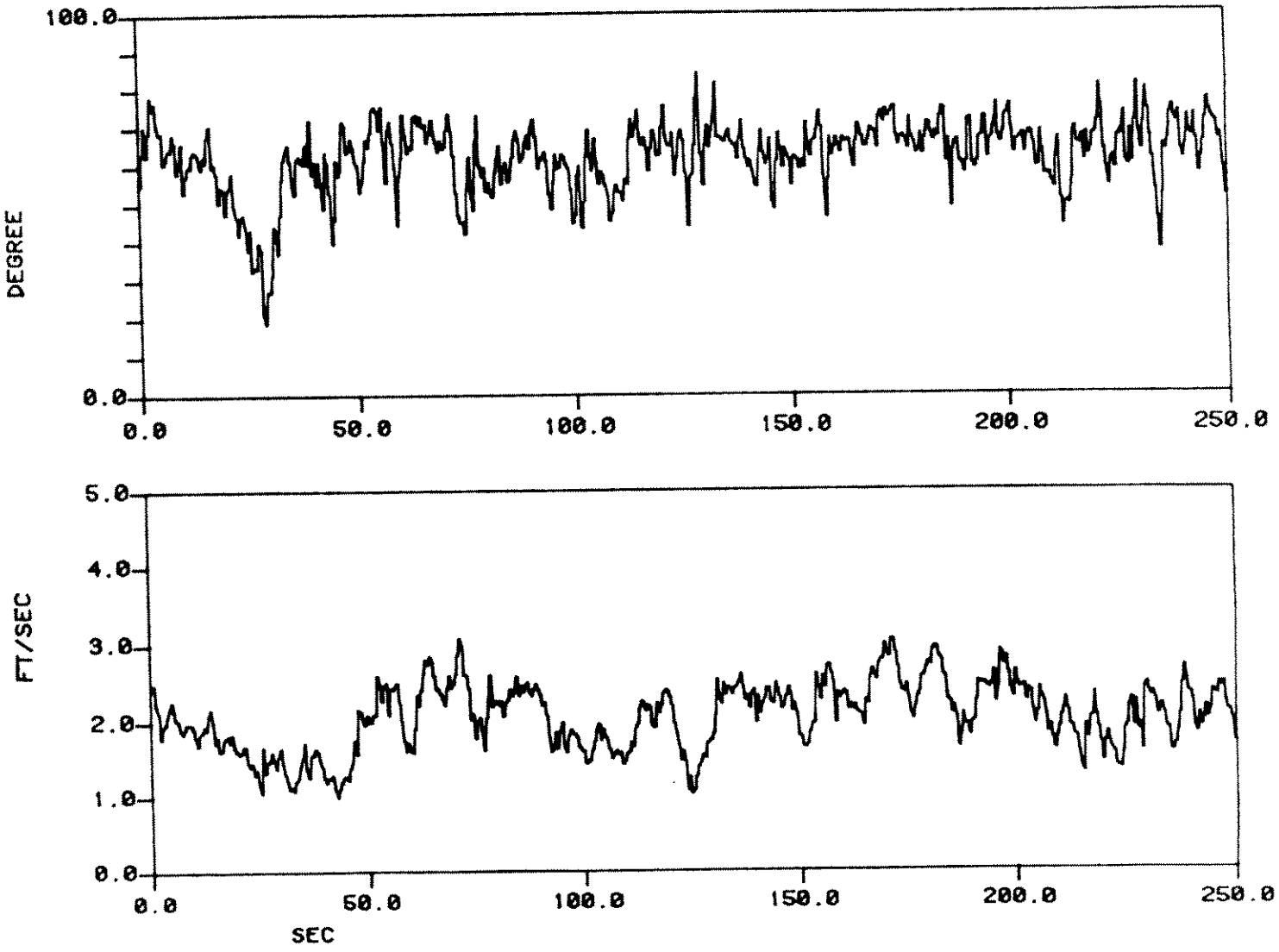

Figure 6.1: Raw current direction and speed signals at $32ft$ from north side for the highly sheared flow case

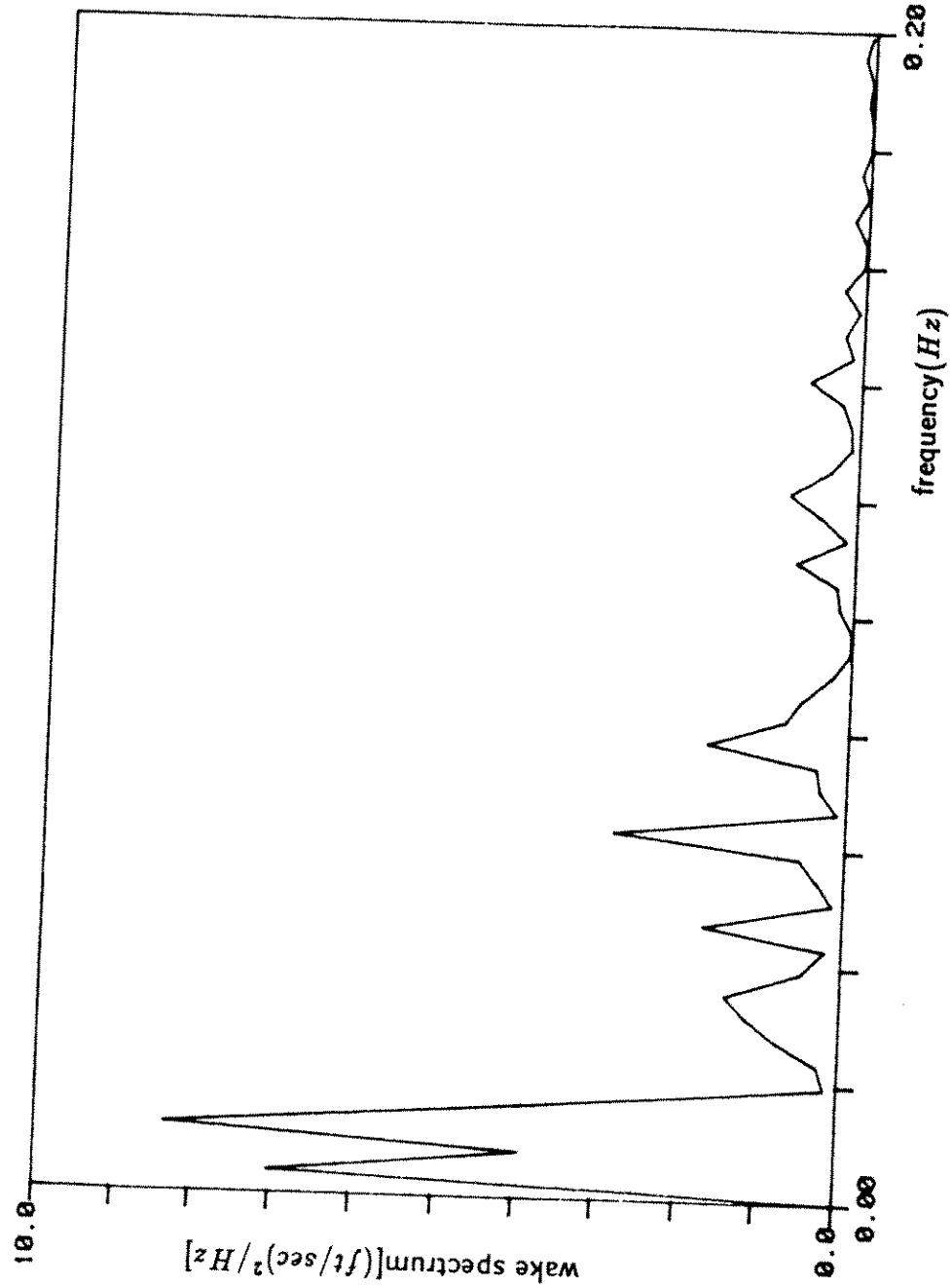

Figure 6.2: Spectrum of the raw current speed signal shown in Figure 6.1

Table 6.1: Statistics of highly sheared flow case

Location	$V_{par}(ft/sec)$		$V_{nor}(ft/sec)$	
(ft)	average	standard dev.	average	standard dev.
2	-0.416	0.300	0.273	0.199
6	-0.032	0.417	0.547	0.213
10	-0.058	0.353	0.382	0.236
14	0.322	0.358	0.316	0.264
18	0.606	0.418	0.202	0.243
22	0.952	0.344	0.033	0.265
26	1.478	0.420	-0.075	0.264
30	1.769	0.412	-0.110	0.277
32	2.015	0.442	-0.070	0.277
34	2.286	0.382	-0.034	0.303
36	2.540	0.368	-0.024	0.271
38	2.593	0.398	-0.029	0.311
40	2.938	0.381	0.075	0.330
42	3.079	0.443	0.121	0.318
44	3.194	0.391	0.191	0.336
46	3.486	0.358	0.312	0.299
48	3.555	0.323	0.383	0.311
50	3.581	0.300	0.494	0.315
52	3.639	0.306	0.627	0.257
54	3.308	0.492	0.310	0.167
56	2.412	0.578	0.107	0.157

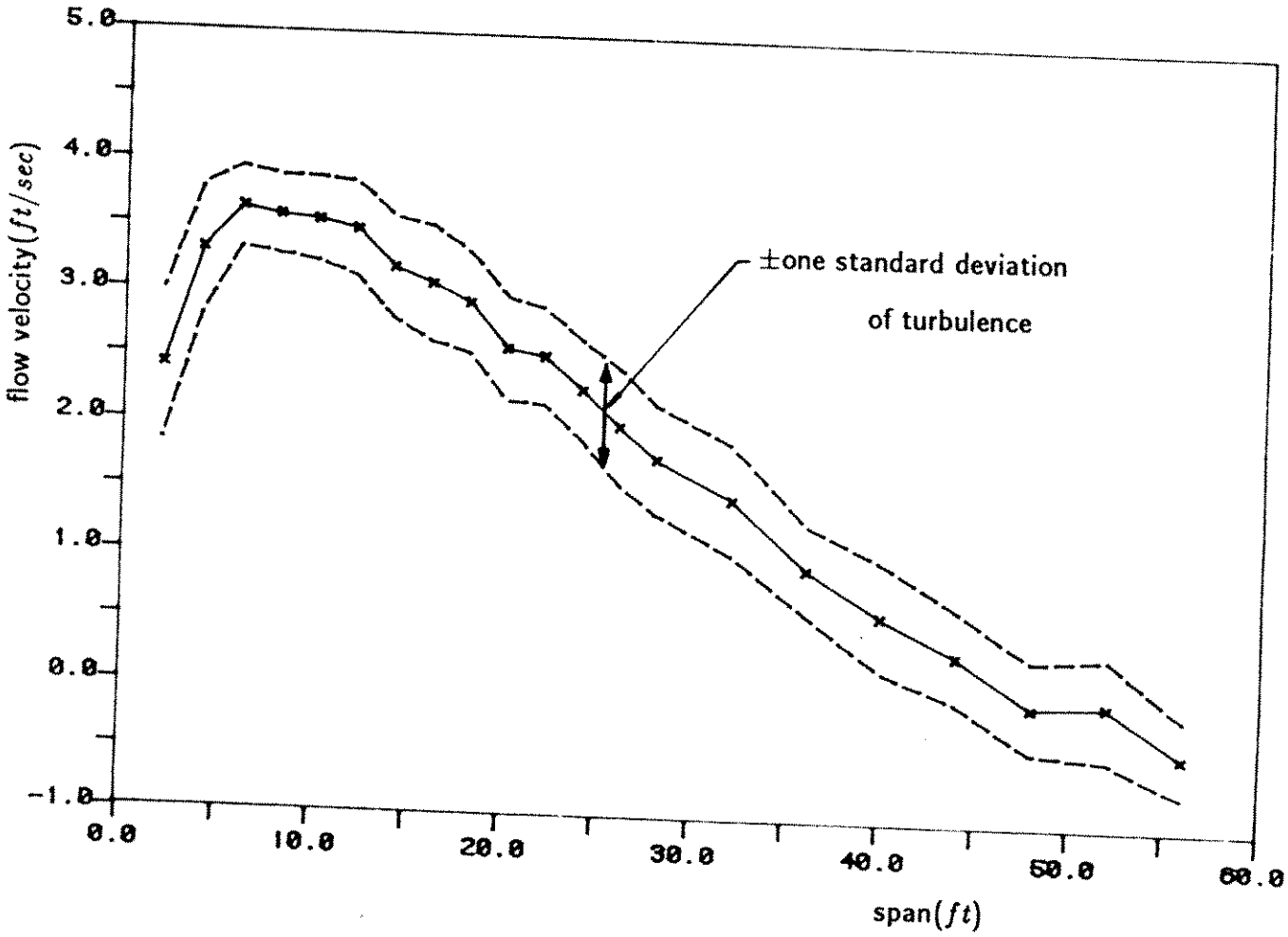

Figure 6.3: Flow velocity profile for the highly sheared flow case

6.3 Acceleration Signals

6.3.1 Vector Rotation of the Acceleration Raw Time Series

The orientation of the bi-axial accelerometers installed in the test cable was initially unknown. It was necessary to resolve the measured accelerations into in-line and cross-flow components. The same technique used in previous experiments (Jong and Vandiver 1983[8]) was used here.

The accelerometers were sensitive to gravity and gave a DC offset to the recorded signal. By vector rotation of the bi-axial acceleration signals the cross-flow direction was identified by having maximum DC offset values due to gravity. The in-line vibration component had zero DC offset due to gravity.

6.3.2 Spectrum Analysis

The auto power spectra of acceleration signals were estimated by squaring the output values from an FFT performed on the acceleration time histories. The FFT's were computed with record lengths of 1024 data points. The sampling frequencies (30 Hz, 50 Hz, or 60 Hz) were selected in the field to avoid aliasing error.

The mean square displacement was calculated by double integration of the auto power spectra of the acceleration signal in the frequency domain:

$$E[y^2(t)] = \int_{f_c}^{\infty} \frac{1}{(2\pi f)^4} \tilde{S}_{\ddot{y}\ddot{y}}(f) df \tag{6.2}$$

where

$E[y^2(t)]$ =mean square displacement

$\tilde{S}_{\ddot{y}\ddot{y}}(f)$ =estimated acceleration spectrum

In order to prevent low frequency noise expansion in the integration, the lower bound of integration, f_c , was determined after reviewing the acceleration spectrum. These

cut-off frequencies had to be low enough to include data of significance and still prevent noise expansion.

Chapter 7

Experimental Results and Discussion

7.1 General Description

The dynamic response characteristics of the test cable in sheared flows showed strong dependence on the velocity profile and the tension of the test cable. For the purpose of illustration, three different sheared flow cases are presented in this report. The velocity profiles are shown in Figure 7.1. They are designated sheared flow profile 1, 2, and 3 (SFP1, etc.).

SFP3 was the steepest shear with a peak flow velocity at times exceeding 4 feet per second and a minimum flow velocity of minus 0.5 feet per second. The minus indicates reverse flow. SFP1 was made as close to uniform as possibly by careful positioning of the gates. SFP2 ranged from 2 feet per second down to zero in a nearly linear profile.

For each sheared flow case, an example of response with high and low tension are presented. The description for each test condition is summarized in Table 7.1. In Table 7.1, the test condition is revealed in the name. For example, Test (1-H) represents the test carried out under the SFP1 and high tension, and Test (2-L) represents the test carried out under the SFP2 and low tension.

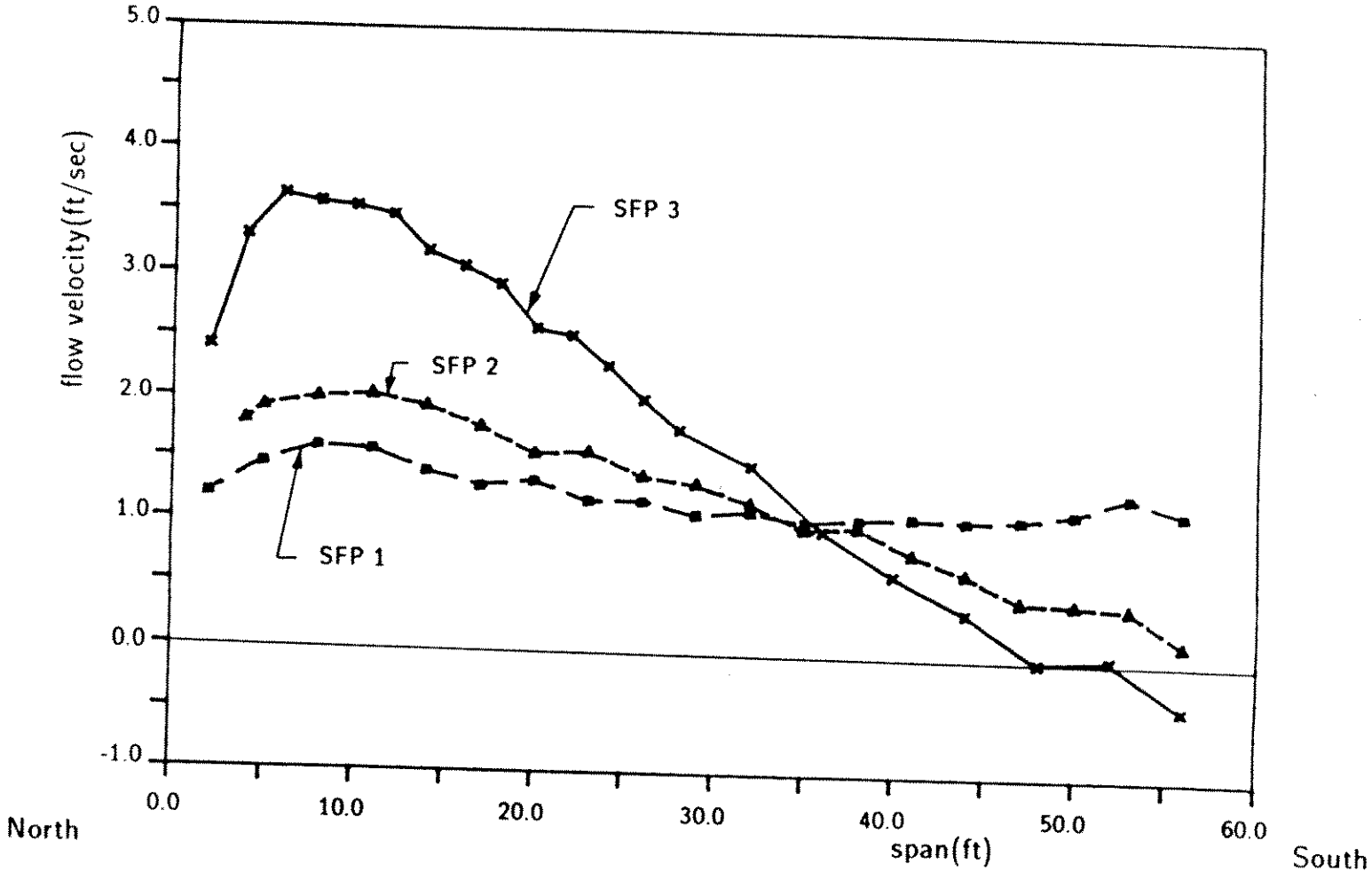

Figure 7.1: Measured sheared flow profiles

Important findings and key results will be discussed in detail in the following sections.

Table 7.1: Summary of the test conditions

Test condition	Test (1-H)	Test (1-L)	Test (2-H)	Test (2-L)	Test (3-H)	Test (3-L)
Sheared flow profile	Almost Uniform SFP1	Almost Uniform SFP1	Slightly Sheared SFP2	Slightly Sheared SFP2	Highly Sheared SFP3	Highly Sheared SFP3
Flow velocity (ft/sec)						
min.	1.0	1.0	0	0	-0.5	-0.5
max.	1.6	1.6	2.0	2.0	3.6	3.6
Vortex shedding frequency (Hz)*						
min.	1.8	1.8	0	0	0	0
max.	2.9	2.9	3.6	3.6	6.5	6.5
Tension (Lbs)	318.4	96.4	348.9	62.4	343.6	145.1
1st natural frequency (Hz)						
in air	1.16	0.64	1.22	0.51	1.21	0.78
in water**	0.88	0.48	0.92	0.38	0.91	0.59

* Vortex shedding frequencies were calculated from equation $f_s = S_t V/D$, where $S_t = 0.17$.

**An added mass coefficient of 1.0 was used in the calculation of the fundamental natural frequency in water.

7.2 The Values of Relevant Non-dimensional Parameters

The value of length-to-diameter ratio of the test cable was 611 implying that for this experiment end effects on the vortex shedding mechanism were negligible as discussed in Section 3.2.1.

The values of Reynolds number for all test conditions were in the subcritical region so that we may expect that differences in Reynolds numbers between tests did not make significant differences in the dynamic response characteristics of the test cable.

The value of mass ratio of the test cable as 0.952. The corresponding value of specific gravity of the test cable is 1.34. The test cable is a relatively low density structure. The lockin range expressed in reduced velocity terms is much broader for low density cylinders than for high density ones as discussed in Section 3.2.3. The cross-flow lockin of this test cable in a uniform flow would be expected to occur in the range of $3.5 \leq \frac{V}{f_n D} \leq 9$ (refer to Figure 3.2).

The most significant dimensionless parameter variations in these tests were the variation in the maximum responding mode number, the variation in the number of modes simultaneously participating in the response, and the variations in damping. The cable tension determined the variation in modal separation or inversely the modal density. For a given modal density the amount of shear in the flow speed determined the number of excited modes and the frequency of the highest responding mode. The damping had very large variation due to hydrodynamic effects.

For the six cases to be described here the values of nondimensional parameters for the test conditions are summarized in Table 7.2. The effective damping in water was estimated by two separate means, one experimental and one analytical. The experimental determination was obtained by striking the cable impulsively with a pole and measuring the decay of the resulting pulse as it passed successive accelerometers. The results of these estimations are given in Section 7.4. The analytical estimation of hydrodynamic damping was obtained by assuming a drag coefficient appropriate to

transverse vibration, and then calculating the damping force on the cable as presented in Section 4.4.1.

In air transient decay tests of the first few modes of the cable were conducted. For the tension ranges later used in water the structural damping was about 0.3%, which is negligible compared to the hydrodynamic losses experienced by the cable, except under uniform flow lockin conditions.

Table 7.2: The values of nondimensional parameters

Test condition	Test (1-H)	Test (1-L)	Test (2-H)	Test (2-L)	Test (3-H)	Test (3-L)
Flow profile	SFP1	SFP1	SFP2	SFP2	SFP3	SFP3
Tension (lbs)	318.4	96.4	348.9	62.4	343.6	145.1
Max. R_e (10^4)	1.4	1.4	1.7	1.7	3.1	3.1
Max. mode number $f_{s,max}/f_1$	3.3	6.0	3.9	9.5	7.1	11.0
Min. mode number $f_{s,min}/f_1$	2.0	3.8	1	1	1	1

7.3 Response Dependence on Sheared Flow Profile and Tension

The cross-flow response spectra at $x = L/8$ for all six test conditions are given in Figures 7.2 to 7.7 in order to illustrate the dependence of the dynamic response of the cable on the sheared flow profile and tension. Each figure contains an acceleration spectrum, a displacement spectrum obtained by dividing the acceleration spectrum by ω^4, and the square root of the integral of the displacement spectrum. The later provides a cumulative estimate of the rms displacement as a function of frequency. A lower cut-off frequency of 1.0 Hz was used to prevent the blow up of low frequency noise during the division of the acceleration spectrum by ω^4. The cut-off frequency of 1 Hz was usually low enough to include all data of interest and still prevent noise expansion. Integration of the displacement spectrum to get the rms values was carried out numerically in reverse, from high to low frequencies. This reverse integration gives an estimate of the rms displacement from the more reliable high frequency components first and allows the reader to determine where low frequency noise expansion begins and therefore allows the reader to choose the total rms values.

The amount of shear determines the total excitation force bandwidth because the local flow velocity largely determines the local vortex shedding frequency as approximately predicted by the Strouhal relationship. The acceleration spectra shown in Figures 7.2 to Figure 7.7 reveal broader bandwidth in cases of greater shears, as expected.

The principal observations concluded from examination of these response spectra are as follows:

1. The steepness of the sheared flow in the canal determines the broadness of the response spectra for the case of non-lockin. A steeper shear results in a greater variation in velocity over the length and therefore makes a broader excitation force bandwidth. Low tension cases of three different sheared flow conditions (Test (1-L) in Figure 7.3, Test (2-L) in Figure 7.5, Test (3-L) in Figure 7.7

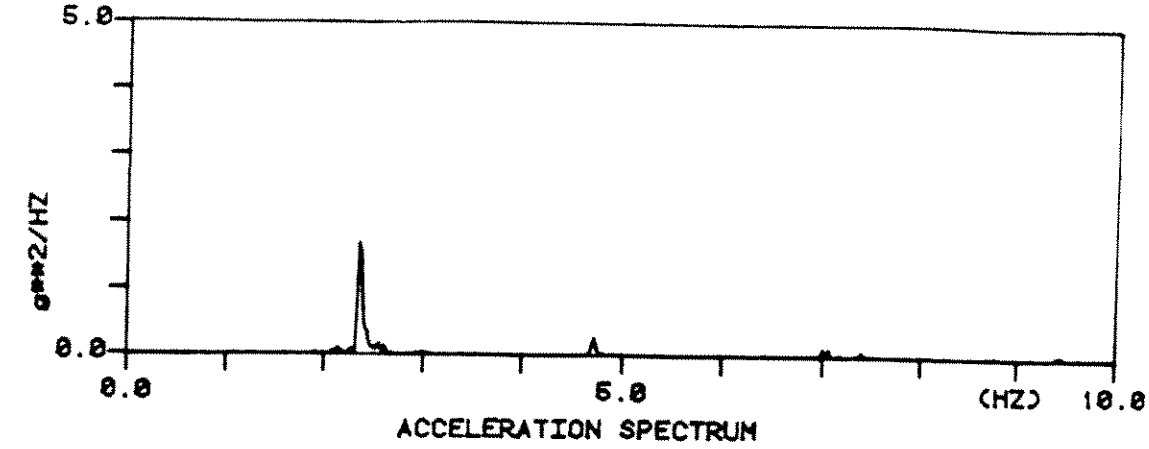

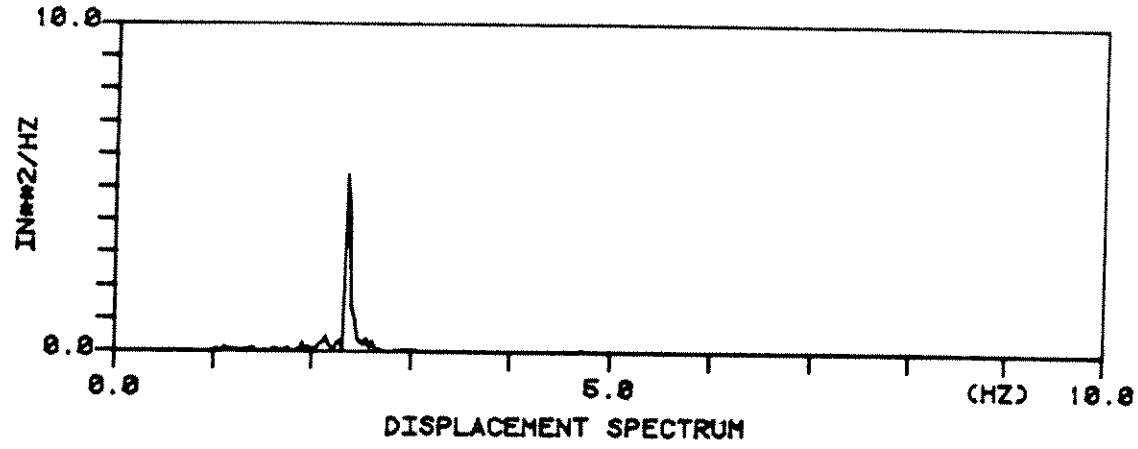

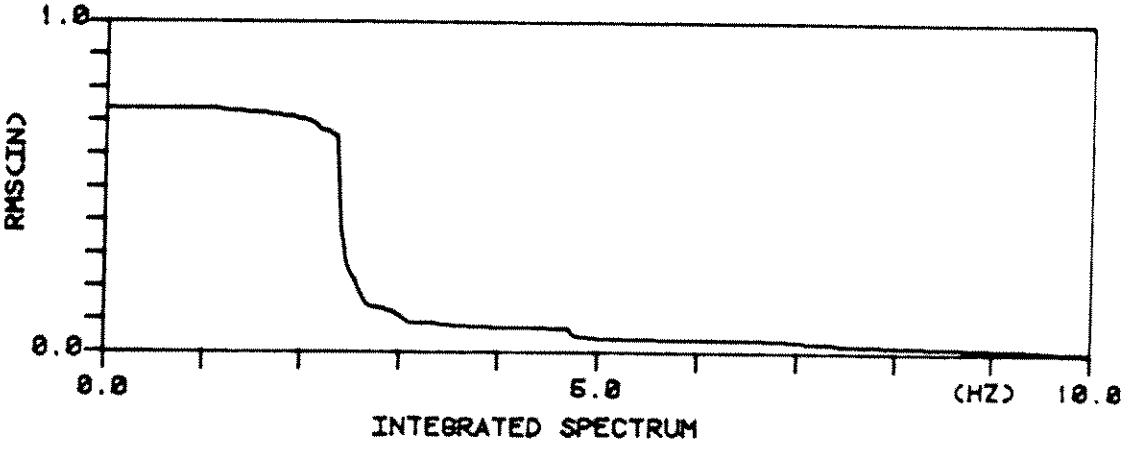

Figure 7.2: Response spectra at $x = L/8$ for Test(1-H)(SFP1 and T=318 lbs)

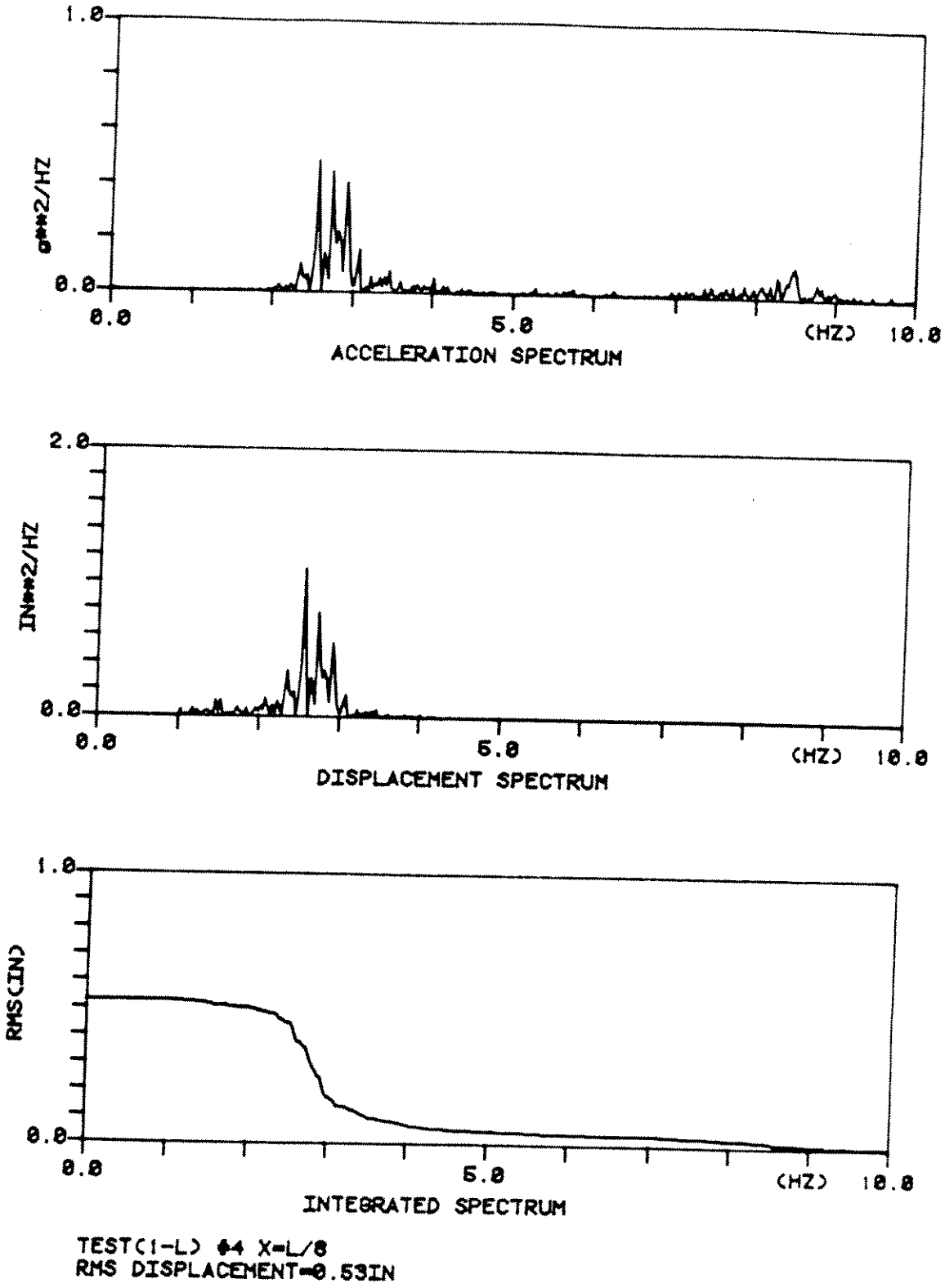

Figure 7.3: Response spectra at $x = L/8$ for Test(1-L)(SFP1 and T=96 lbs)

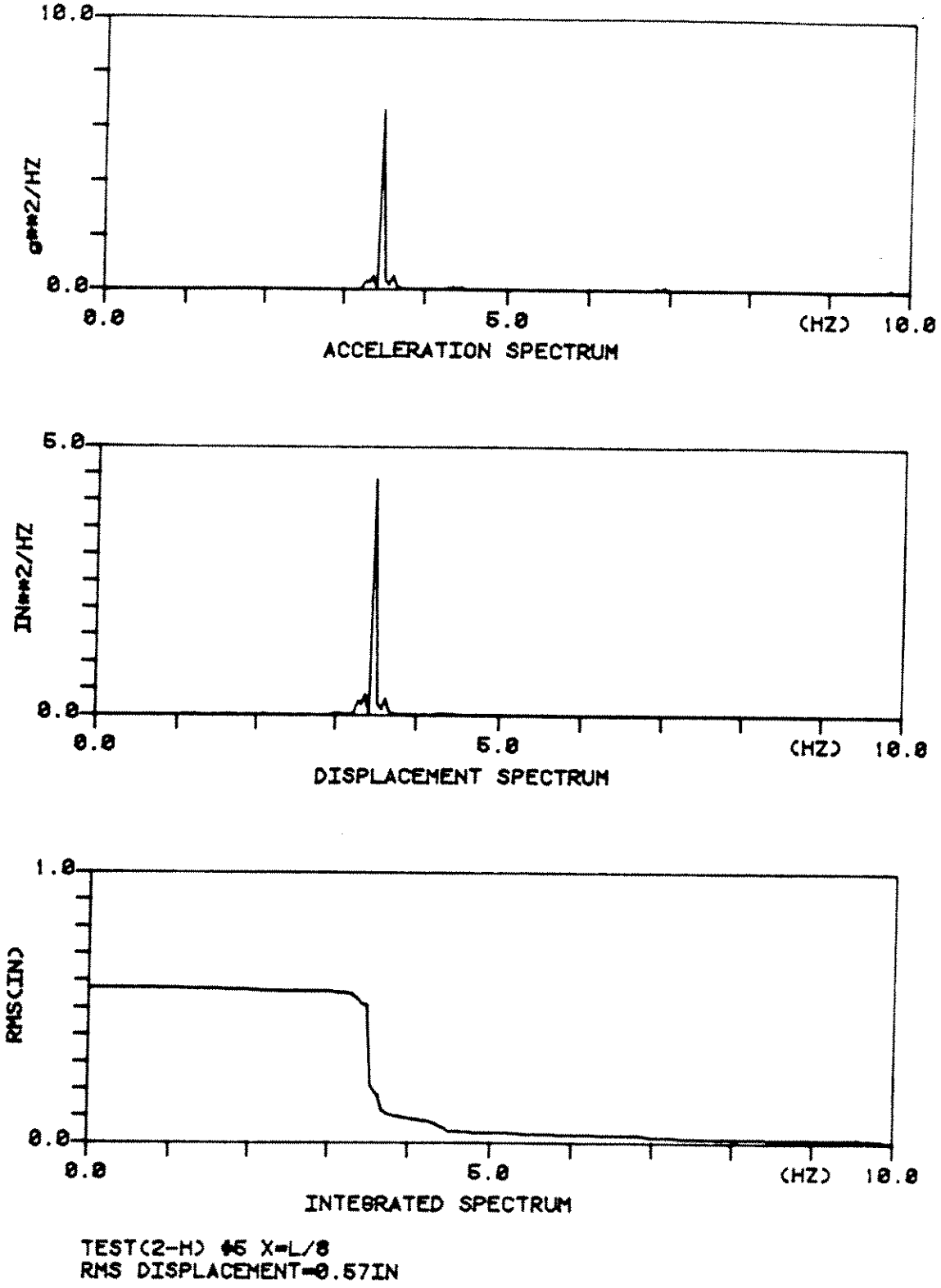

Figure 7.4: Response spectra at $x = L/8$ for Test(2-H)(SFP2 and T=349 lbs)

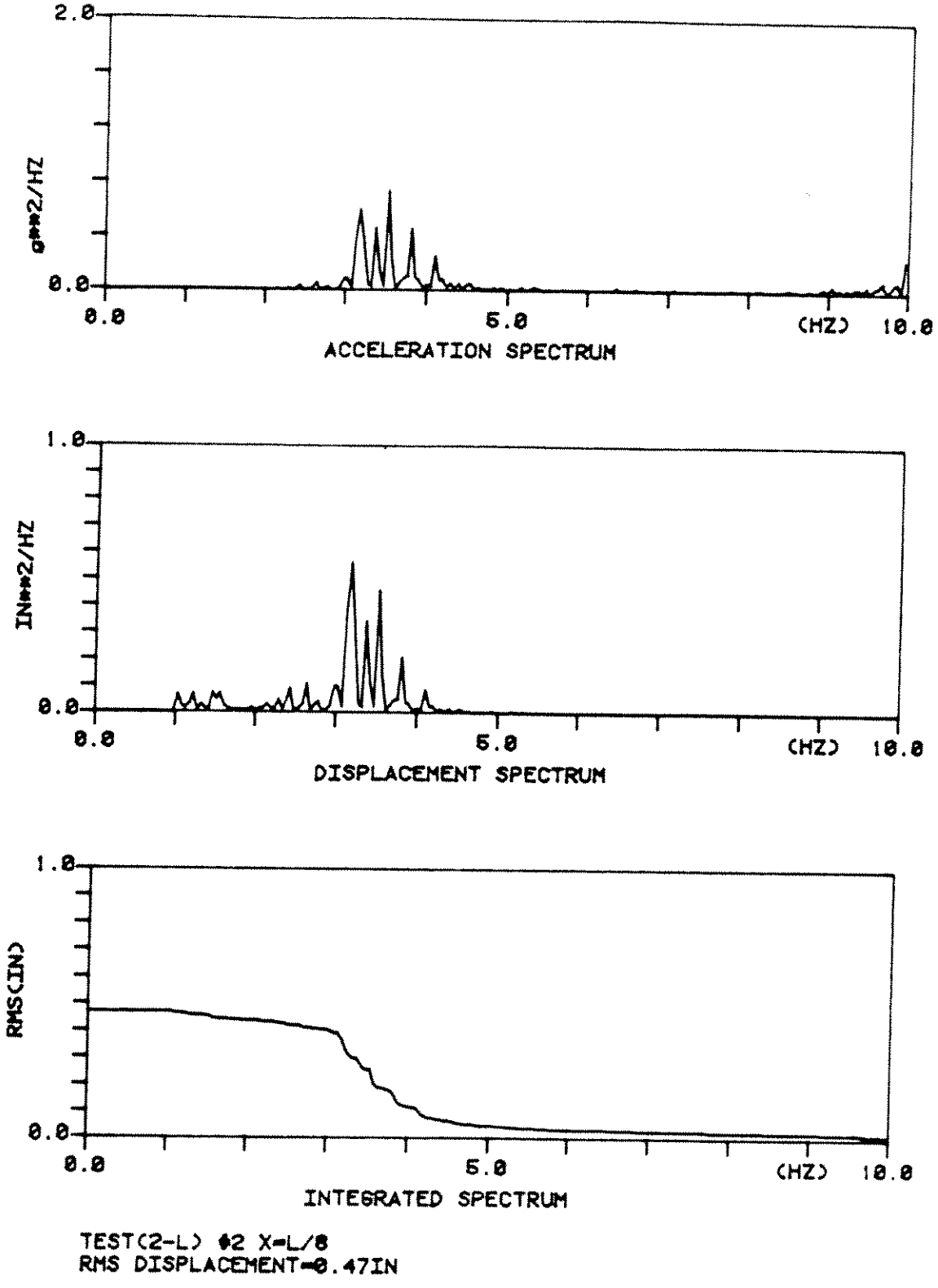

Figure 7.5: Response spectra at $x = L/8$ for Test(2-L)(SFP1 and T=62 lbs)

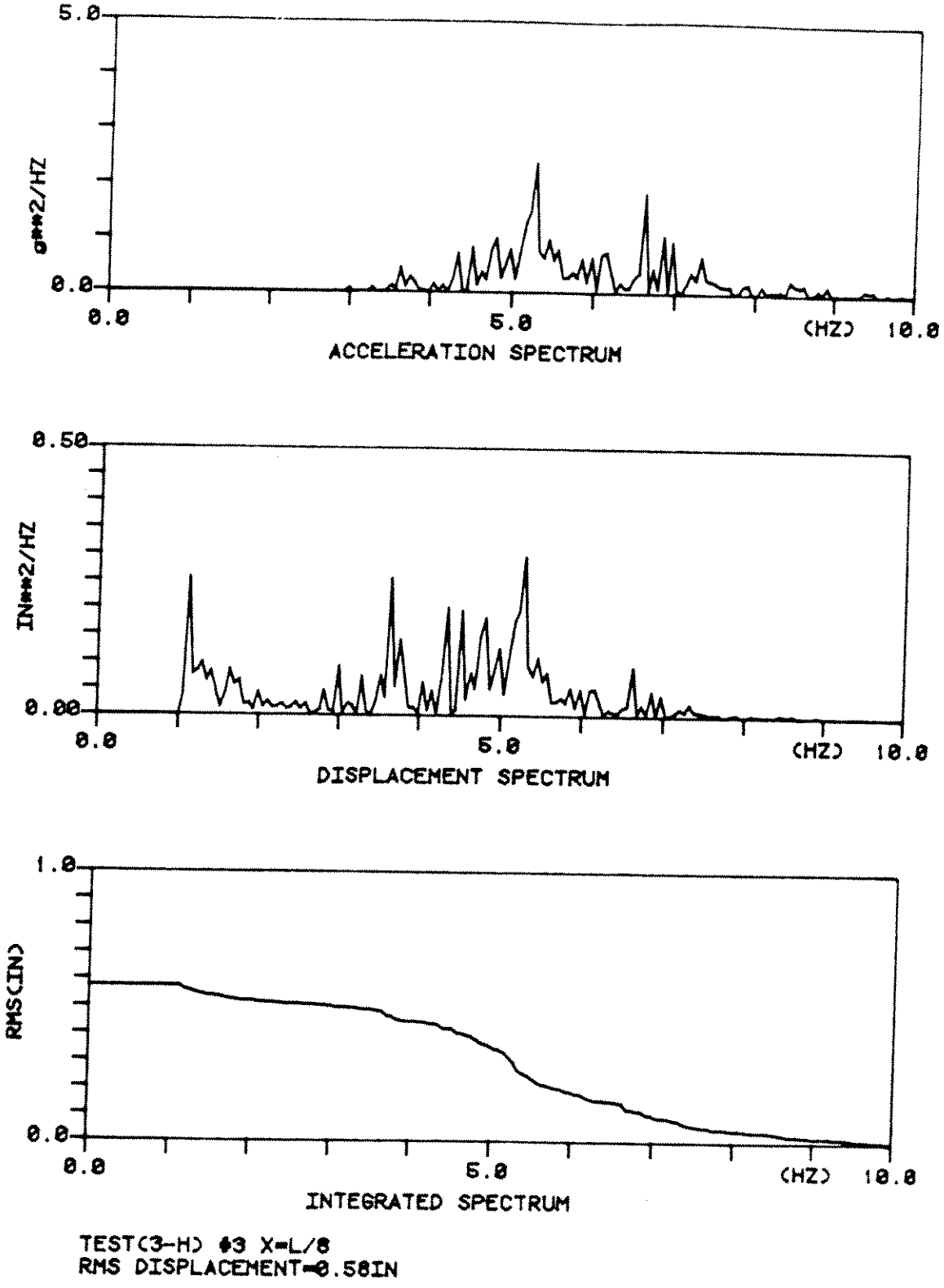

Figure 7.6: Response spectra at $x = L/8$ for Test(3-H)(SFP3 and T=344 lbs)

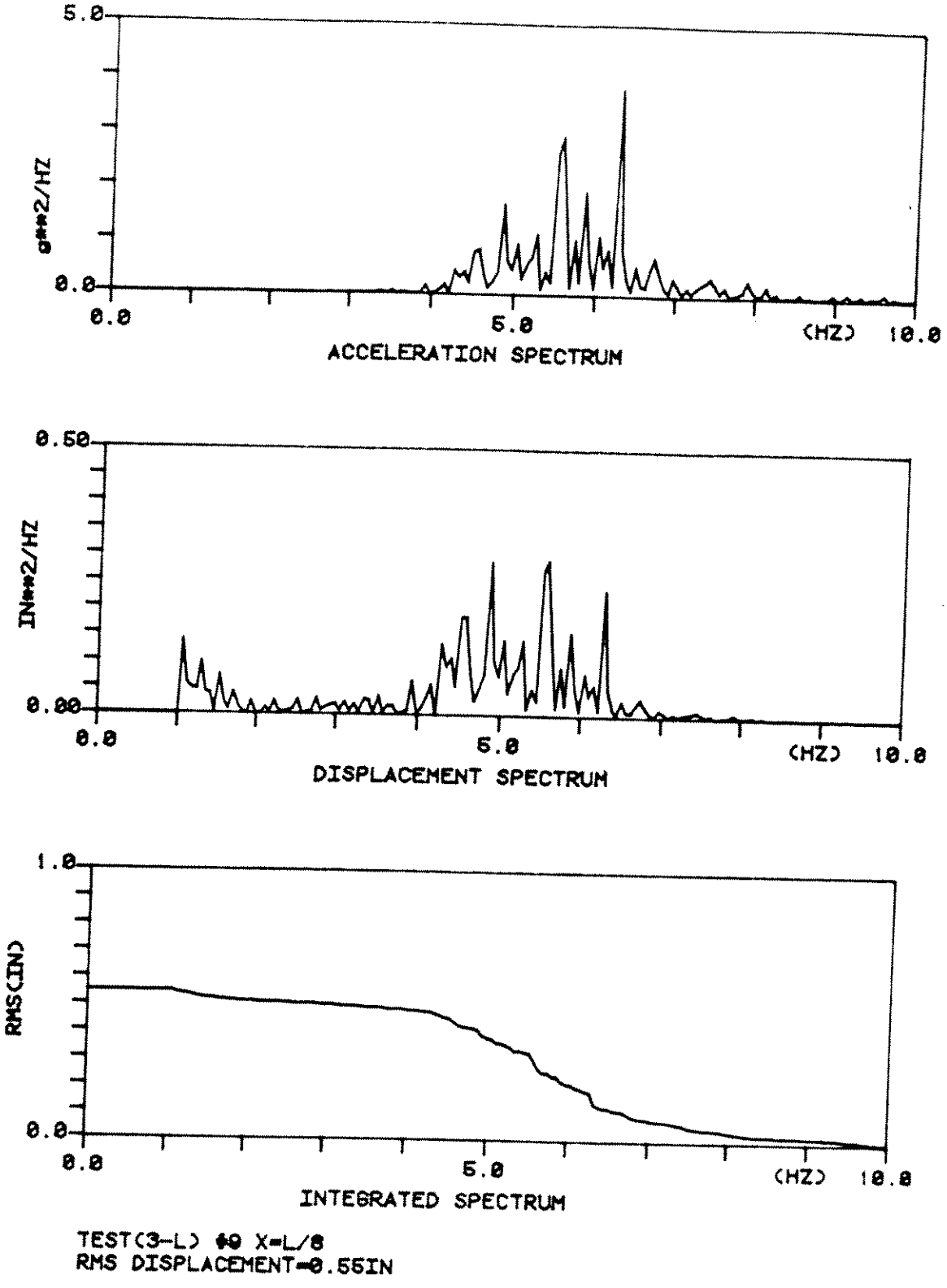

Figure 7.7: Response spectra at $x = L/8$ for Test(3-L)(SFP3 and T=145 lbs)

illustrate this conclusion.

2. Different tension in test conditions with the same flow profile causes different modes and a different number of modes to be involved in the response. However, if there is a strong shear, little difference can be seen in the respective response spectra. The results of Test (3-H) in Figure 7.6 and Test (3-L) in Figure 7.7 illustrate this conclusion.

3. Under less sheared conditions than discussed in item (2) above, the dynamic response characteristics can be totally different due to the difference of the given tension, particularly if lockin occurs. In high tension Test (2-H) in Figure 7.4 and the low tension Test (2-L) in Figure 7.5 were carried out with the same medium shear flow condition (SFP2). The two response spectra are totally different. The reason for this difference is that the possible modes excited by the flow in Test (2-H) is much smaller than those in Test (2-L). The possible modes excited by the flow in Test (2-H) Figure 7.4 are from the 1st to 4th modes but the possible modes excited by the flow in Test (2-L) are from the 1st to 9th modes.

4. In Test (2-H) a single mode was able to dominate the response, whereas in Test (2-L) several modes contributed. A similar lockin case was observed in the response spectra of Test (1-H) (almost uniform flow, SFP1, and high tension) as shown in Figure 7.2. Qualitatively speaking, as the number of modes excited by the flow decreases, the likelihood of lockin increases. When lockin of any single mode occurs, it is usually the highest mode of the possibly excited modes which dominates as seen in the response spectra of Test (2-H) in Figure 7.4. In that case the possible resonantly responding modes were the 1st, 2nd, 3rd, and 4th mode, but the 4th mode was the dominant one. Figure 7.8 shows spatial variation of the response spectra of Test (2-H).

5. The most important experimental result was the observation of substantial response amplitude and frequency variation from high to low velocity regions of

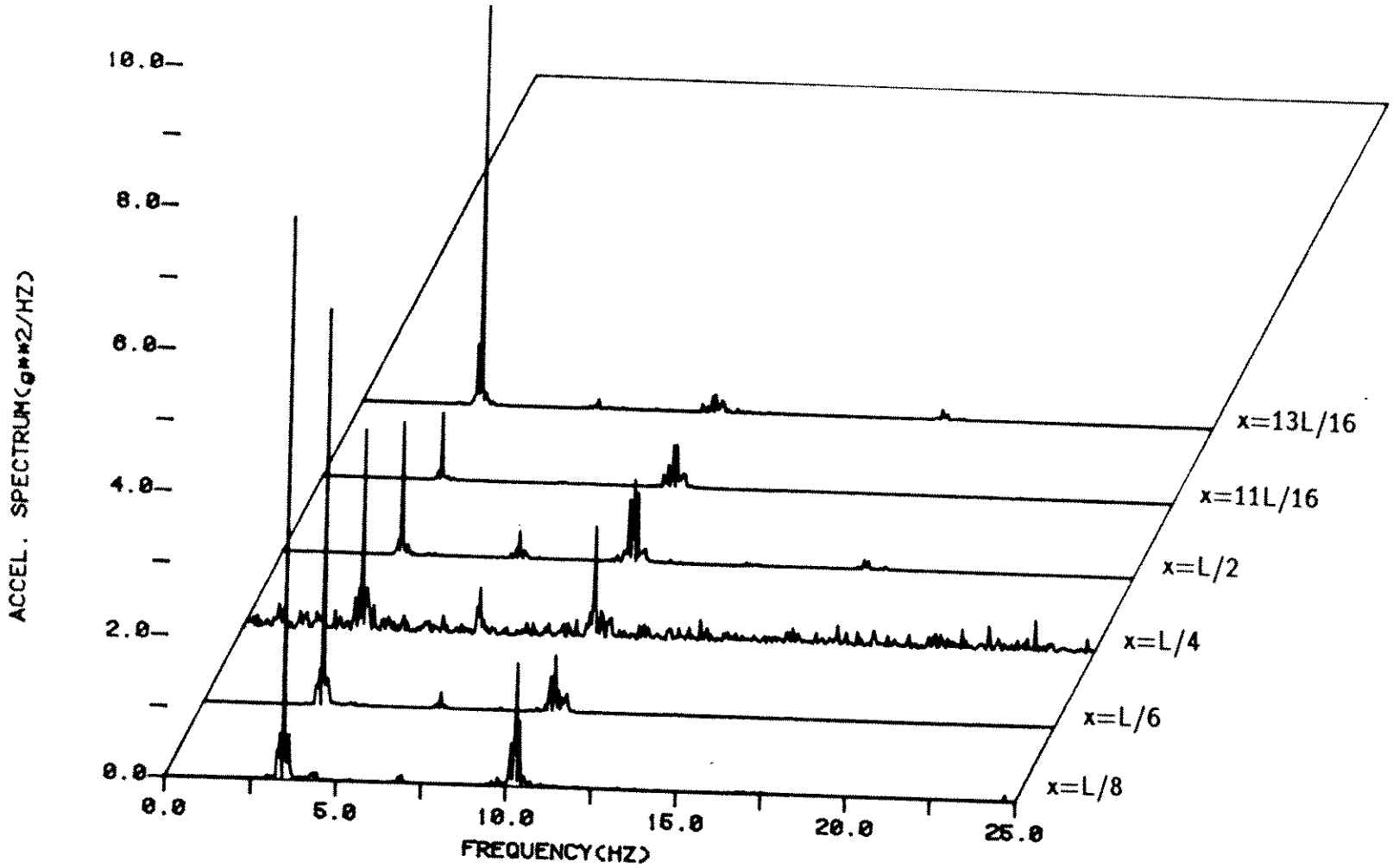

Figure 7.8: Acceleration response spectra for Test(2-H) (SFP2 and T=349 lbs)

the cylinder. Hydrodynamic damping is responsible for this variation. This will be discussed at length in the next section. Generally, for non-lockin cases, the high velocity locations had higher response than the lower velocity regions. The representative value of the rms displacement to diameter ratio was 0.4 to 0.5 for the high velocity region and 0.2 to 0.3 for the low velocity region.

7.4 Experimental Observations of Hydrodynamic Damping

Under ideal, uniform flow, single mode, lockin conditions, experiments of many investigators have revealed that the non- hydrodynamic sources of damping (structural damping) regulate the response. The reduced damping parameter incorporates this concept. The interpretation of the reduced damping parameter under sheared flow conditions is discussed at length in reference(Vandiver 1985[19]). In that paper the author suggests that under sheared conditions hydrodynamic sources of damping must be included in any attempt to predict response. In this paper compelling evidence is given to support that conclusion.

The structural damping measured by free vibration decay tests in air for the test cable in this experiment was about 0.3% of critical for modes corresponding to the frequency ranges and tensions later experienced in the water. As will be shown, observed response in sheared flows could only result from effective dampings of 3 to 5% and greater. This additional damping could only come from hydrodynamic sources.

7.4.1 Response of a Low Tension Flexible Hose in a Highly Sheared Flow

Figure 7.9 is a sample time history of the response of the test cable in SFP3, the highly sheared case. Simultaneous sample time histories of cross-flow acceleration

are given for all six measurement locations. It is quite obvious that the high velocity locations had higher response than the low velocity regions. Figure 7.10 is for the same case and shows the acceleration response spectra at three locations, $L/8$ (high speed), $L/2$ (medium flow), and $13L/16$, a location where the mean flow speed was very close to zero. The spectra was clearly attenuated in the low velocity regions. In this case the rms displacement was 0.3 diameters at $x = 13L/16$ and 0.5 diameters at $x = L/8$. The tension was 151 pounds and the natural modes were 0.6 Hz apart. The peak vortex shedding frequency corresponded to about the 10th natural frequency. Enough modes are involved in the response that variation in mode shape is not a particularly important factor when comparing the rms response of one location to another.

In order for the response to have been spatially attenuated as shown, hydrodynamic damping must have been a significant influence. If there had been only structural damping of less than 1%, then $n\zeta$ would have been at most 0.1 and the response of the cable would have revealed essentially no variation in magnitude from the high to low velocity regions. Even though the excitation varies dramatically with position on the cable, the response would only show significant spatial decay if substantial hydrodynamic damping were available. In order to determine the effective modal damping from response records, predictions from a dynamic response model were compared to observations. Considerable insight may be gained from the following simplified example.

Figure 7.11 shows the magnitude squared of the response of the cable to a unit harmonic input force at $L/8$ from one end. The frequency is the natural frequency of the tenth mode. The Green's function is plotted for damping ratios of 3, 4, 6, and 8%. This is similar to the experimental case corresponding to Figures 7.9 and 7.10. The highest velocity portion of the shear near $L/8$ corresponded to resonance with the tenth mode. The author feels that the response observed only could result from a total effective damping in the 3 to 8% range.

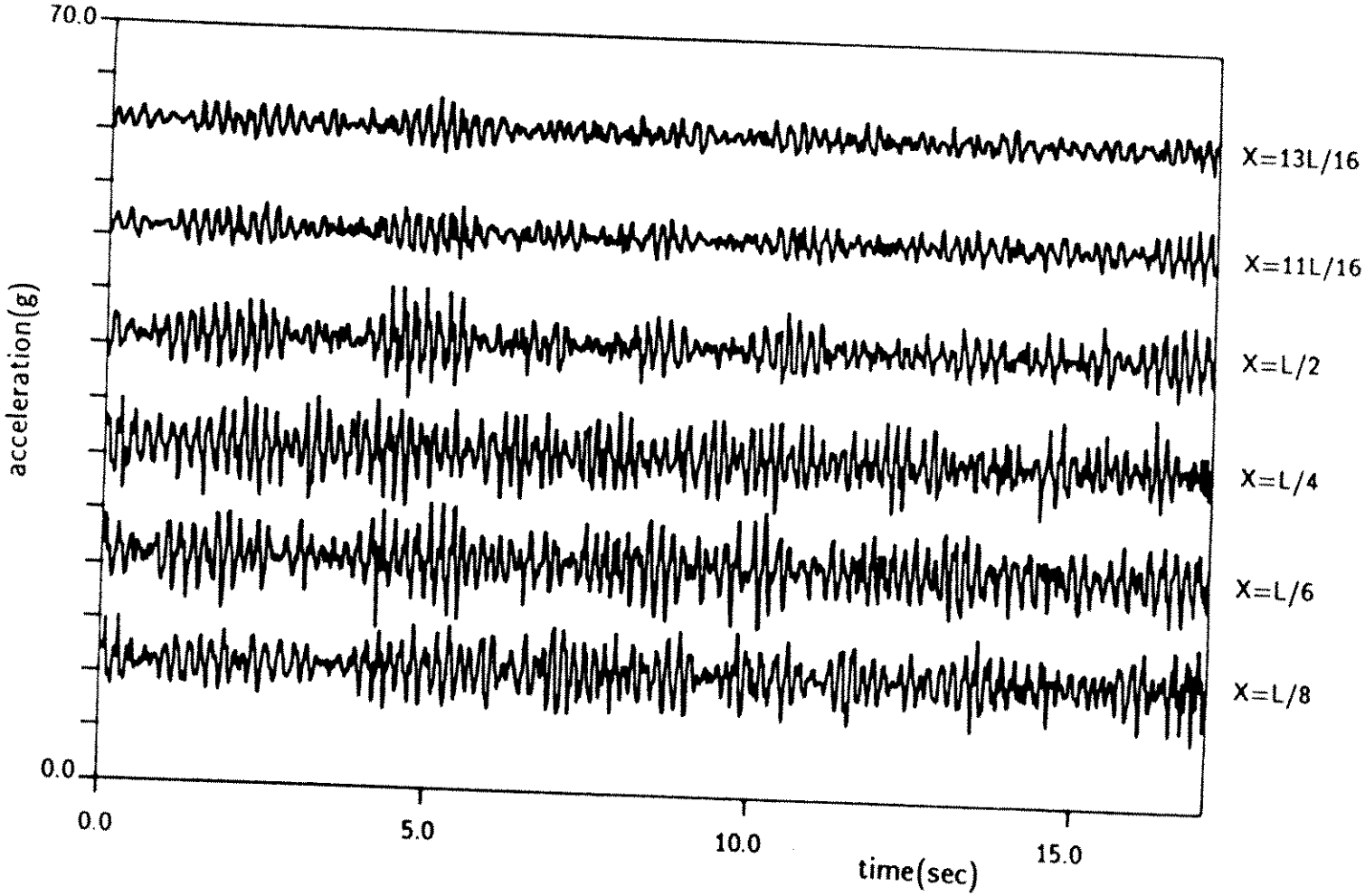

Figure 7.9: Spatially attenuated acceleration time histories in SFP3; T=151lbs

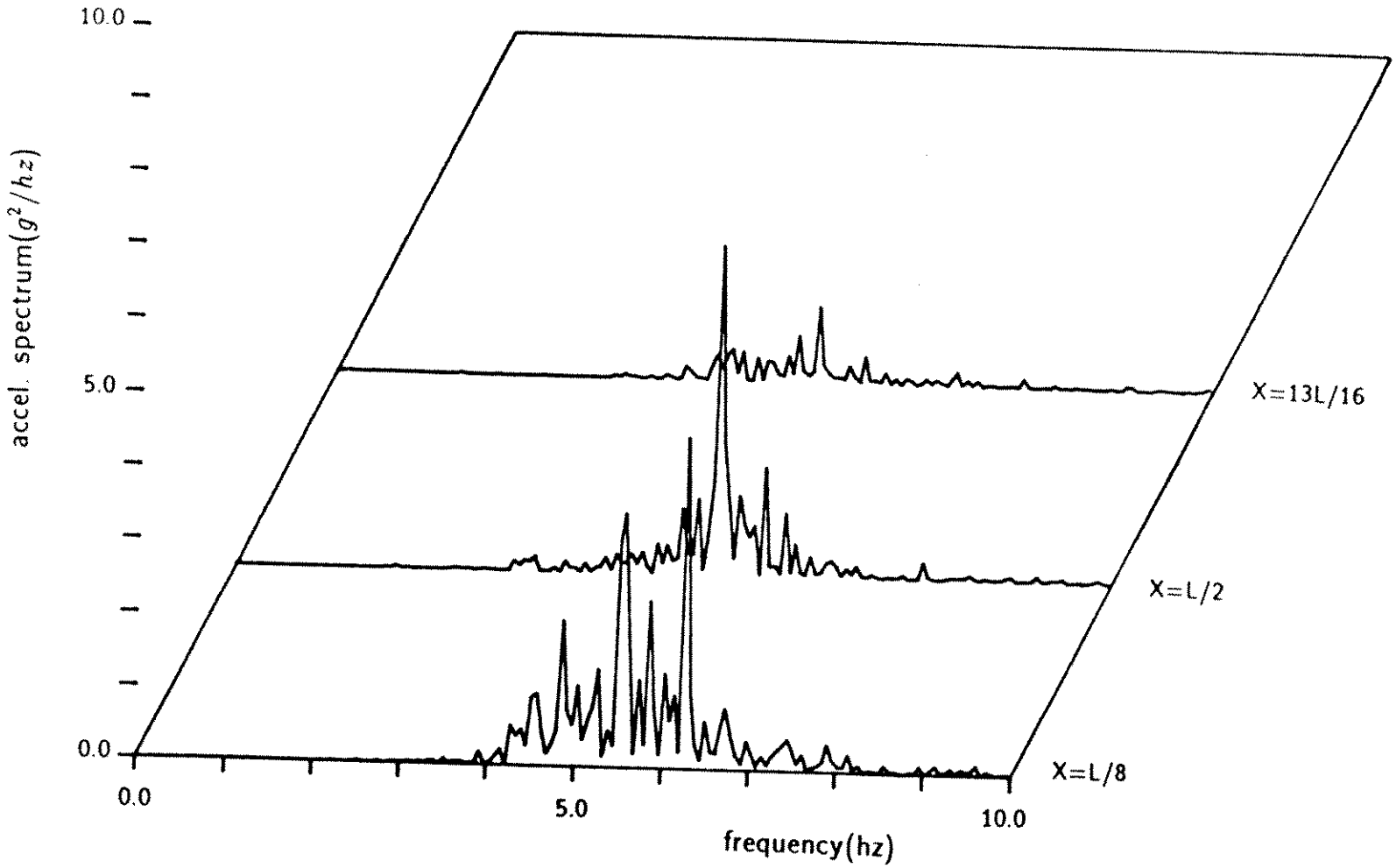

Figure 7.10: Acceleration response spectra for SFP3 and T=151 lbs

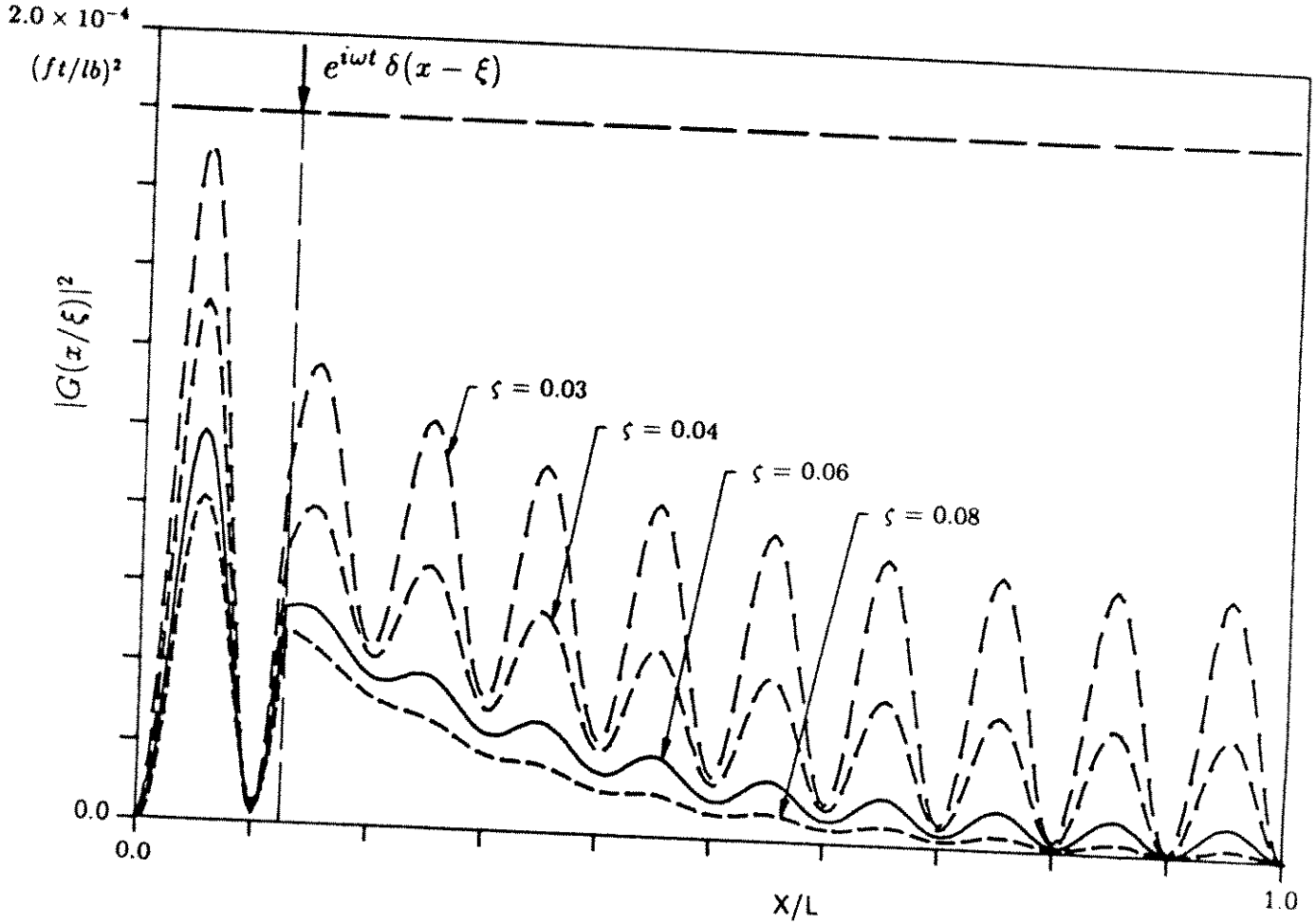

Figure 7.11: Green's function squared: response to a tenth mode resonant excitation applied at $L/8$

7.4.2 Impulse Response Under High Tension in a Turbulent Uniform Flow

With large hydrodynamic damping the vibration excited at one location is attenuated as it travels through the cable to distant points. This was confirmed by an independent measurement. Under steady state flow-induced vibration conditions, the cable was struck impulsively with a wooden pole, at a location near one end. The impulse generated, propagated through the cable. Figure 7.12 shows the simultaneous time histories at all six accelerometer locations. The impulse can be seen to travel from one location to the next with a travel time delay and an attenuation due to damping. By independently examining the spectrum of each accelerometer time history it was possible to estimate the frequency content of the impulse and the effective damping coefficient. The cable tension was 450 pounds, the current was approximately uniform (SFP1). The impulse had most of its energy in the 15 to 24 Hz range. The dominant vortex shedding frequency is indicated in the response peak at 3 Hz in the spectra shown in Figure 7.13. The cable response was dominated by third mode response at a natural frequency of 3.0 Hz. The reduced velocity was approximately 5 corresponding to an average but turbulent flow speed of 1.4 ft/sec.

By assuming an exponential decay with distance traveled, it was possible to estimate the effective damping by comparing the magnitudes of the acceleration response spectra in the 15 to 24 Hz band. Figure 7.13 is an example. Two spectra are shown. The locations were separated by 19.3 feet. If one assumes that the ratios of the two spectra are exponentially related then

$$\frac{S(x+l,\omega)}{S(x,\omega)} = e^{-2\varsigma kl} = e^{-2\varsigma\omega l/C_p} \simeq \frac{1}{6} \tag{7.1}$$

Choosing a typical frequency of f=18 Hz , and noting that $\omega = 2\pi f$, l=19.3 feet, C_p=120 feet/sec, and the ratio of the spectra is approximately six to one, results in an estimate of ς=0.049 or 4.9%. Many similar calculations were performed between different locations and for different impulse events. The results fell into a range of 4 to 6% damping. The spectra shown in Figure 7.13 are typical in that the attenuation

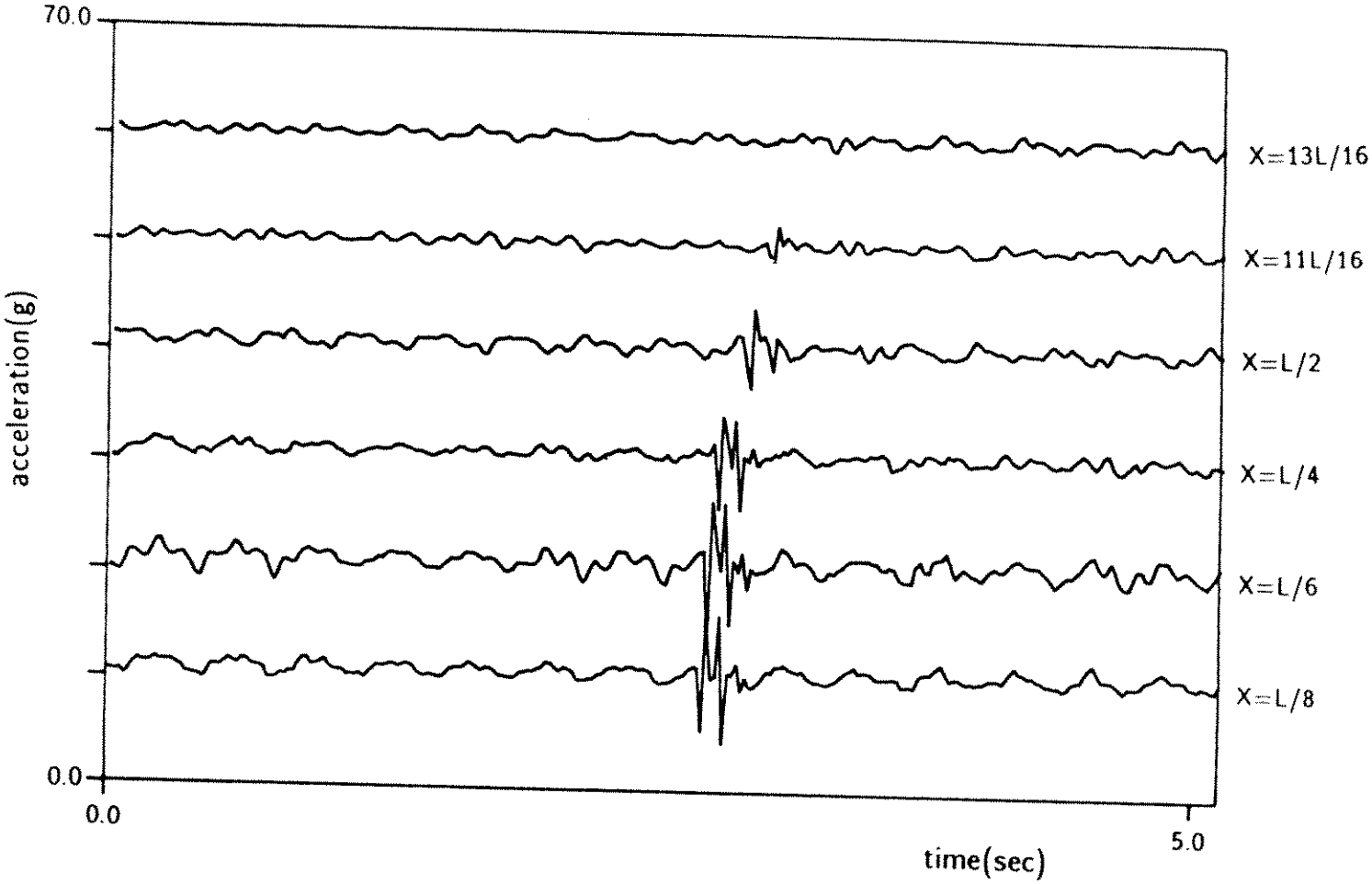

Figure 7.12: Impulse propagation time histories; impulse at L/20, T=450 lbs, V=1.4 ft/sec

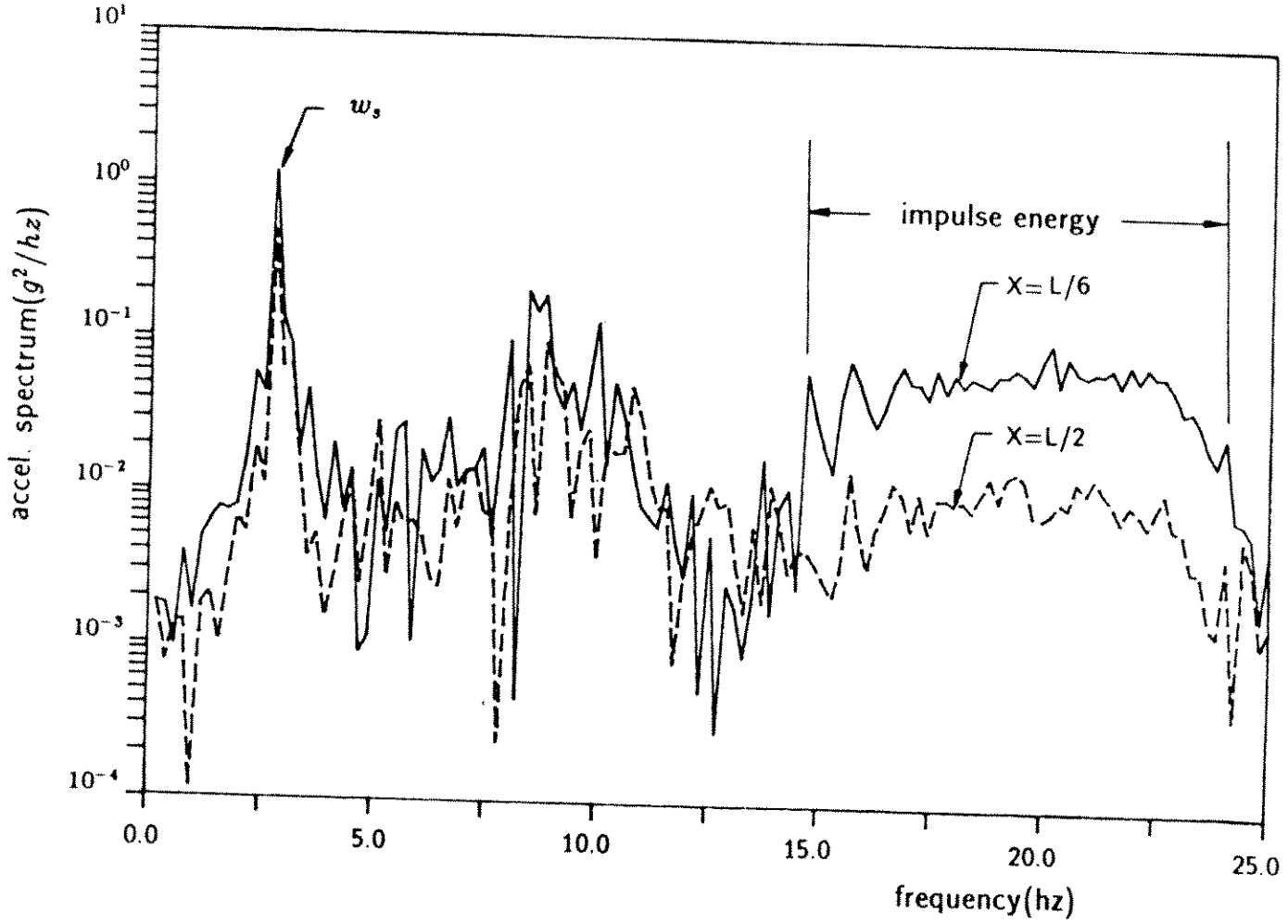

Figure 7.13: Response spectra at L/6 and L/2 with impulse and flow excitation

between the two spectra in the 15 to 24 Hz band is approximately constant which indicates a frequency dependent damping which decreases with increasing frequency. This agrees with the conclusion explained in the section on damping prediction for infinite cables.

Chapter 8

Comparison between Predicted and Experimental Results

8.1 Implementation of the Response Prediction Model

A computer program was written to implement the response prediction method described in chapter four. This program can at present be applied to the response prediction of a constant tension, uniform cable in a monotonically increasing sheared flow.

Estimation of damping is completed based on the hydrodynamic damping model in Section 4.4.1. The lift force spectrum (as modeled in Section 4.4.2) is calculated at numerous discrete points in space and frequency. Using the estimated damping value and the lift force spectrum, the displacement response spectrum at location x is obtained numerically:

$$\begin{aligned} S_{vv}(x,\omega_k) &= \int_0^L d\xi \int_0^L d\xi' S_{f_\xi f_{\xi'}}(\xi,\xi',\omega) G(x/\xi) G^*(x/\xi') \\ &= (\frac{L}{n_s})^2 \sum_{i=1}^{n_s} \sum_{j=1}^{n_s} S_{f_\xi f_{\xi'}}(i,j,\omega_k) G(x/i) G^*(x/j) \end{aligned} \tag{8.1}$$

where

$S_{yy}(x,\omega_k)$ = the displacement response spectrum
at location x and $\omega = \omega_k$

$\Delta\omega$ = resolution in frequency domain

n_s = number of segments in the span L

L/n_s = resolution in space

$S_{f_\xi f_{\xi'}}(i,j,\omega_k)$ = lift force spectrum
at $\xi = \frac{iL}{n_s}$, $\xi' = \frac{jL}{n_s}$ and $\omega = \omega_k$

$G(x/\xi)$ = the Green's function at x excited at $\xi = \frac{iL}{n_s}$

$G^*(x/\xi')$ = conjugate of the Green's function at x excited at $\xi' = \frac{jL}{n_s}$

The acceleration spectrum is calculated from the displacement spectrum as shown below.

$$S_{\ddot{y}\ddot{y}}(x,\omega_k) = \omega_k^4 S_{yy}(x,\omega_k) \tag{8.2}$$

In order to confirm the validity of the present response prediction model for the non-lockin case, sample runs were made for four different test conditions and were compared with the experimental results. The values of input parameters used to determine hydrodynamic damping and hydrodynamic lift force are summarized in Table 8.1. Linear sheared flow profiles which closely approximated the experimental profiles were used in the prediction. C_D, C_a, and C_L were chosen to give good agreement with Test(3-L) and then kept at those values for all other cases. The measured acceleration spectra were averaged 14 times with recordlengths of 1024 data points. The sampling frequencies were 50 Hz for Test(2-H) and Test(2-L)and 60 Hz for Test(3-H) and Test(3-L). Resolution in space was $0.02L$ and resolution in frequency was $0.2Hz$ in the numerical calculation for all test condition. All of the important outputs including the predicted and measured rms displacement are summarized in Table 8.2.

Table 8.1: Summary of the input parameters

Test condition	Test (2-H)	Test (2-L)	Test (3-H)	Test (3-L)
Flow profile	SFP2	SFP2	SFP3	SFP3
Flow velocity(ft/sec)				
min.	0	0	0	0
max.	2.15	2.0	3.5	3.5
One standard deviation of turbulence(ft/sec)	0.25	0.25	0.4	0.4
Tension (lbs)	349	62	344	145
Structural damping ratio	0.003	0.003	0.003	0.003
Drag force coeff. C_D	1.0	1.0	1.0	1.0
γ^*	1.0	1.0	1.0	1.0
Added mass coeff. C_a	1.0	1.0	1.0	1.0
Correlation length coeff. l_c^{**}	0.125	0.06	0.07	0.05
Mean square lift coeff. C_L^2	2.0	2.0	2.0	2.0
Coeff. of higher harmonics				
$C_{L,2}$	0.1	0.04	0.04	0.04
$C_{L,3}$	0.15	0.06	0.06	0.06
$C_{L,4}$	0.0025	0.001	0.001	0.001
$C_{L,5}$	0.025	0.01	0.01	0.01

* γ is the parameter which accounts for the effect of the response amplitude on the hydrodynamic damping. $\gamma = 1$ neglects the response amplitude effect on the hydrodynamic damping. This gives a lower bound estimate of damping for any assumed C_D.

** $l_c = \frac{1}{2n_{max}}$ for each case

Table 8.2: Summary of the output

Test condition	Test (2-H)	Test (2-L)	Test (3-H)	Test (3-L)
Flow profile	SFP2	SFP2	SFP3	SFP3
Flow velocity(ft/sec)				
min.	0	0	0	0
max.	2.15	2.0	3.5	3.5
Tension (lbs)	349	62	344	145
Calculated first natural freq.(Hz)	0.92	0.39	0.91	0.59
Standard deviation of excitation spectrum(Hz)	1.07	1.07	1.71	1.71
Peak mode number excted by the flow, n	4	9	7	11
Estimated damping ratio for the peak mode, ζ_n	0.046	0.056	0.058	0.064
$n\zeta_n$	0.18	0.50	0.41	0.70
Rms displ. at $x = L/8(in)$				
predicted	0.59	0.55	0.62	0.52
*measured**	0.57	0.45	0.51	0.50
Rms displ. at $x = 13L/16(in)$				
predicted	0.54	0.38	0.37	0.34
*measured**	0.53	0.46	0.39	0.41

* Cut-off frequency for integration of acceleration spectra to get rms dispacement was 1.0 Hz.

The results which will be shown for each test condition consist of four figures:

1. Predicted acceleration spectra at $x = L/8$(high flow velocity region) and $x = 13L/16$(near zero flow velocity region)

2. Predicted and measured acceleration spectra at $x = L/8$(high flow velocity region)

3. Predicted and measured acceleration spectra at $x = 13L/16$ (near zero flow velocity region)

4. Predicted and measured integrated displacement spectra at $x = L/8$ and $x = 13L/16$

In this chapter, two extreme cases will be shown. One is the high tension and low shear case (Test(2-H)) and another is the low tension and high shear case(Test(3-L)). The results of two other cases(Test(2-L) and Test(3-H)) are shown in Appendix B.

The results for Test (2-H)(the slightly sheared flow, SFP2, and high tension) are shown in Figure 8.1 to Figure 8.4. The predicted acceleration spectra at the two locations, $x = L/8$ and $x = 13L/16$, in Figure 8.1 do not show much spatial attenuation of the response. As discussed in chapter 3 and chapter 4, $n\zeta_n$ is an important parameter in determining the cable's behavior. When $n\zeta_n$ is less than 0.2, single mode resonant response may dominate the total response. For Test (2-H) $n\zeta_n = 0.18$, and is therefore on the borderline in behavior. In this case the response was not lockin. The predicted result shows quite good agreement with the experimental results as shown in Figure 8.2 to Figure 8.4. Figure 8.4 shows the rms displacement response or a cumulative integral of the spectrum from high to low frequency.

The results for Test (3-L)(the highly sheared flow, SFP3, and low tension)are shown in Figure 8.5 to Figure 8.8. The predicted acceleration spectra at the two locations, $x = L/8$ and $x = 13L/16$, as shown in Figure 8.5 reveal a large spatial attenuation of response. The estimated value of $n\zeta_n$ was 0.7. For values of $n\zeta_n$ between 0.2 and 3, significant spatial attenuation occurs over the length of the cable

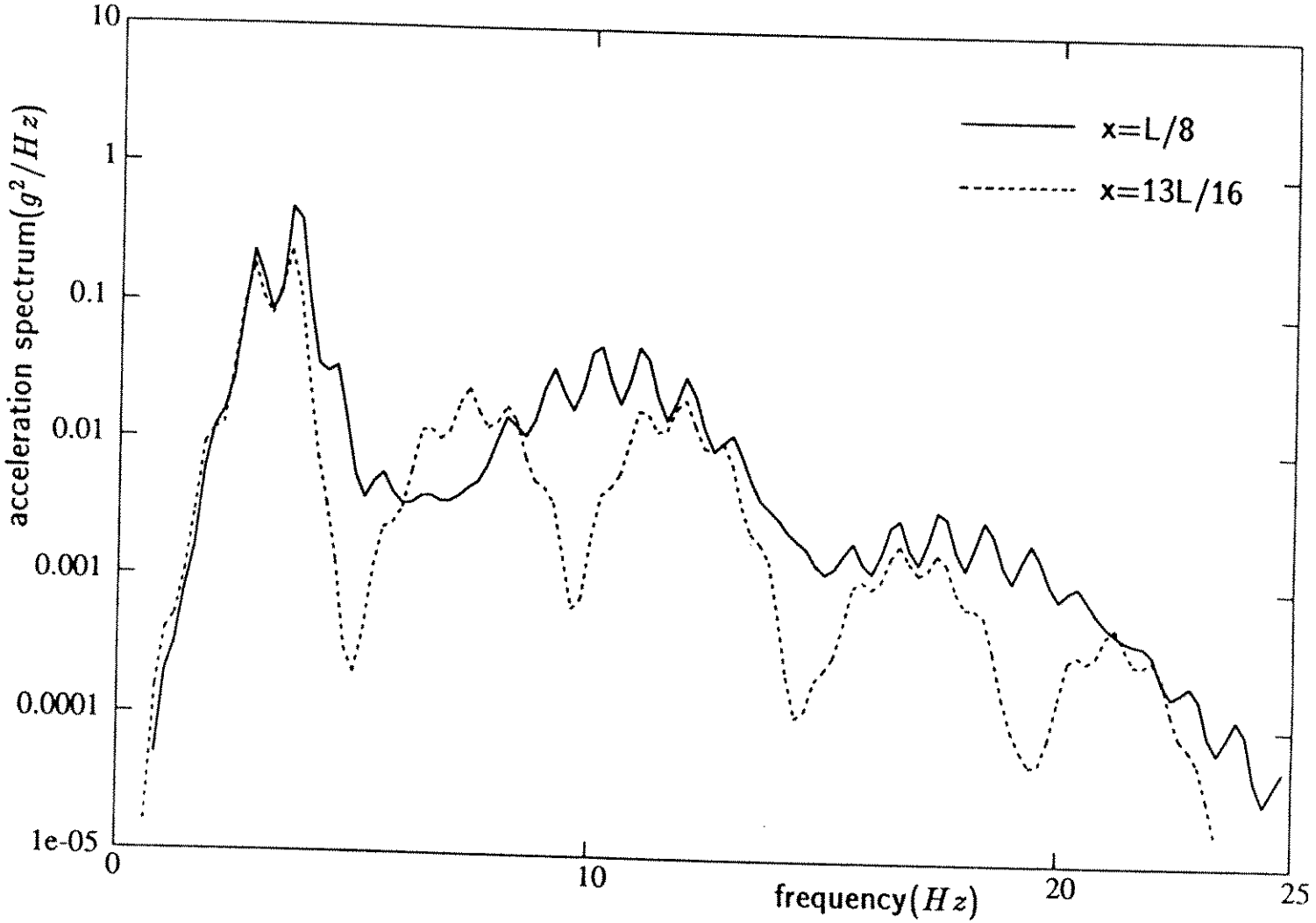

Figure 8.1: Predicted acceleration spectra at $L/8$ and $13L/16$ for Test(2-H)(slightly sheared flow, SFP2, and T=349 *lbs*)

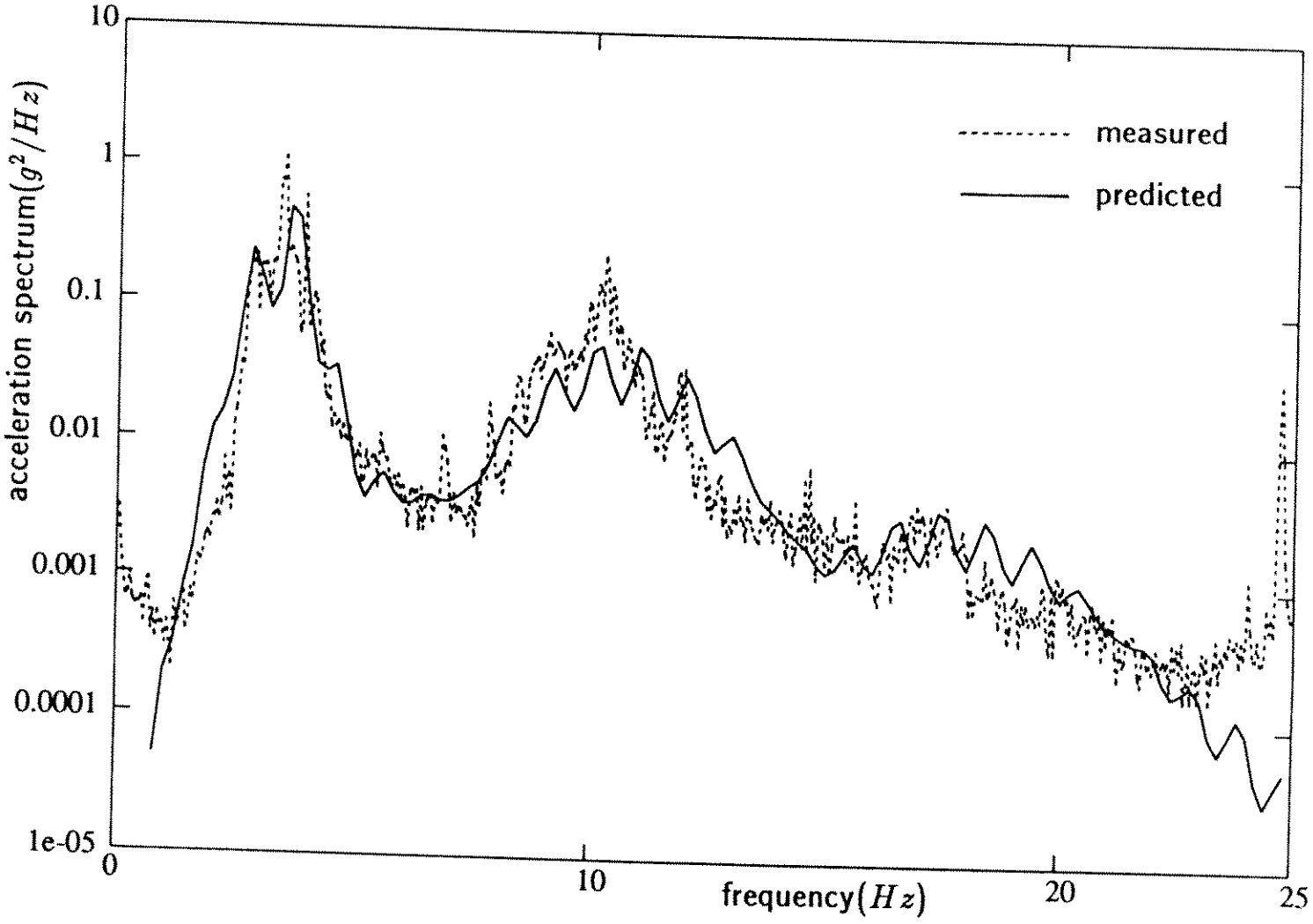

Figure 8.2: Predicted and measured acceleration spectra at $L/8$ for Test(2-H)(slightly sheared flow, SFP2, and T=349 *lbs*)

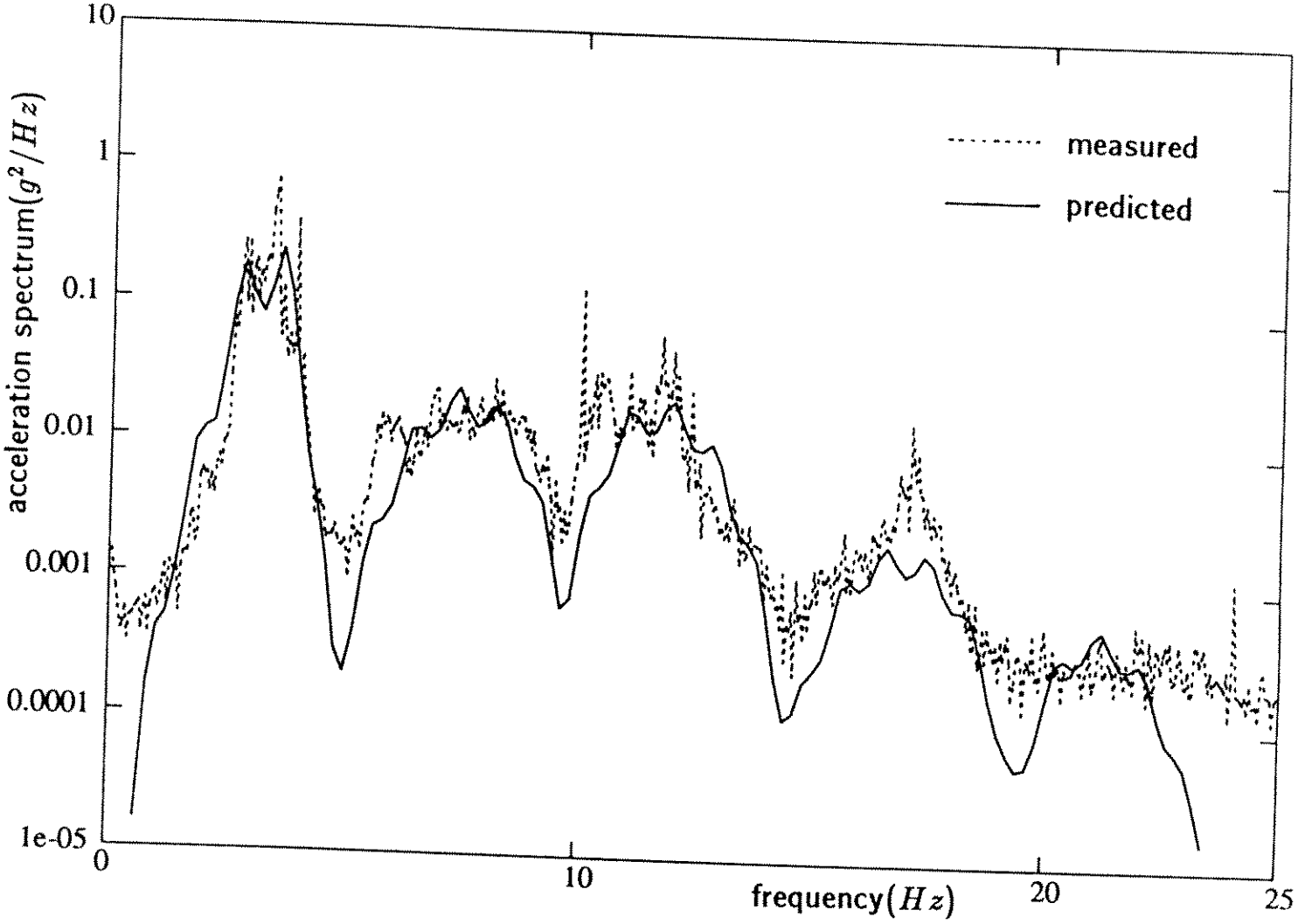

Figure 8.3: Predicted and measured acceleration spectra at $13L/16$ for Test(2-H)(slightly sheared flow, SFP2, and T=349 *lbs*)

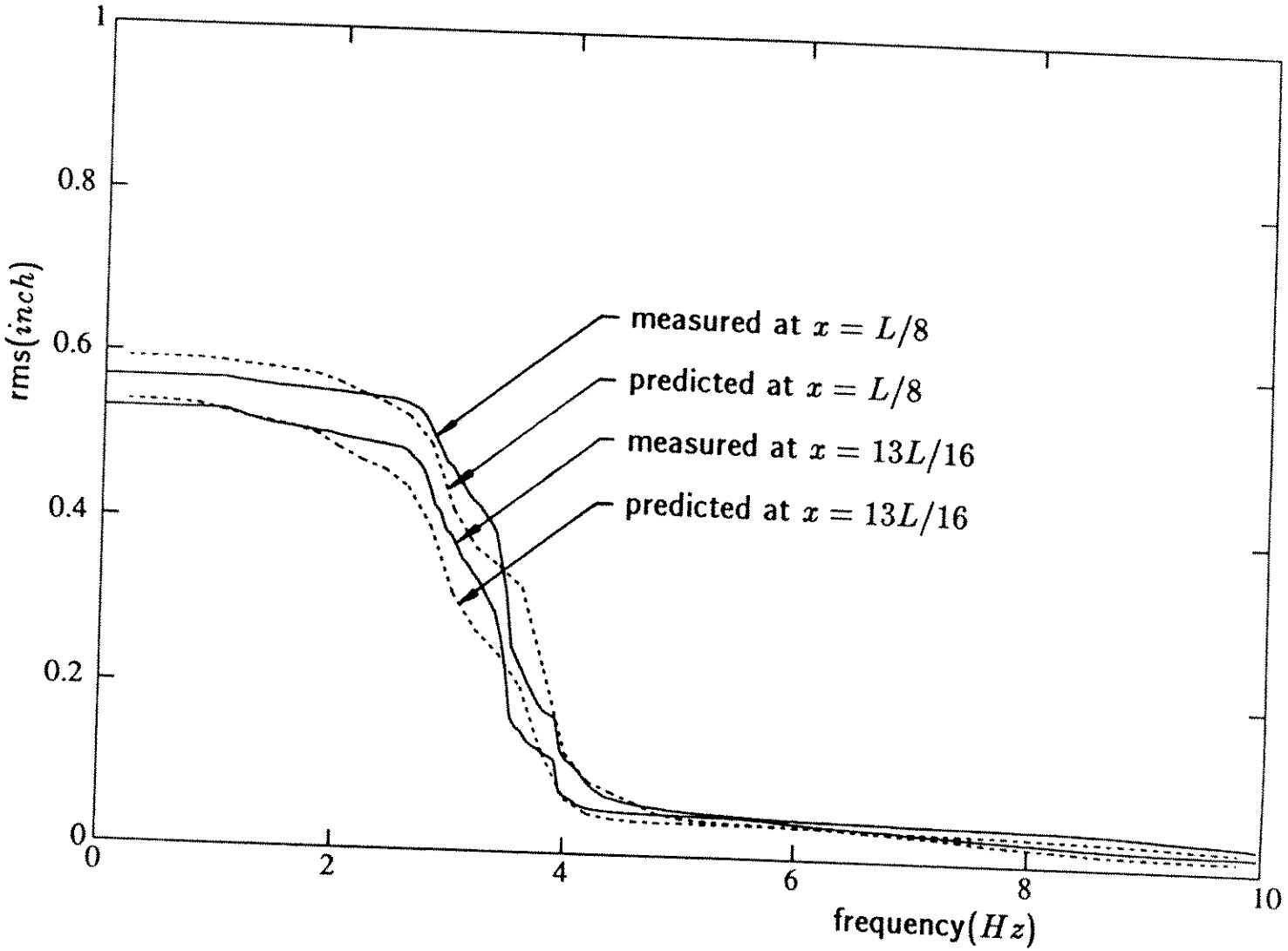

Figure 8.4: Predicted and measured integrated displacement spectra at $L/8$ and $13L/16$ for Test(2-H)(slightly sheared flow, SFP2, and T=349 lbs)

as discussed in chapter3 and chapter4. The greatest difference between the predicted and measured accelerlation spectra at $x = L/8$ in Figure 8.6 occurs in the frequency range of 8 to 11 Hz. The possible reasons for this difference are:

1. Non-stationarity in the flow velocity over the 14 records used in computing the averaged spectrum. The total record length was 4 minutes.

2. Time varying mean tension due to non-stationarity in mean flow velocity and mean drag coefficient.

3. Linear assumption of sheared flow profile

In the prediction model, mean flow velocity and tension are assumed to be stationary in time and in space, but in fact varied with the current. The standard deviation of the reference current velocity measured in the peak flow region was about $\pm 10\%$. The flow profile is assumed to be linear but it is not linear, especially near the canal boundaries. The measured acceleration spectrum at $x = 13L/16$ in Figure 8.7 is larger than predicted in the range of 8 to 13 Hz. The possible error for this may occur in the vector decomposition of acceleration signals. In-line vibration occurs at twice the frequency of the cross-flow and if contained errorneously in the cross-flow data would push up the result in the 8-13Hz range. It should be noted that the measured acceleration spectrum at $x = 13L/16$ is much smoother than the predicted one. The slowly varying mean flow velocity in space and time can be a possible reason for this smoothed result in the acceleration measurement.

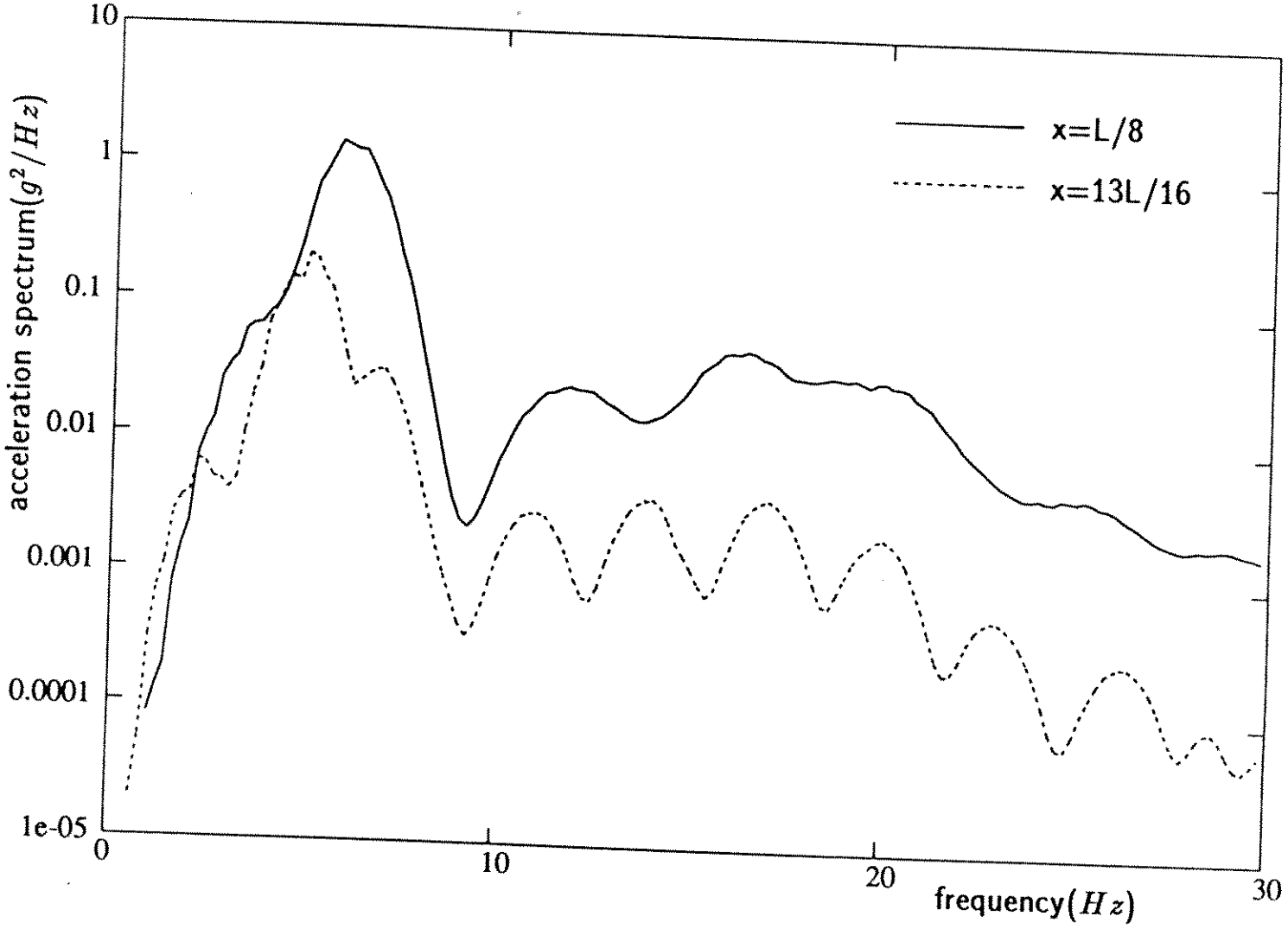

Figure 8.5: Predicted acceleration spectra at $L/8$ and $13L/16$ for Test(3-L)(highly sheared flow, SFP3, and T=145 *lbs*)

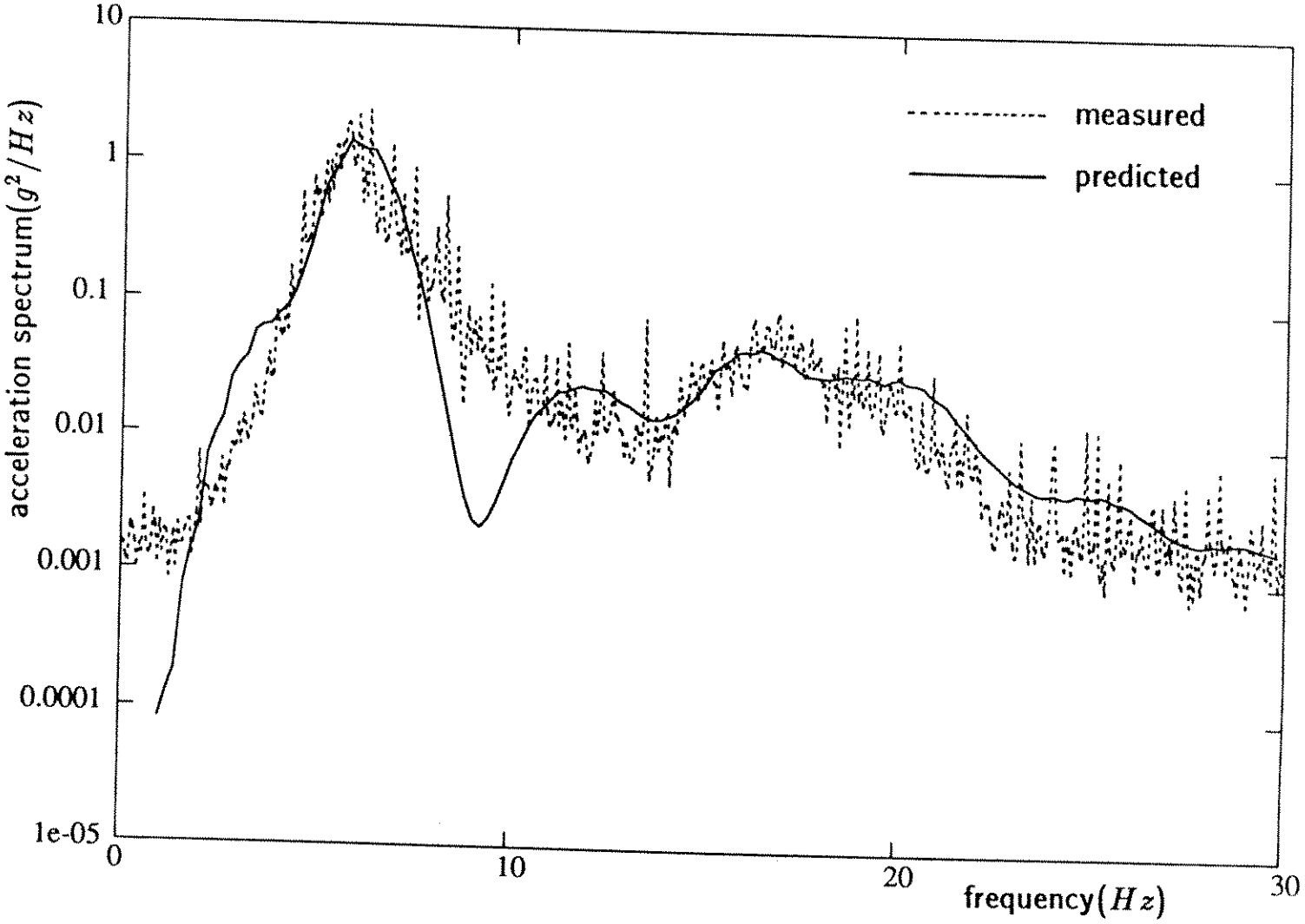

Figure 8.6: Predicted and measured acceleration spectra at $L/8$ for Test(3-L)(highly sheared flow, SFP3, and T=145 *lbs*)

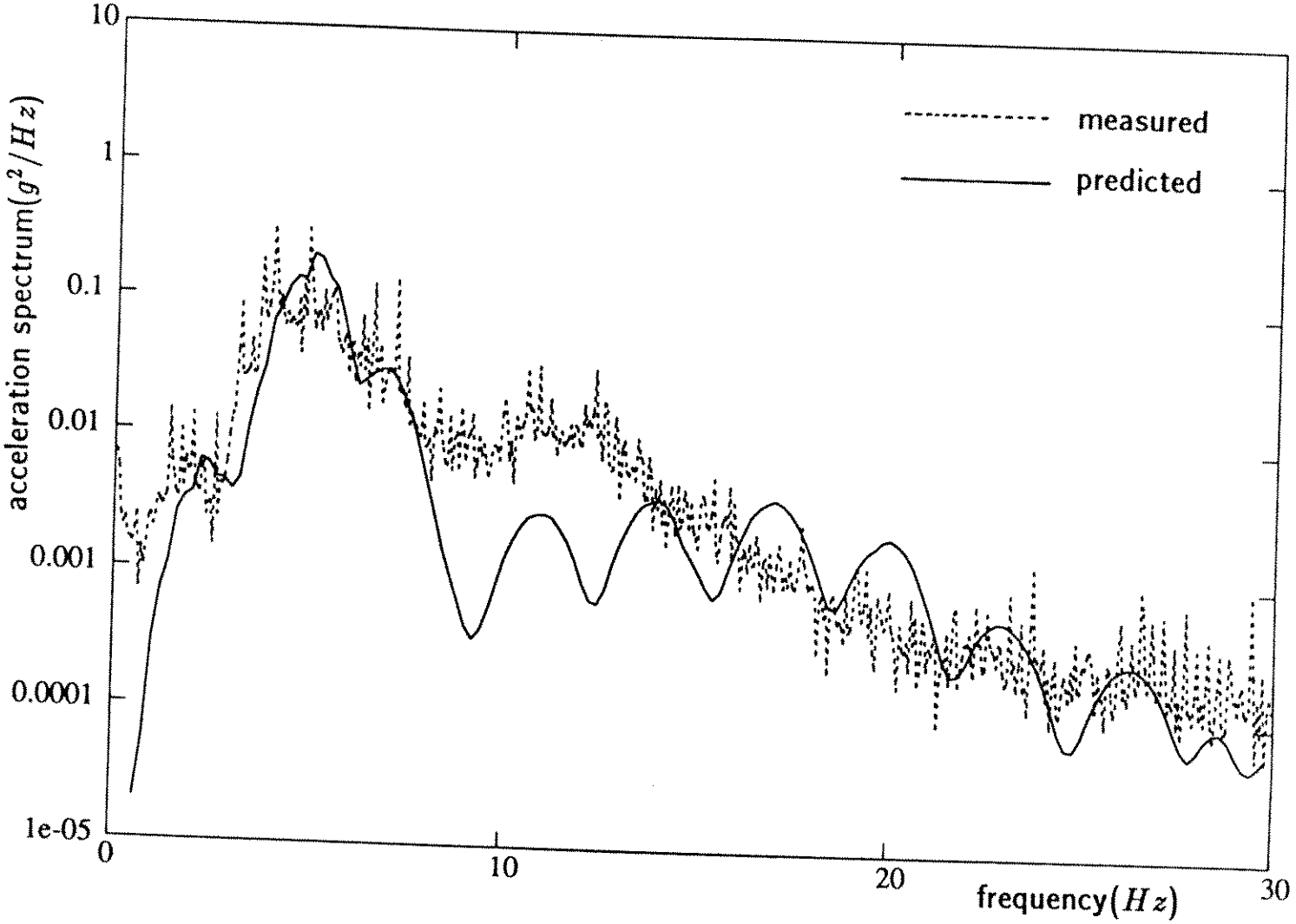

Figure 8.7: Predicted and measured acceleration spectra at $13L/16$ for Test(3-L)(highly sheared flow, SFP3, and T=145 *lbs*)

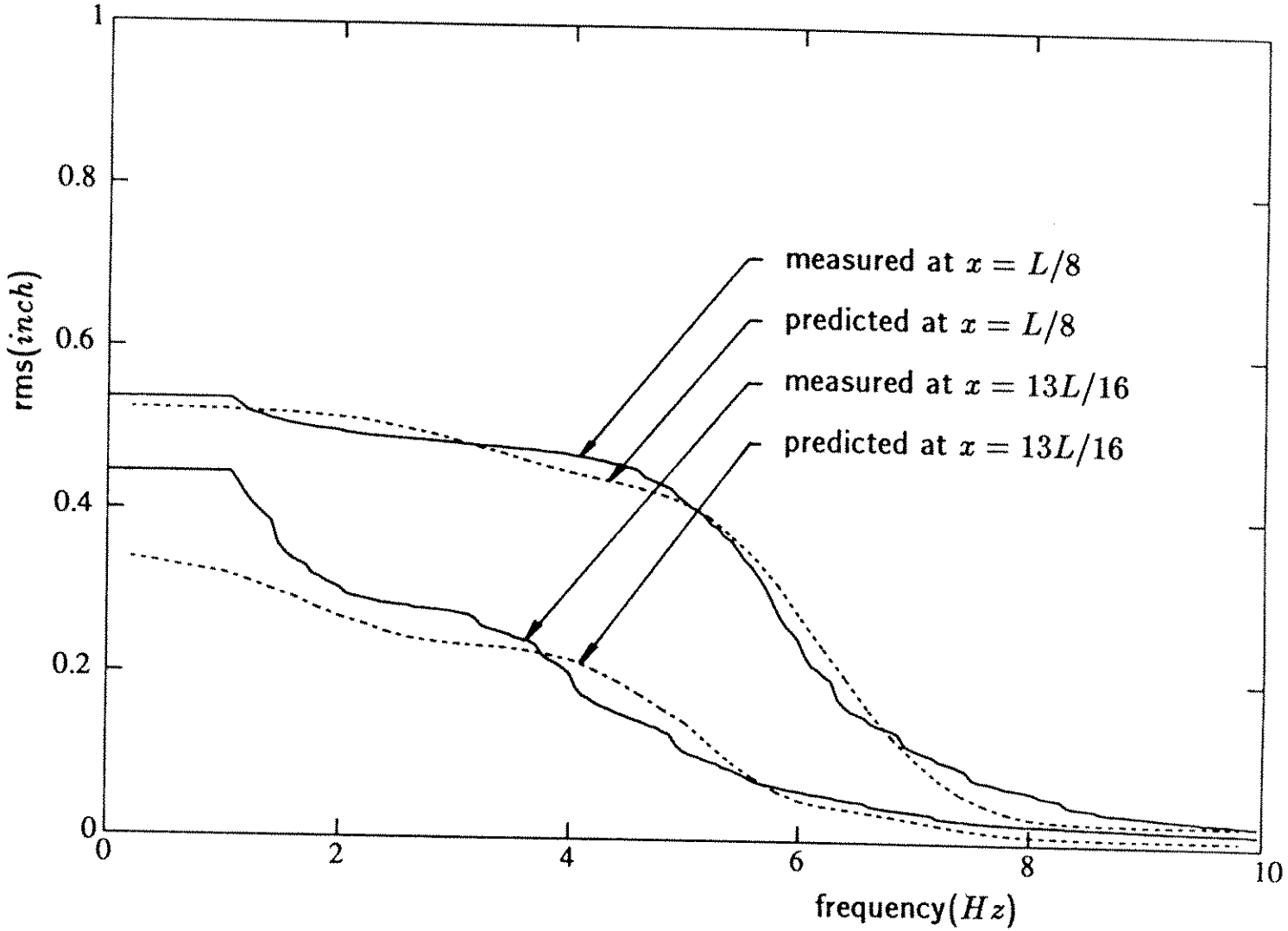

Figure 8.8: Predicted and measured integrated displacement spectra at $L/8$ and $13L/16$ for Test(3-L)(highly sheared flow, SFP3, and T=145 *lbs*)

8.2 Parametric Study in C_L^2, C_D, ΔV_{rms}, l_c and V_{rms}

A parametric study was undertaken to investigate the sensitivity of the predicted response due to variation in the mean square lift coefficient, C_L^2 , drag coefficient, C_D, variation in the standard deviation of turbulence, ΔV_{rms} , spatial correlation length coefficient, l_c , and variation in the maximum flow velocity of the sheared flow profile, V_{max}. Parametric Studies were made for Test (3-L)(highly sheared flow, SFP3, and low tension) by varying one parameter and keeping the other parameters fixed. The values of input parameters used to carry out the sensitivity analysis with the values of predicted rms displacement are summarized in Table 8.3.

Table 8.3: The values of input parameters for sensitivity analysis and predicted responses

Input parameter	C_L^2	y_{rms}^{**}	C_D	y_{rms}	ΔV_{rms}^{***}	y_{rms}	l_c	y_{rms}	V_{max}^{****}	y_{rms}
1	0.25	0.19	0.5	0.67	0.2	0.46	0.025	0.41	3.0	0.53
2	1.0	0.37	[1.0]	0.52	[0.4]	0.52	[0.05]	o.52	[3.5]	0.52
3	[2.0]*	0.52	2.0	0.41	0.6	0.62	0.1	0.59	4.0	0.59

* The values in [ ] represent the values used in the prediction which came closest to the experimental observations.

** y_{rms} is in *inch* scale.

*** ΔV_{rms} is in ft/sec scale

**** V_{max} is in ft/sec scale

Figure 8.9 shows the result of parametric variation of the mean square lift coefficient C_L^2. Three different values of C_L^2, 0.25, 1.0 and 2.0 were used in the prediction of the acceleration spectra at $x = L/8$(high flow velocity region). The results show that increase of the response spectra is linearly proportional to the increase of the mean square lift coefficient C_L^2 as anticipated.

The results of the sensitivity of the computed response to variation in the drag coefficient, C_D , are shown in Figure 8.10. The predicted integrated spectra at $x = L/8$ and $x = 13L/16$ are shown for the values of C_D=0.5, 1.0 and 2.0. Increasing C_D gives not only a decrease in the rms displacement but also more spatial attenuation of the response.

Figure 8.11 shows the results of a parametric variation of the standard deviation of flow turbulence ΔV_{rms}. The predicted acceleration spectra at $L/8$ are shown for the values of ΔV_{rms} of 0.2, 0.4 and $0.6 ft/sec$. Increasing ΔV_{rms} makes the response spectra broader and larger.

The results of variation of the spatial correlation length coefficient l_c is shown in Figure 8.12. The predicted acceleration spectra at $x = L/8$ are shown for the values of l_c of 0.025, 0.05 and 0.1. Increase of the spatial correlation length coefficient l_c makes the response spectrum broader and larger, but for the range of variation used here, from 0.025 to 0.1, variation in l_c has little import.

The change of the maximum flow velocity in the linear flow profile shifts the peak frequency in the response spectrum. Figure 8.13 shows the result of a parametric variation of the maximum flow velocity V_{max}. Generally rms response increases with the increase of V_{max}.

A final variation is shown to reveal the significance of the higher harmonic terms. Figure 8.14 shows the predicted response with and without the higher order lift terms. The variation at high frequencies is very significant. However, this pronounced variation at high frequencies does not make a big difference in the rms displacement results, but is important for acceleration prediction.

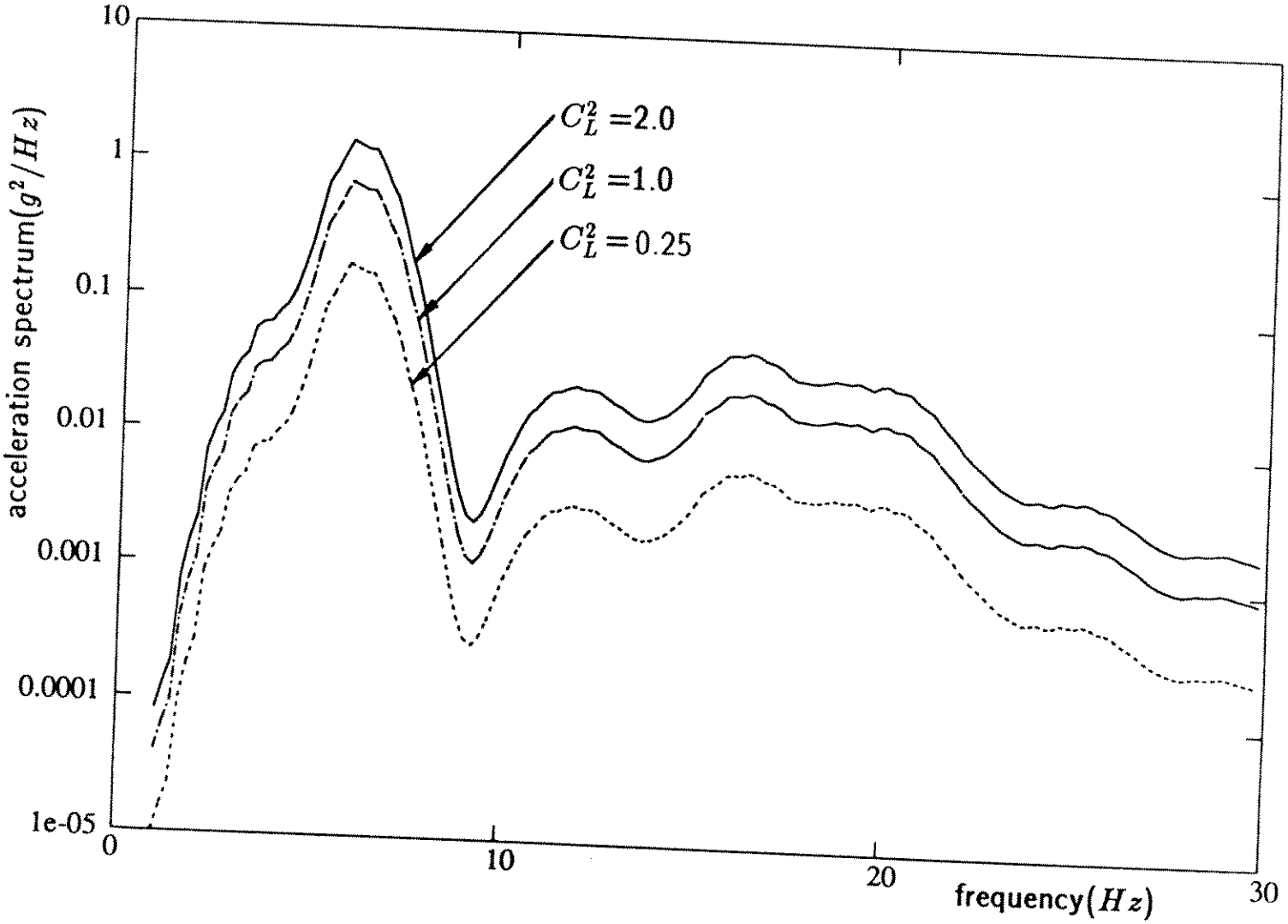

Figure 8.9: **Predicted acceleration spectra at $L/8$ for Test(3-L) : mean square lift coefficient C_L^2=0.25, 1.0 and 2.0**

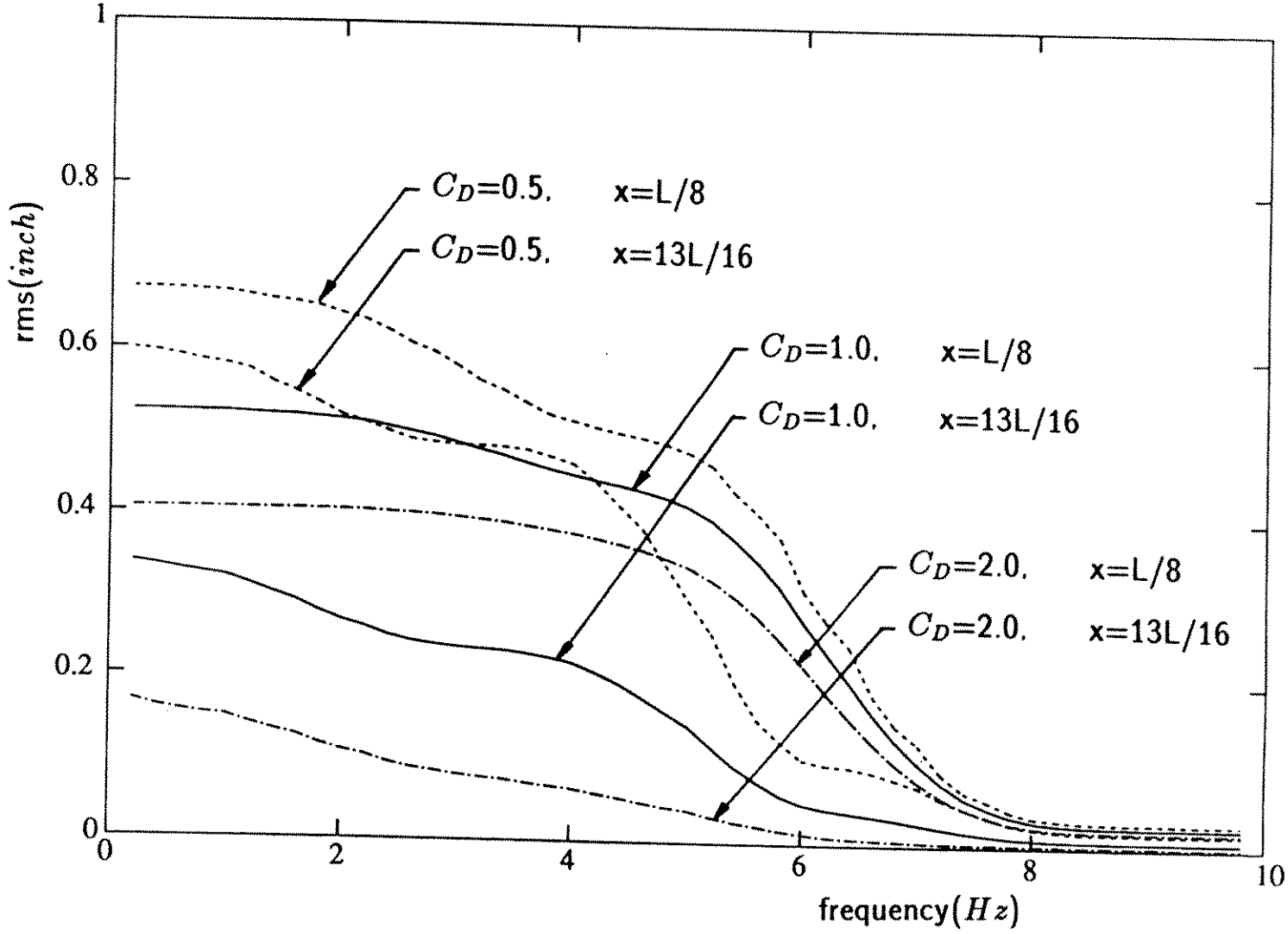

Figure 8.10: Predicted integrated spectra at $L/8$ and $13L/16$ for Test(3-L) :drag coefficient C_D=0.5, 1.0 and 2.0

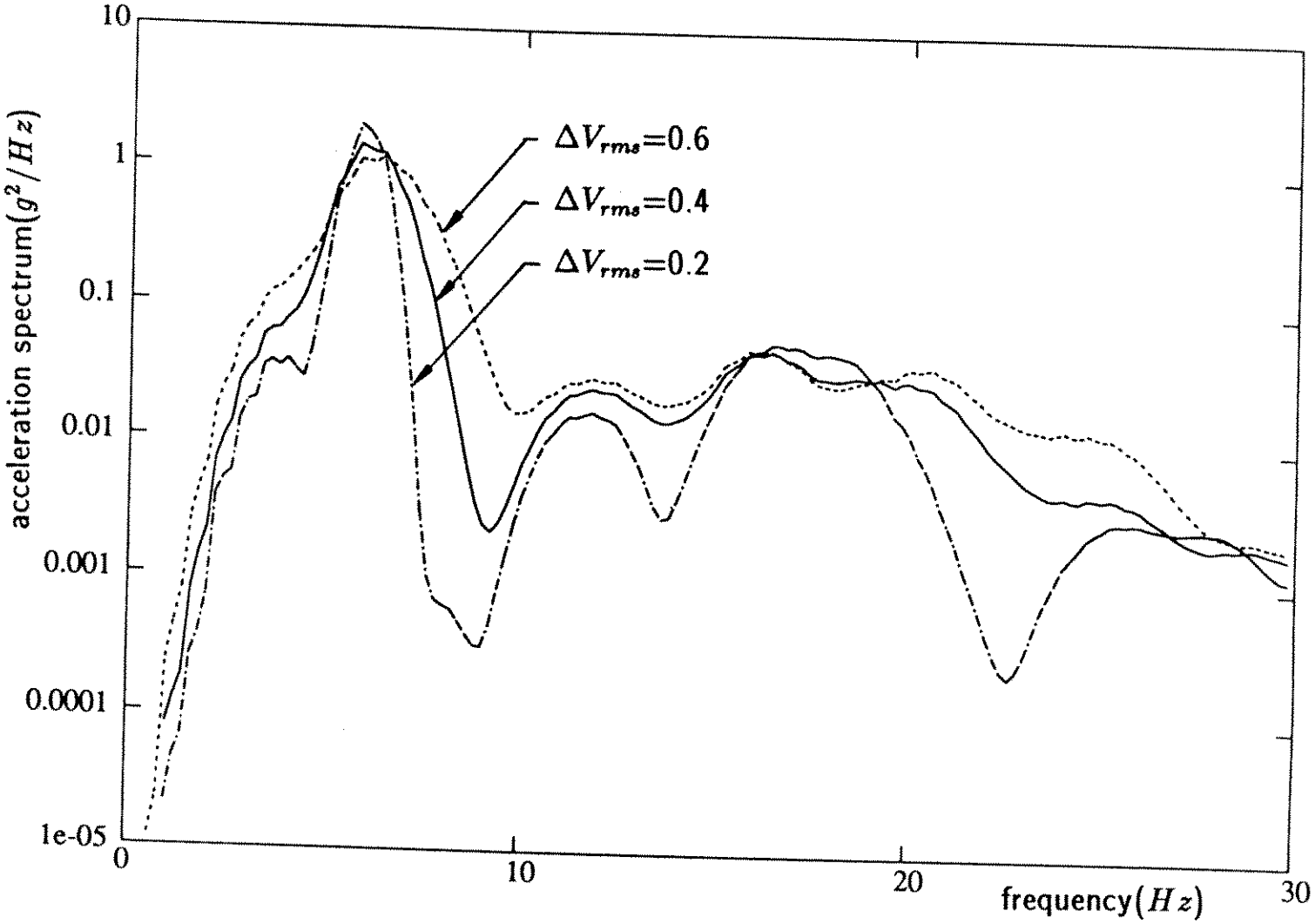

Figure 8.11: Predicted acceleration spectra at $L/8$ for Test (3-H) :standard deviation of turbulence ΔV_{rms}=0.2, 0.4 and 0.6 ft/sec

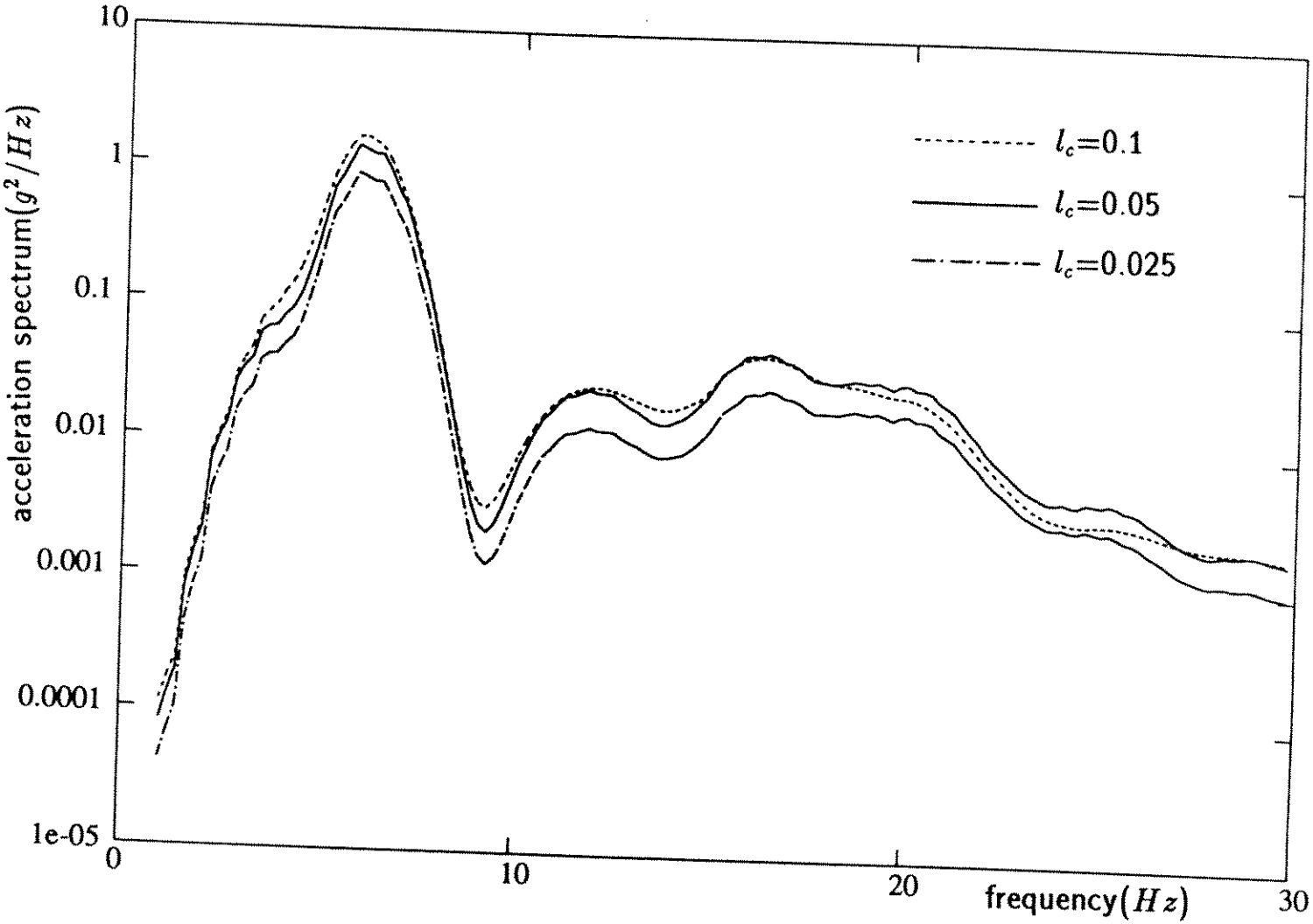

Figure 8.12: Predicted acceleration spectra at $L/8$ for Test (3-L) :spatial correlation length coefficient l_c=0.025, 0.05 and 0.1

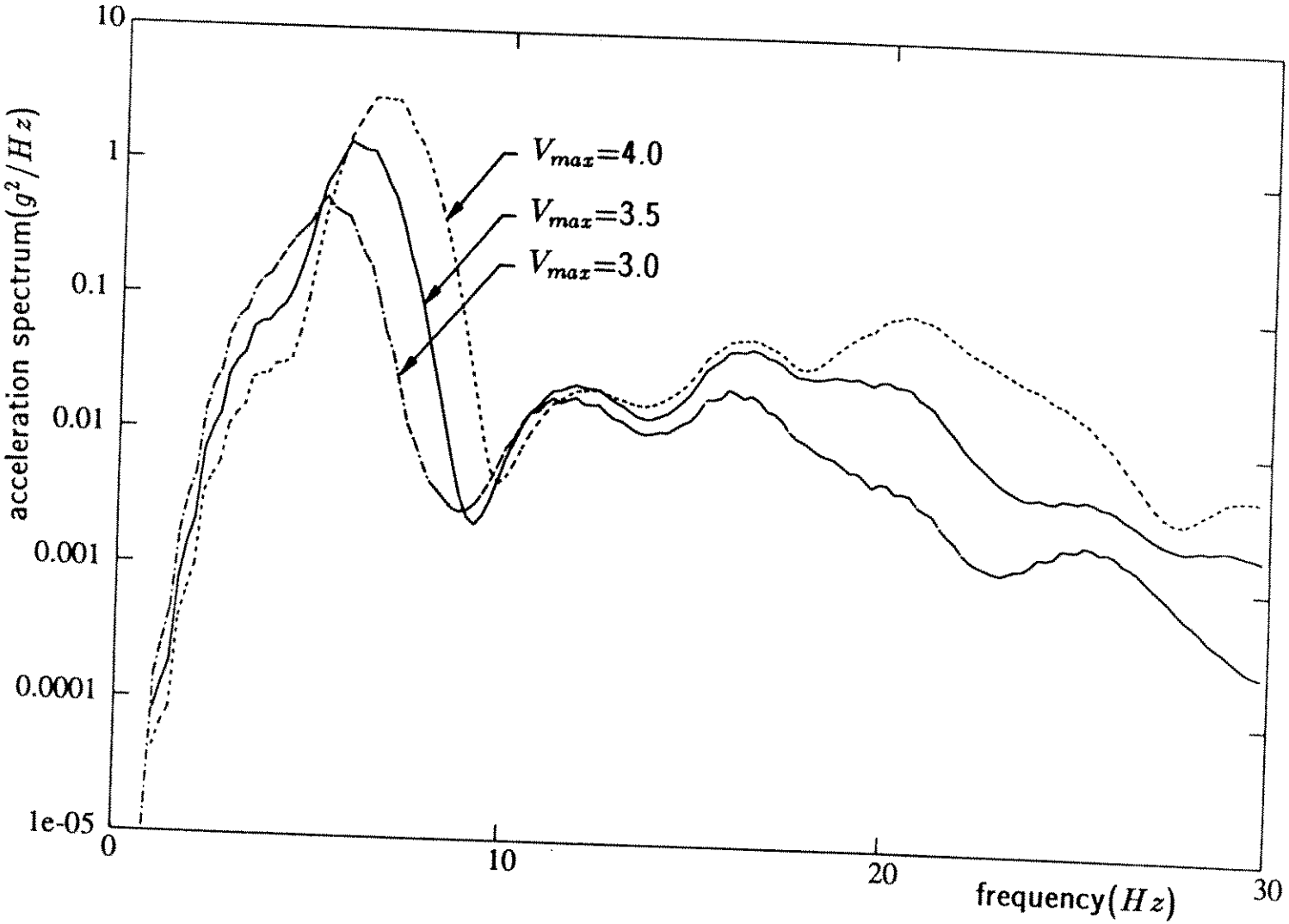

Figure 8.13: Predicted acceleration spectra at $L/8$ for Test (3-L) :the maximum flow velocity V_{max}=3.0, 3.5 and 4.0ft/sec

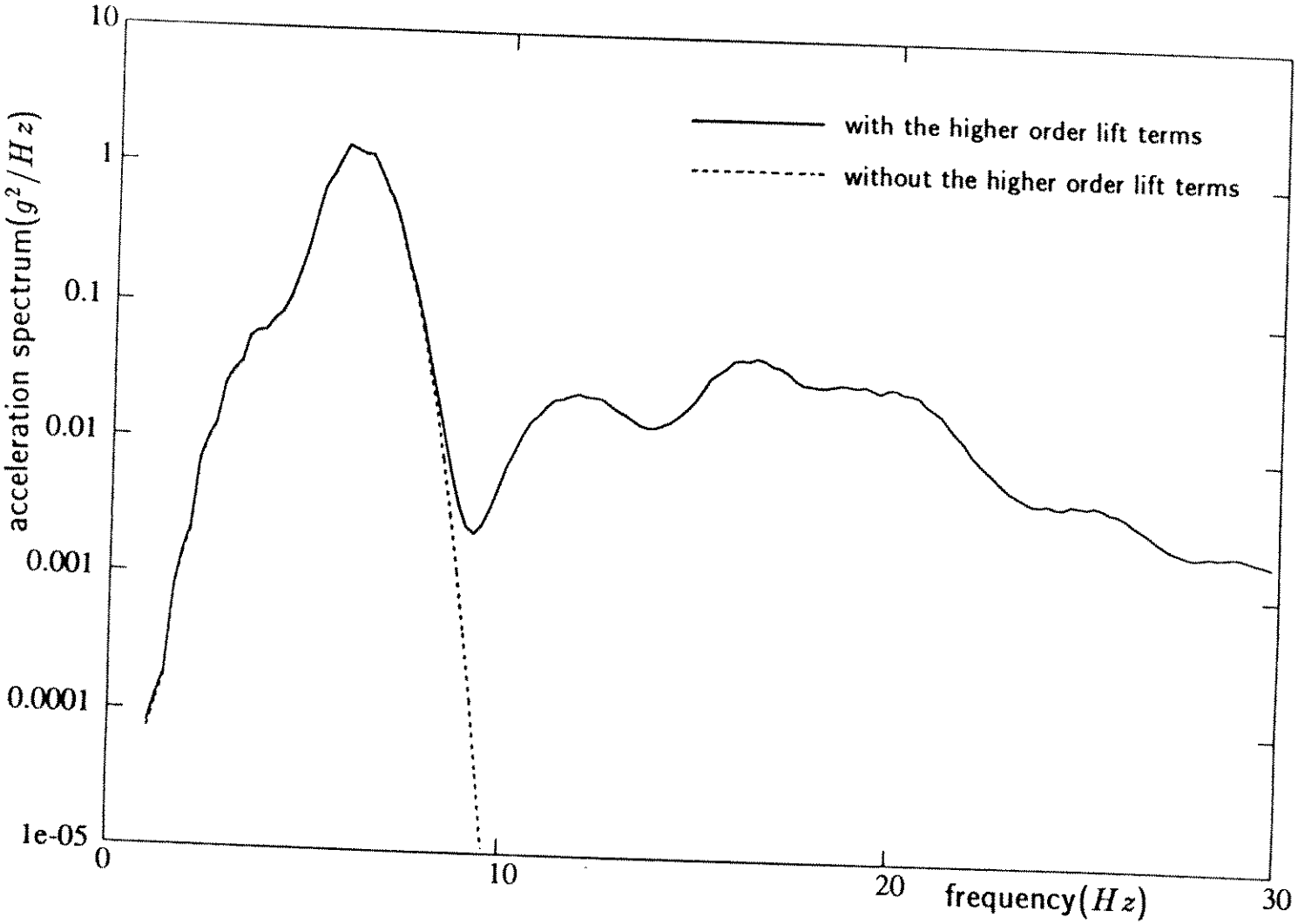

Figure 8.14: Predicted acceleration spectra at $L/8$ for Test (3-L) with and without the higher order lift terms

Chapter 9

Summary and conclusions

Field experiments were conducted to investigate the dynamic response characteristics of a tensioned cable in sheared flows. The tests were conducted under realistic field conditions with a length to diameter ratio of approximately 600. Uniform to highly sheared flows were achieved.

A response prediction method was proposed for the non-lockin, vortex-induced vibration of a tensioned cylinder in sheared flow based on a Green's function approach. An hydrodynamic damping and an excitation model are proposed based on linear random vibration theory. The predicted response, using parameters estimated from the same experiments, is compared with the experimental observations.

Findings obtained in this study are as follows:

1. For the non-lockin case, the steepness of sheared flow profile determines the broadness of the response spectrum through a local Strouhal relationship.

2. The non-dimensional parameters $f_{s,max}/f_1$ and $\Delta f_s/f_1$ are important in estimating the likelihood of the occurrence of single mode lockin.

3. With the exception of pure single mode lockin, hydrodynamic modal damping plays an important role in determining flow induced vibration response. In these experiments hydrodynamic damping was 10 to 20 times larger than structural damping.

4. The product $n\zeta_n$, determines whether the cylinder behaves like a infinite cable or not. When this parameter exceeds 3, then infinite length behavior takes over. When it is less than 0.1, single modes may dominate the response.

5. The mode superposition method requires many modes when $n\zeta_n$ exceeds about 0.2. In such cases non-resonant modal contributions are substantial and account for the spatial attenuation.

6. The predicted and observed damping ratio varied inversely with frequency.

Suggestions for further Research

As an immediate extension of this work, it is suggested that the response prediction model be extended to cylindrical structures other than uniform cables with constant tension. Non uniform tension, diameter, and bending stiffness need all be considered.

Another suggestion for further research is to carry out more experiments in sheared flow using a very high density cable. In uniform flow, the lockin bandwidth in the reduce velocity domain is mainly dependent upon the mass ratio. It would be interesting to see the differences between the response characteristics in sheared flow of cables with differences in their mass ratios. More research needs to be conducted to understand hydrodynamic damping mechanisms.

Bibliography

[1] R. D. Blevins. *Flow-Induced Vibration.* Van Nostrand Reinhold Co., 1977.

[2] D. L. R. Botelho. *An Empirical Model for Vortex-Induced Vibrations.* Report No. EERL82-02, Calif. Institute of Technology, Earthquake Engineering Research Laboratory, August 1982.

[3] K. F. Graff. *Wave Motion in Elastic Solids.* Ohio State University Press, 1975.

[4] O. M. Griffin. "The Effect of Current Shear on Vortex Shedding". In *The International Symposium on Separated Flow Around Marine Structures*, The Norwegian Institute of Technology, June 1985.

[5] O. M. Griffin. *Vortex-Induced Vibrations of Marine Cables and Structures.* NRL Memorandum Report 5600, Naval Research Laboratory, June 1985.

[6] O. M. Griffin and S. E. Ramberg. "Some Recent Studies of Vortex shedding with Application to Marine Tubulars and Risers". *Journal of Energy Resources Technology*, Vol. 104, March 1982.

[7] J. Y. Jong. *The Quadratic Correlation Between In-Line and Cross-Flow Vortex-Induced Vibration of Long Flexible Cylinders.* Ph. D. Thesis, Massachusetts Institute of Technology, Ocean Engineering Department, August 1984.

[8] J. Y. Jong and J. K. Vandiver. *Response Analysis of the Flow-Induced Vibration of Flexible Cylinders Tested at Castine, Maine in July and August of 1981.* Technical Report, Massachusetts Institute of Technology, Ocean Engineering Department, January 1983.

[9] M. B. Kennedy. *A Linear Random Vibration Model for Cable Strumming.* Ph. D. Thesis, Massachusetts Institute of Technology, Ocean Engineering Department, February 1979.

[10] Y. H. Kim. *Vortex-Induced Response and Drag Coefficients of Long Cables in Ocean Currents.* Ph. D. Thesis, Massachusetts Institute of Technology, Ocean Engineering Department, October 1984.

[11] Y. H. Kim, J. K. Vandiver, and R. A. Holler. "Vortex-Induced Vibration and Drag Coefficients of Long Cables Subjected to Sheared Flows". *Journal of Energy Resources Technology*, Vol. 108, March 1986.

[12] R. King. "A Review of Vortex Shedding Research and It's Application". *Ocean Engineering*, Vol. 4, 1977.

[13] N. M. Patrikalakis and C. Chryssostomidis. "Vortex-Induced Response of a Flexible Cylinder in a Sheared Current". *Journal of Energy Resources Technology*, Vol. 108, March 1986.

[14] S. E. Ramberg and O. M. Griffin. "Velocity Correlation and Vortex Spacing in the wake of a Vibrating Cable". *Journal of Fluids Engineering*, Vol. 10, March 1976.

[15] T. Sarpkaya. *Transverse Oscillations of Circular Cylinder in Uniform Flow, Part1.* Report No. NPS-69SL77071-R, Naval Postgraduate School, Monterey, MA, December 25 1977.

[16] T. Sarpkaya. "Vortex Induced Oscillations. A Selective Review". *ASME Journal of Applied Mechanics*, Vol. 46:PP 241–258, June 1979.

[17] P. K. Stansby. "The Locking-on of Vortex Shedding due to the Cross-Stream Vibration of Circular Cylinders in Uniform and Shear Flows". *Journal of Fluids Mechanics*, Vol. 74, Part 4, 1976.

[18] D. T. Tsahalis. "Vortex-Induced Vibrations of a Flexible Cylinder Near a Plane Boundary Exposed to Steady and Wave-Induced Currents". *Journal of Energy Resources Technology*, Vol. 106, June 1984.

[19] J. K. Vandiver. "The Prediction of Lockin Vibration on Flexible Cylinders in a Sheared Flow". In *Proceedings of 1985 Offshore Technology Conference*, Houston, May 1985. OTC5006.

[20] J. K. Vandiver and J. Y. Jong. "The Relationship Between In-Line and Cross-Flow, Vortex-Induced, Vibration of Cylinders". In *Proceedings ASME, ETCE Conference*, New Orleans, February 1986. Paper No. OMAE-No-170.

[21] E. Wang, D. K. Whitney, and K. G. Nikkel. "Vortex-Shedding Response of Long Cylindrical Structures in Shear Flow ". In *Proceedings Fifth International Symposium on Offshore Mechanics and Arctic Engineering*, Tokyo, April 1986.

Appendix A

Dynamic characteristics of the test cable in air

During field experiments, the dynamic characteristics of the test cable in air were investigated. After making the test cable oscillate in a specific mode, the free decay signals were obtained. Figure A.1 shows the cross-flow acceleration time histories at $L/8$, $L/6$, $L/4$, $L/2$, $11L/16$, and $13L/16$. As a result of the modal identification process, natural coordinate time histories for the 1st, 2nd, 3rd, and 5th modes were extracted and plotted in Figure A.2. Figure A.2 shows free decay of the 3rd mode acceleration. A similar free decay test was done for the 2nd mode. For lightly damped structures, the natural frequency and the damping ratio for the jth mode are given by:

$$f_j = \frac{N_c}{\Delta T} \tag{A.1}$$

$$\varsigma_j = \frac{1}{2\pi N_c} \ln \frac{A_i}{A_{i+N_c}} \tag{A.2}$$

where

f_j = the jth mode natural frequency

ς_j = damping ratio for the jth mode

ΔT = time duration between the amplitudes of two peaks which are n cycles apart

N_c = the number of cycles between two peaks

A_i = amplitude of the initial peak

A_{i+N_c}= amplitude of the peak after N_c cycles from initial peak

Table A.1 shows the measured natural frequencies and damping ratios for the 2nd and 3rd modes. Table A.1 includes the calculated natural frequencies under the tension of 230 pounds using the simple equation for a taut string.

Table A.1: Dynamic characteristics of the test cable in air

Mode No.	Natural frequency		Damping ratio
	measured	calculated	
2nd mode	1.98	1.98	0.0032
3rd mode	2.99	2.97	0.0028

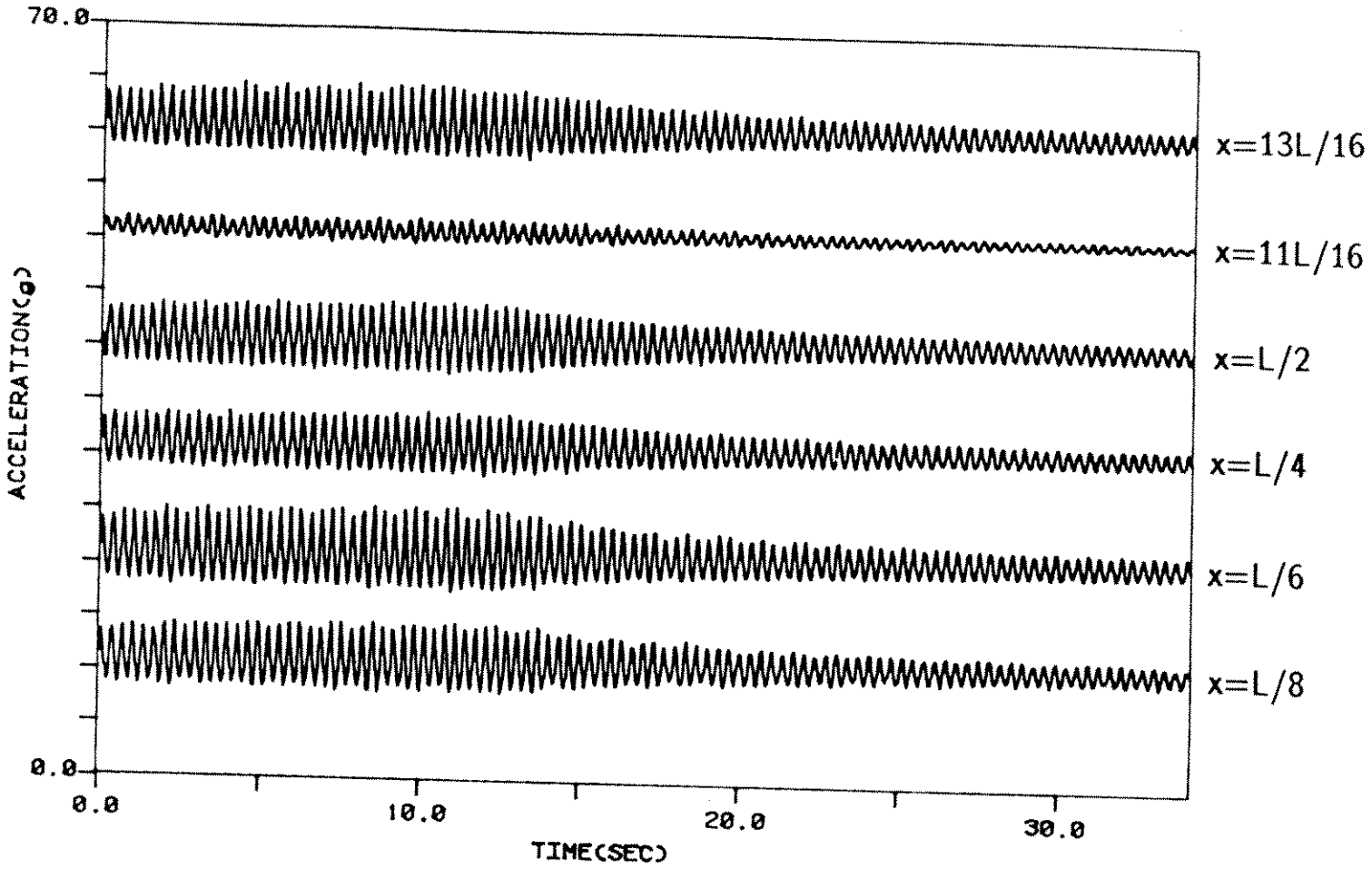

Figure A.1: Cross-flow acceleration time histories of free decay test in air

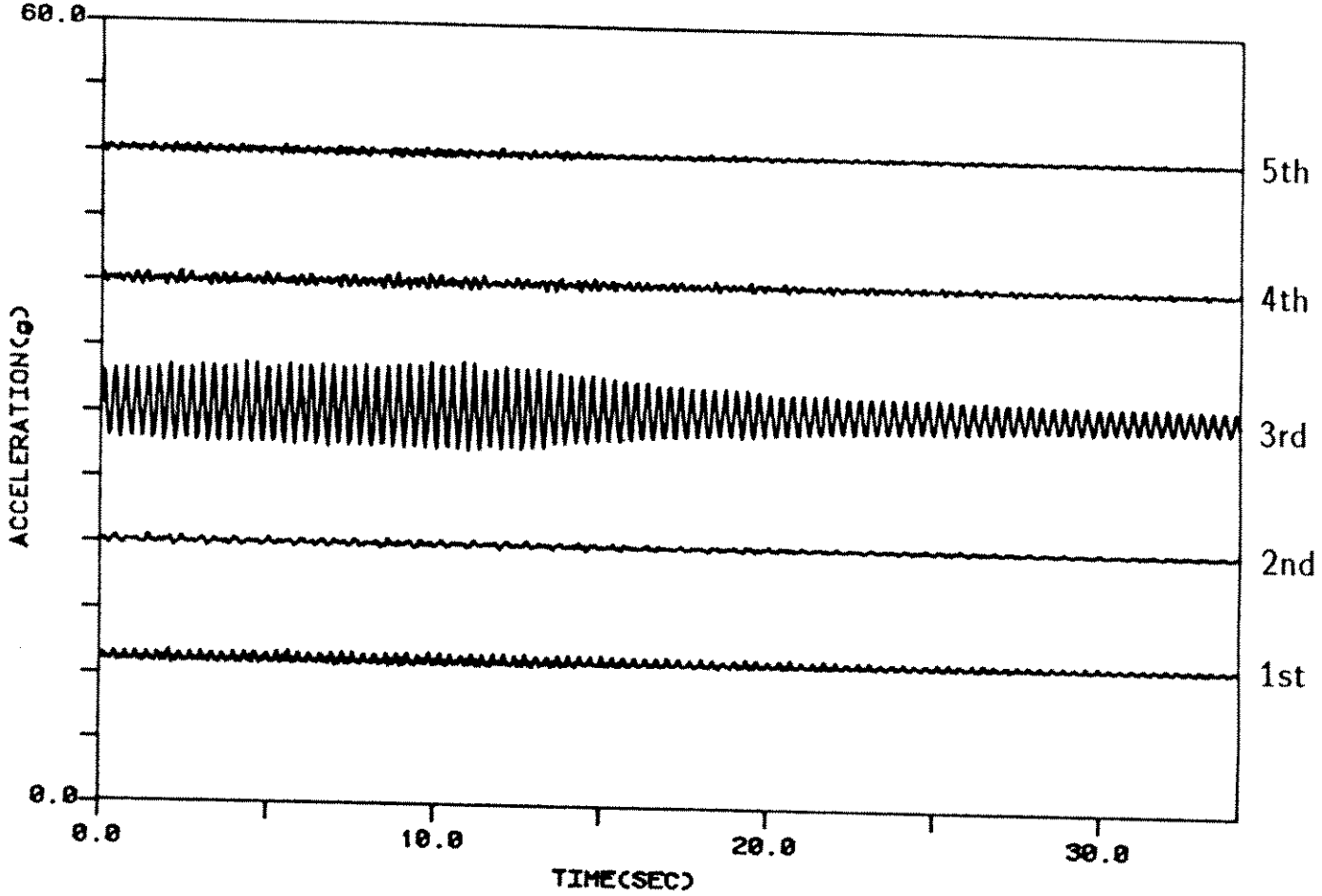

Figure A.2: Modal identification result of free decay test in air

Appendix B

Predicted and Experimental Results for Test(2-L) and Test(3-H)

The predicted results and experimental results for two test conditions which were not shown in chapter 8 are shown in here. One is the low tension and low shear case (Test(2-L)) and another is the high tension and high shear case (Test(3-H)). The results which will be shown for each test condition consist of four figures:

1. Predicted acceleration spectra at $x = L/8$(high flow velocity region) and $x = 13L/16$(near zero flow velocity region)

2. Predicted and measured acceleration spectra at $x = L/8$ (high flow velocity region)

3. Predicted and measured acceleration spectra at $x = 13L/16$(near zero flow velocity region)

4. Predicted and measured integrated displacement spectra at $x = L/8$ and $x = 13L/16$

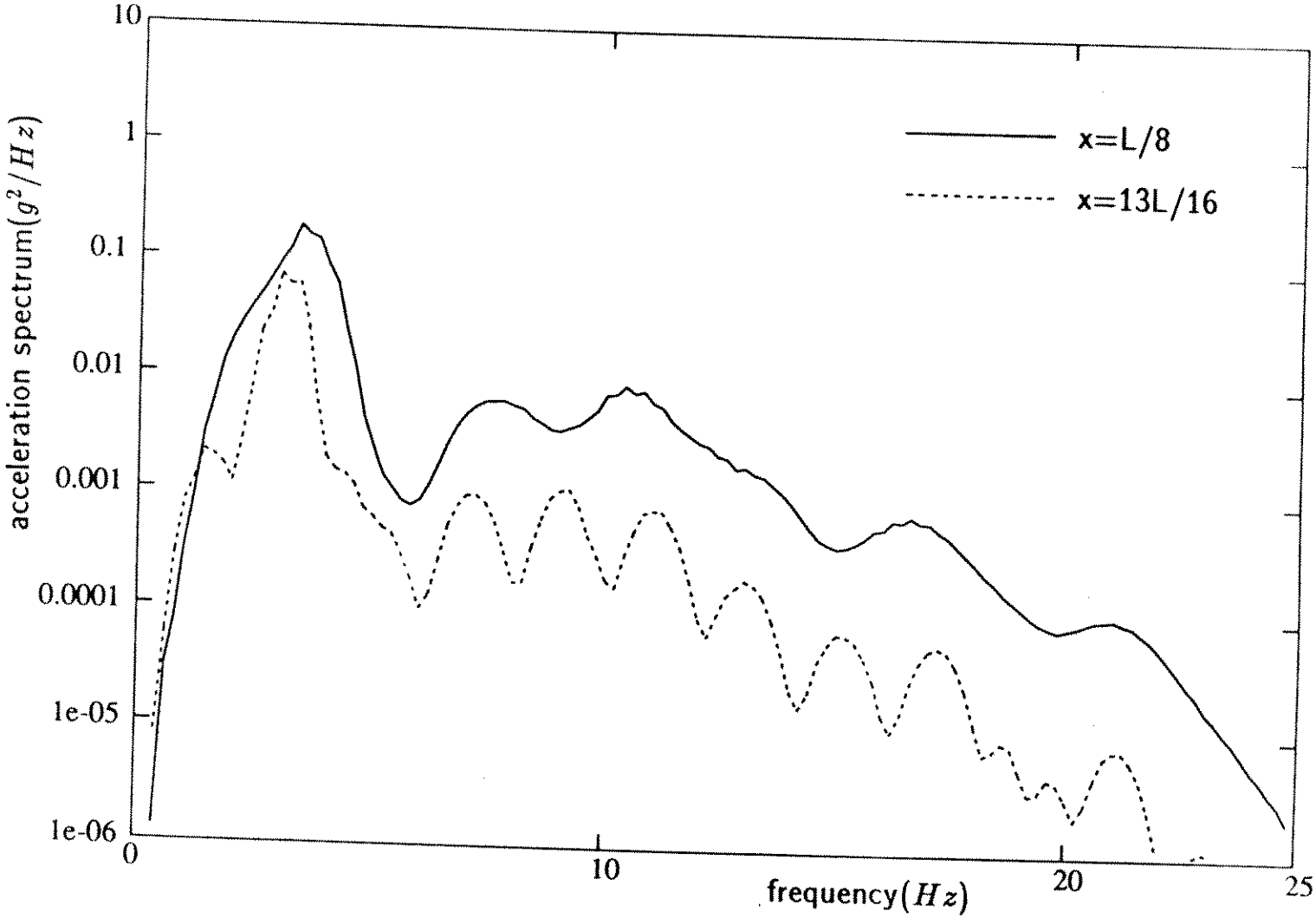

Figure B.1: Predicted acceleration spectra at $L/8$ and $13L/16$ for Test(2-L)(slightly sheared flow, SFP2, and T=62 *lbs*)

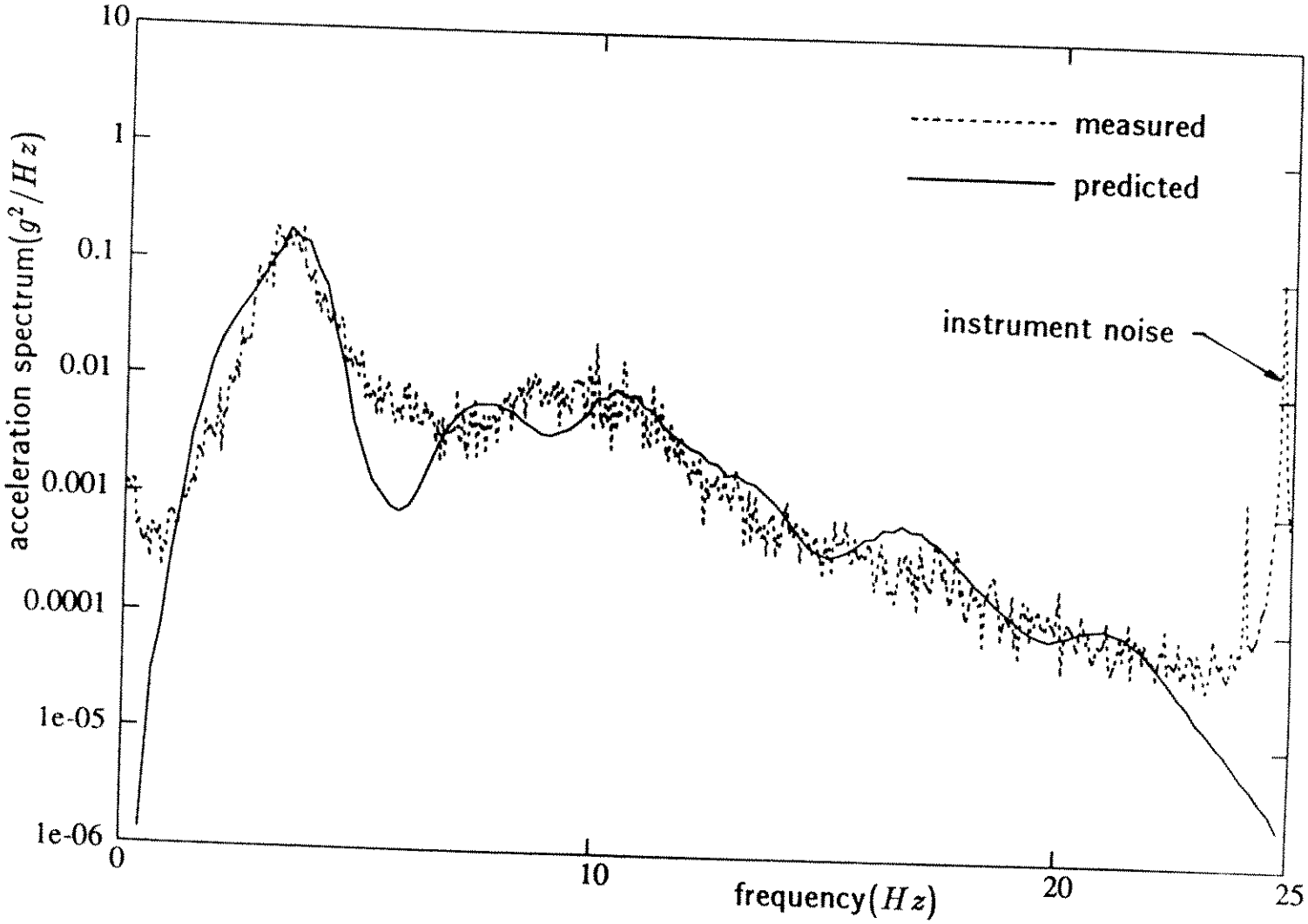

Figure B.2: Predicted and measured acceleration spectra at $L/8$ for Test(2-L)(slightly sheared flow, SFP2, and T=62 *lbs*)

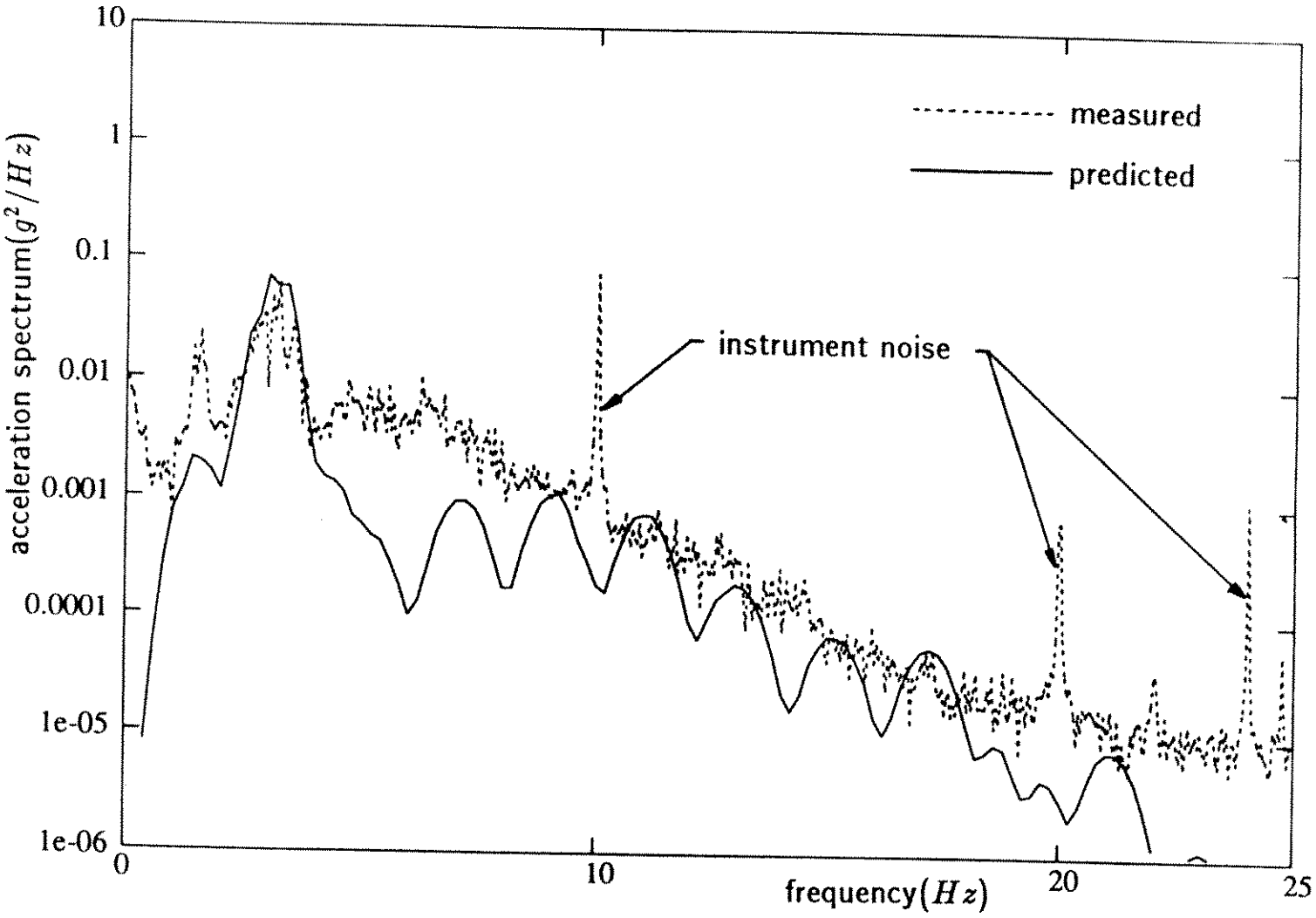

Figure B.3: Predicted and measured acceleration spectra at $13L/16$ for Test(2-L)(slightly sheared flow, SFP2, and T=62 *lbs*)

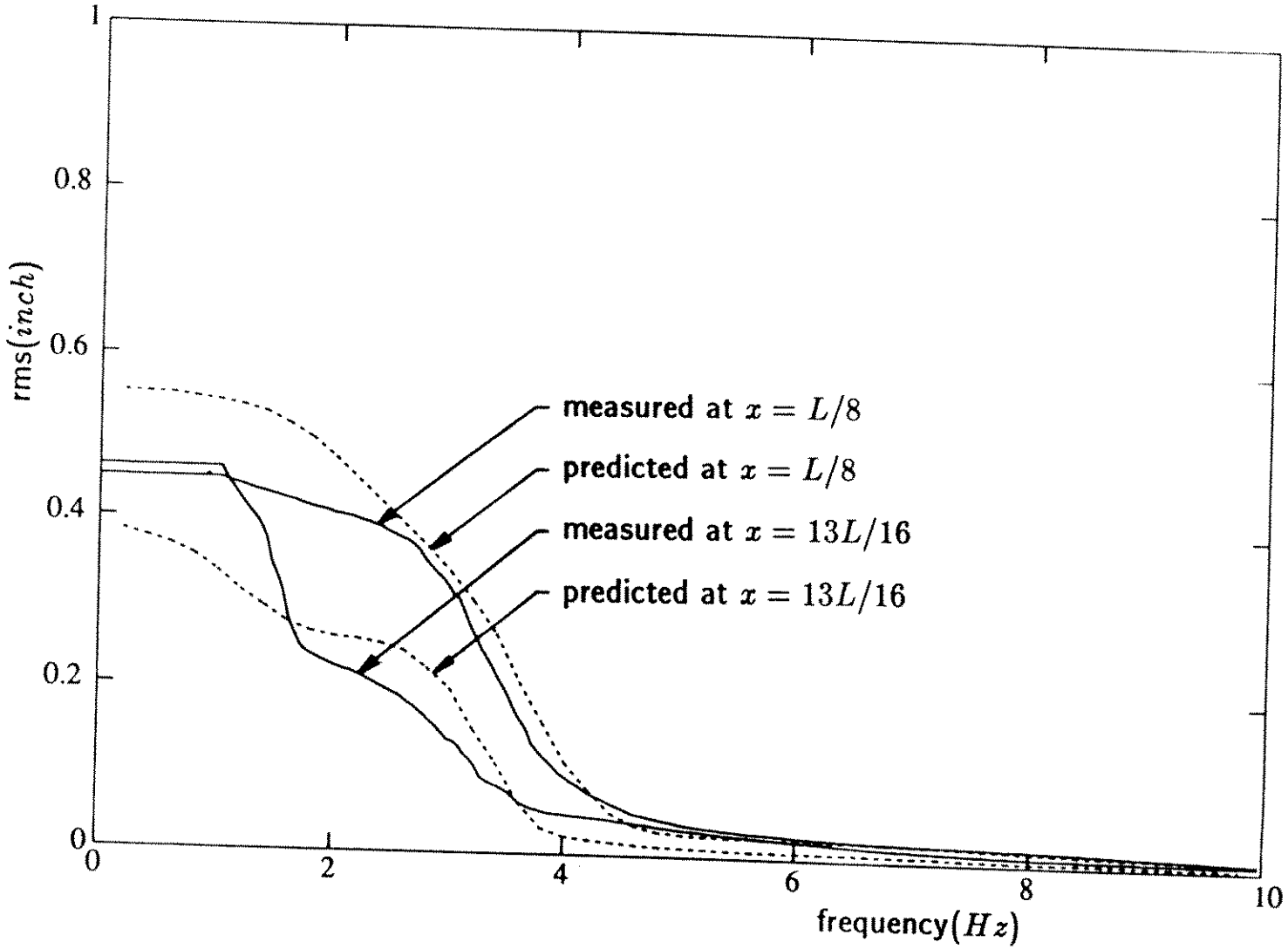

Figure B.4: Predicted and measured integrated displacement spectra at $L/8$ and $13L/16$ for Test(2-L)(slightly sheared flow, SFP2, and T=62 *lbs*)

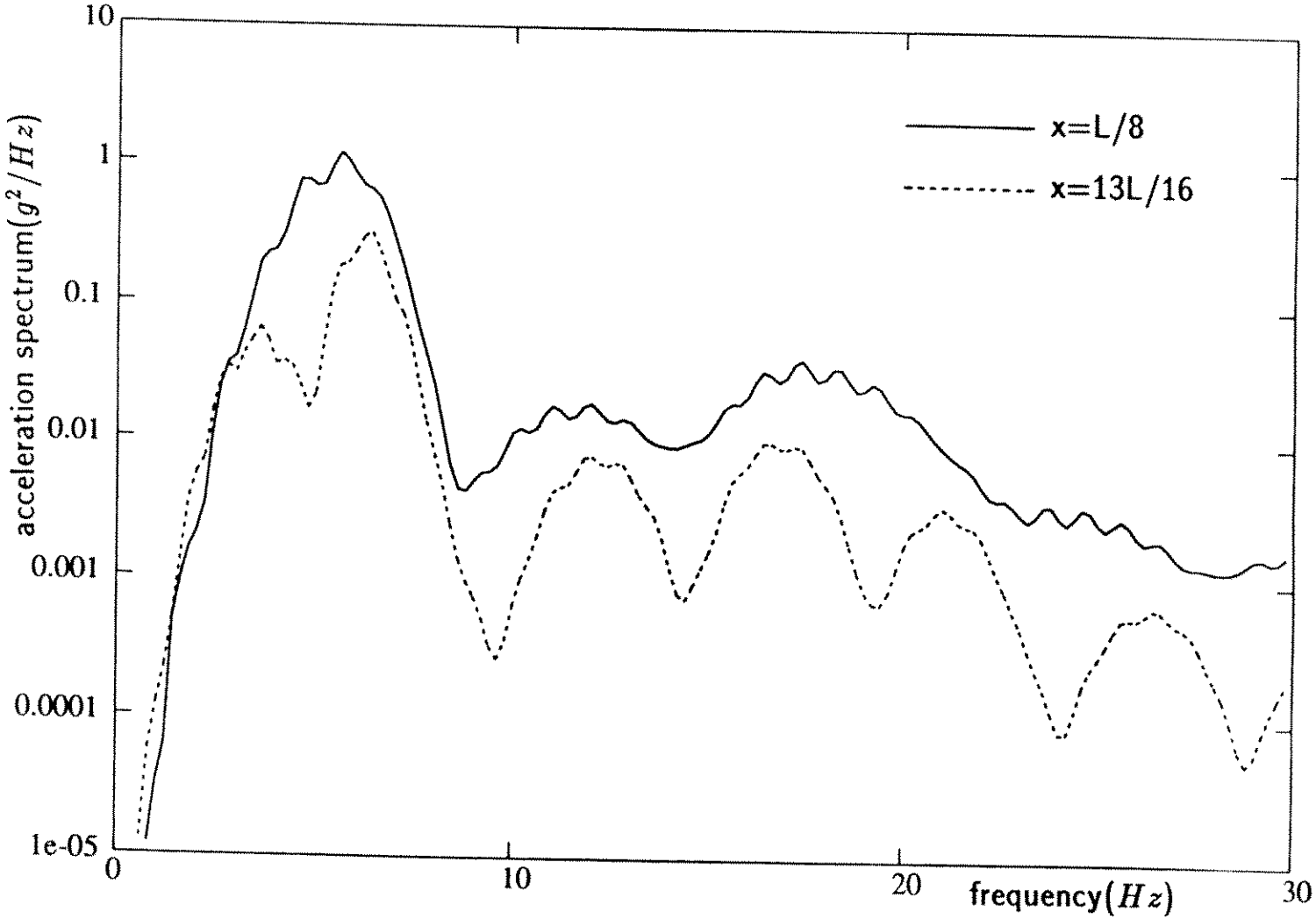

Figure B.5: Predicted acceleration spectra at $L/8$ and $13L/16$ for Test(3-H)(highly sheared flow, SFP3, and T=344 *lbs*)

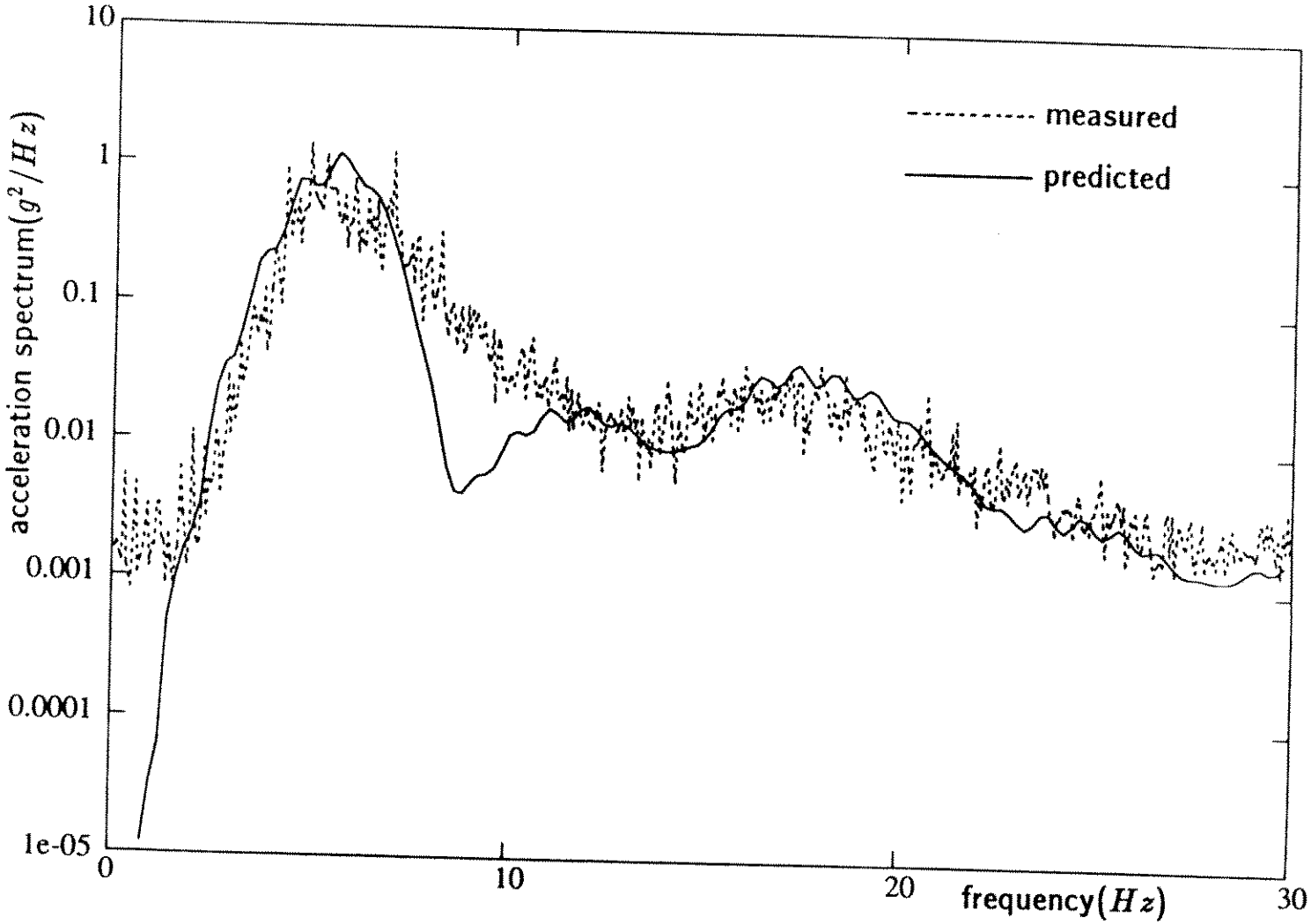

Figure B.6: Predicted and measured acceleration spectra at $L/8$ for Test(3-H)(highly sheared flow, SFP3, and T=344 *lbs*)

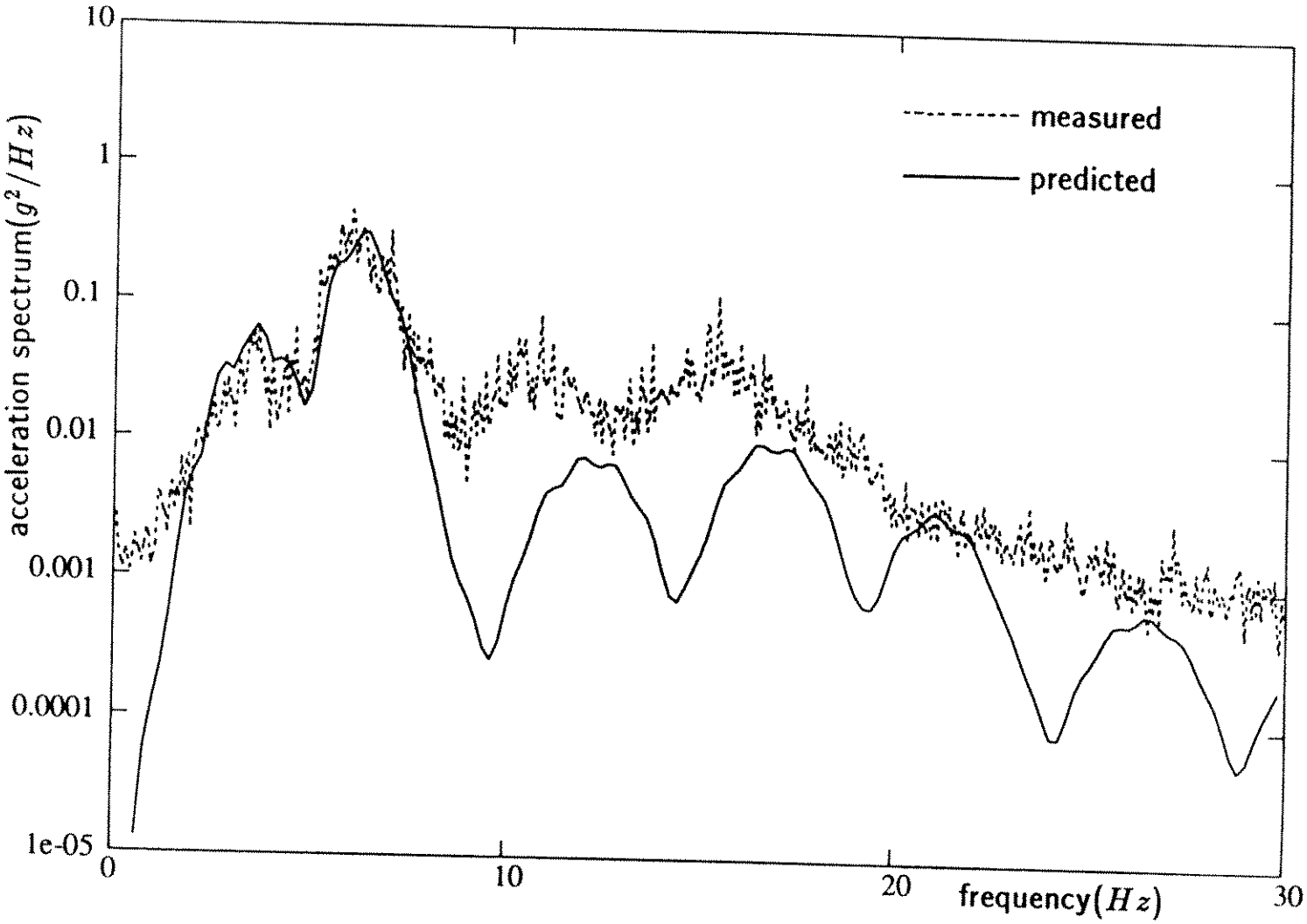

Figure B.7: Predicted and measured acceleration spectra at $13L/16$ for Test(3-H)(highly sheared flow, SFP3, and T=344 *lbs*)

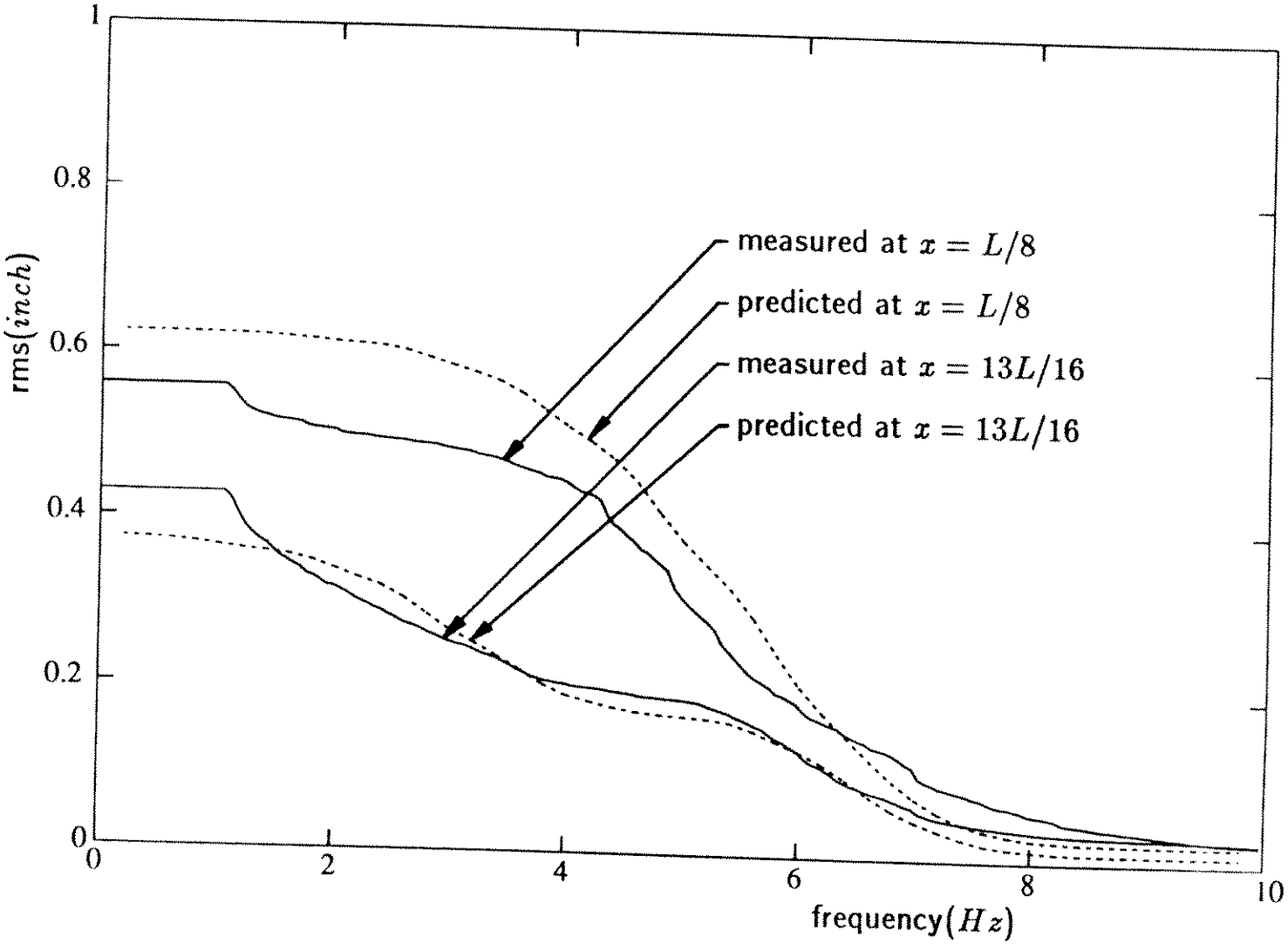

Figure B.8: Predicted and measured integrated displacement spectra at $L/8$ and $13L/16$ for Test(3-H)(highly sheared flow, SFP3, and T=344 *lbs*)